

MASTER'S THESIS

---

# CdSe nanoplatelets

Synthesis, heterostructures, ion exchange and optical properties

---

*Author:*

Annelies van der Bok

*Supervisor:*

Jaco Geuchies

Relinde van Dijk - Moes

Prof. Dr. Daniël Vanmaekelbergh

Condensed Matter and Interfaces

Utrecht University

May 13, 2015



Universiteit Utrecht



---

## Abstract

CdSe nanoplatelets (NPLs) exhibit interesting opto-electronic properties. For example, they have narrow excitonic features and can therefore be used as monochromatic light emitters. Synthesis methods for CdSe NPLs emitting at 460 nm (460NPLs), 510 nm (510NPLs) and 550 nm (550NPLs) were reported by Dubertret et al. This thesis reports that these synthesis methods are reproducible and that the surface of the NPLs can be modified. The knowledge obtained from investigating surface modifications of quantum dots and nanorods could be used to modify the surface of the NPLs. This resulted in the formation of CdSe/CdS core/shell NPLs. A CdS/Cd<sub>0.5</sub>Zn<sub>0.5</sub>S/ZnS shell using SILAR with oleyl amine as a coordination ligand was also synthesized. Synthesis of multishell quantum dots results in particles with a high quantum yield (QY), but the QY of the multishell NPLs was reduced compared to bare NPLs. Furthermore, the thickness of the multishell NPLs was not homogeneous. The edge of the particle was thicker and an excess of cadmium and sulphur could be found at the edge. Zinc and selenium were homogeneously distributed in the multishell NPLs.

A second modification reported in this thesis is the cadmium-to-mercury ion-exchange of CdSe NPLs, but this modification did not result in stable dispersions of NPLs. The exchange was only partially successful on CdSe QDs with a multishell.

Furthermore, an adaptation to the synthesis of 510NPLs is reported. Instead of adding only cadmium acetate during the reaction, a mixture of cadmium- and sodium acetate was added. The cadmium acetate is added during the reaction to induce 2D growth, but addition of different acetate salts also resulted in the formation of CdSe NPLs. When cadmium acetate is added, a small amount of thicker or thinner NPLs are present in the sample. Addition of a mixture of sodium acetate and cadmium acetate resulted in the formation of 510NPLs only with a high QY of 60 %.

The optical properties of CdSe NPLs are also investigated. Plausible energy transfer is observed between NPLs. The fluorescence intensity decay of the NPLs is multi-exponential. Photoluminescent lifetime measurements on NPLs in solvents with different refractive indices showed that none of the components of the multi-exponential decay are predominantly radiative. Trends obtained with these measurement could not be fitted by the models used in literature.



## Contents

1	Introduction	7
2	Theory	8
2.1	Quantum confinement	8
2.2	Synthesis of nanocrystals	9
2.3	Stability and shape control of nanocrystals	10
2.4	Heteronanocrystals	10
2.5	Ion exchange	12
3	Previous studies on CdSe nanoplatelets	13
4	Experimental methods	16
4.1	Chemicals	16
4.2	Synthesis of nanoplatelets	16
4.2.1	Synthesis of 460NPLs	16
4.2.2	Preparation Cadmium myristate for synthesis 510NPLs and 550NPLs	16
4.2.3	Synthesis of 510NPLs	17
4.2.4	Preperation Se-precursor for synthesis 550NPLS	17
4.2.5	Synthesis of 550NPLs	17
4.3	Synthesis of heteronanoplatelets	17
4.3.1	Synthesis CdSe/CdS core/shell nanoplatelets	17
4.3.2	Synthesis of CdS/Cd <sub>0.5</sub> Zn <sub>0.5</sub> S/ZnS multishell nanoplatelets using layer by layer method	18
4.3.3	Synthesis of CdS/Cd <sub>0.5</sub> Zn <sub>0.5</sub> S/ZnS multishell nanoplatelets using SILAR method	18
4.4	Hg-Exchange	18
4.5	Optical measurements	19
5	Results and Discussion	20
5.1	CdSe nanoplatelets	20
5.1.1	Nanoplatelets emitting at 460 nm	20
5.1.2	Nanoplatelets emitting at 510 nm	20
5.1.3	Nanoplatelets emitting at 550 nm	24
5.1.4	Conclusion and outlook	24
5.2	Heteronanoplatelets	27
5.2.1	CdSe/CdS core/shell nanoplatelets	27
5.2.2	Nanoplatelets with multishell	28
5.2.3	Conclusion and outlook	33
5.3	Cadmium-to-mercury ion exchange	34
5.3.1	Cadmium-to-mercury ion exchange on CdSe QDs	34
5.3.2	Cadmium-to-mercury ion exchange on CdSe nanoplatelets	36
5.3.3	Cadmium-to-mercury ion exchange on multishell quantum QDs	38

5.3.4	Conclusion and outlook . . . . .	40
5.4	Adaptation to original synthesis . . . . .	41
5.4.1	Addition of different acetates salts . . . . .	41
5.4.2	EDX-measurements . . . . .	47
5.4.3	Photoluminescence quantum yield measurements . . . . .	49
5.4.4	Conclusion and outlook . . . . .	52
5.5	Energy transfer . . . . .	53
5.5.1	Energy transfer in dispersion obtained when adding acetic acid . .	53
5.5.2	Energy transfer between 460NPLs and 510NPLs . . . . .	55
5.5.3	Energy transfer between 510NPLs and 550NPLs . . . . .	57
5.5.4	Conclusion and outlook . . . . .	59
5.6	Influence refractive index on the decay rate and the quantum yield . . . .	61
5.6.1	Background information . . . . .	61
5.6.2	Lifetime measurements . . . . .	62
5.6.3	Dependence lifetime . . . . .	63
5.6.4	Dependence fraction of emission though fast components . . . . .	64
5.6.5	Fitting of the models . . . . .	67
5.6.6	Conclusion and outlook . . . . .	69
6	Conclusion and outlook	70
7	Acknowledgements	73
	References	75
A	Appendix A	79

## 1 Introduction

Semiconductor nanocrystals (NCs) have been of great interest due to their size and shape dependent properties. Especially NCs with at least one dimension smaller than their exciton Bohr radius have received noticeable attention, since their optical properties are dictated by the quantum confinement effect. Due to this effect, the band gap of these materials can be tuned, by changing one of the spatial dimensions of the NC, which makes these materials very interesting for biomedical labelling [1], solar cells [2], LEDs [3] and many other applications.

NCs consisting out of a broad variety of materials can be synthesized. Cadmium based NCs have been researched extensively, because their bandgap lies in the visible range of the electromagnetic spectrum. This extensive research resulted in cadmium based NCs with many different shapes and sizes. Examples of different shapes are dots [5], rods [6], tetrapods [7] and platelets. The synthesis method for nanoplatelets (NPLs) was reported relatively recent compared to the other cadmium based NC shapes. The method for wurtzite NPLs dates from 2006 [8] and the method for zinc blende NPLs is even more recent; the synthesis of these particles was first reported by the group of Dubertret in 2008 [9]. This thesis will focus on these zinc blende NPLs.

Zinc blende NPLs exhibit very narrow excitonic features without inhomogeneous broadening [10], which makes these particles interesting for monochromatic light emitting devices. These NPLs have narrow absorption and emission peaks, because there is only confinement in one dimension. The size of this dimension, the thickness of the NPLs, can be controlled with atomic precision. Because only the NC size in one dimension has to be controlled to obtain narrow excitonic features, it is easier to scale-up the synthesis of NPLs than QDs. Other properties that make platelets interesting for optical applications are their high quantum yield and fast radiative decay rate.

Over the years extensive research has been done on QDs and nanorods. This resulted in the formation of heteronanostructures. Ion exchange on these cadmium based structures also made it possible to obtain NCs of materials which cannot be synthesized directly. It is of course interesting to investigate if the knowledge obtained from research on QDs and nanorods can be translated to NPLs.

This thesis will discuss the synthesis of CdSe NPLs and heteronanoplatelets (section 5.1 and 5.2). The possibility of cadmium-to-mercury ion-exchange was also investigated, because HgSe particles are predicted to have interesting optical properties (see section 5.3). The last part of this thesis will focus on the optical properties of CdSe NPLs. Synthesis methods to obtain NPLs with a high QY, energy transfer between NPLs and the effect of the refractive index of the solvent on the lifetime of the NPLs will be discussed in section 5.4, 5.5 and 5.6 respectively.

## 2 Theory

### 2.1 Quantum confinement

NCs have different properties compared to bulk crystals of the same material due to their size. For example, the bandgap becomes size dependent for nanocrystals with spatial dimensions close to, or below, the exciton Bohr radius (Fig 1). This dependence can be explained from a chemist's or physicist's point of view.

From the chemical point of view this phenomenon is explained using the molecular orbital (MO) theory. MO theory describes the MOs of a material as a linear combination of atomic orbitals (AOs). Due to the combination of many AOs, a band-like structure forms for bulk materials. There are less combinations of AO in NCs because there are less atoms present, which results in discrete energy levels near the band edges. As the number of energy levels decreases with decreasing particles size, the bandgap of the particles increases.

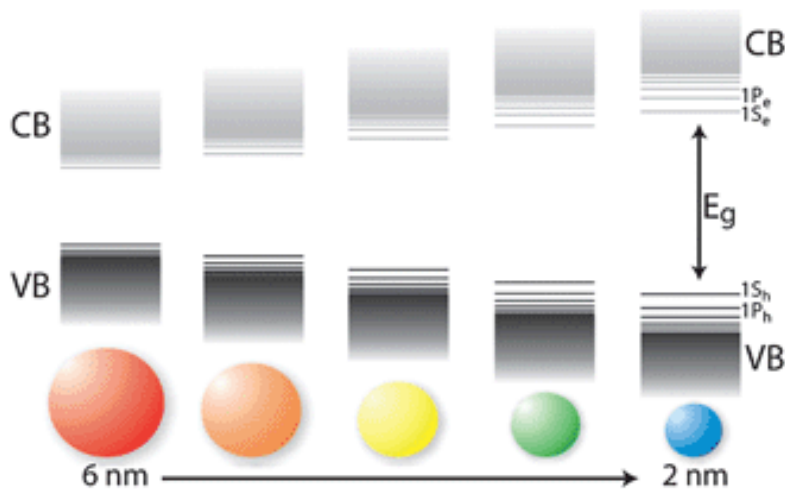


Figure 1: Schematic representation of quantum confinement in NCs. The bandgap ( $E_g$ ) becomes larger when the NC size becomes smaller. Discrete energy levels appear near the edges of the conduction and valence band. Duplicated from ref. [11].

From the physical point of view this phenomenon is explained using the particle in the box method [12]. With this method the NC material is described as a finite potential well with infinite potential barriers at the edges of the crystal. A free particle, e.g. an electron in a bulk crystal, has a energy dispersion relation that is quasi-continuous. This dispersion relation is given in equation (1). Because bulk material can be seen as an infinite crystal when we make use of boundary conditions, there are no restrictions on the wavevector  $k$ . In a NC, however, there are restrictions on the value for  $k$ , as the electron (and hole) wavefunctions have to become zero at the NC edges due to the infinite potential barrier. For a NC with confinement in one dimension (e.g. NPLs), the electron wavefunction is given by equation (2). The  $k_{xy}$  values are continuous, because



there is no confinement in the  $x$  and  $y$  direction. The wavefunction in the  $z$ -direction of the NPLs has to be described by a standing wave, leading to discrete values of  $k_z$ . To solve for this problem we impose new boundary conditions: the standing wave term in the wavefunction has to be zero at  $z = 0$  and  $z = L_z$ . This is true for  $k_z = \frac{2\pi n_z}{L}$  with  $n_z \in \mathbb{N}$ . The energy of the wavefunction is then given by equation (3), which is split into a continuous term and a discrete term.

$$E = \hbar\omega = \frac{\hbar^2 k^2}{2m} \quad (1)$$

$$\psi(r) = \sqrt{\frac{2}{L_x L_y L_z}} \sin(k_z z) \exp(ik_{xy} r) \quad (2)$$

$$E = \frac{\hbar^2 k_{xy}^2}{2m_{e^*}} + \frac{\pi^2 \hbar^2}{2m_{e^*} L_z^2} n_z^2 \quad (3)$$

The values for  $k_x$  and  $k_y$  will also become quantized, if there is confinement in three dimensions (like in QD). The wavefunction will then be described by eq.(4) and the energy by eq. (5). The energy is inversely proportional to the square of the sizes of the NC. If the size of the NC is reduced, then the spacing between the energy levels becomes bigger. Resulting in discrete energy levels at the edges of the band and a larger bandgap.

$$\psi(r) = \sqrt{\frac{2}{L_x L_y L_z}} \sin(k_x x) \sin(k_y y) \sin(k_z z) \quad (4)$$

$$E = \frac{\pi^2 \hbar^2}{2m_{e^*}} \left( \frac{n_x^2}{L_x^2} + \frac{n_y^2}{L_y^2} + \frac{n_z^2}{L_z^2} \right) \quad (5)$$

## 2.2 Synthesis of nanocrystals

There are many methods to synthesize NCs. In this report the focus will be on the wet-chemical synthesis of semiconductor NCs. Two general wet-chemical synthesis methods are the hot-injection method and the heating up method.

The hot-injection method was first reported by Murray et al. [5]. With this method a cold solution of monomer precursors is injected in a hot mixture of solvent, coordinating ligands and another monomer precursor. The sudden injection results in a supersaturated mixture which induces the rapid formation of nuclei. Due to the drop in temperature by the injection of the cold solution, the supersaturation is only short lived. This results in a short period of time where nucleation can take place. After this period only growth of the NCs can take place. This effective separation of the nucleation and

growth stages in the NC formation process ensures a low polydispersity of the NC size. The second method is the heating up method. All precursors, solvents and coordinating ligands are mixed before heating. For this method precursors are used that only become reactive at elevated temperatures. An example is selenium powder. This material is insoluble in ODE at low temperature, but if the temperature is raised to around 200 °C the selenium will dissolve. At this temperature the selenium concentration will increase suddenly and the mixture will become supersaturated. Again, nuclei can be formed together with the cation monomers. The separation between nucleation and growth in this process is realised by slowly heating the reaction mixture [13]. Synthesis of CdSe and CdTe NCs with low polydispersity using this method were reported by Cao et al. [14].

### 2.3 Stability and shape control of nanocrystals

Ligands play an important role during and after the synthesis of NCs. First, they make sure that the NCs do not aggregate. This can be either a result from electrostatic repulsion by charged ligands or due to steric hindrance by the ligands' long organic carbon chains. Second, the ligands influence the shape of the crystal. Facets to which ligands bind strongly are less reactive than facets to which the ligands bind weakly. In this way anisotropic particles can be synthesised, e.g. rods, platelets and tetrapods. Ligands have also an impact on the particle size and size distribution of the NCs [13]. Other factors that influence the shape of the particle are the surface free energy of the NC facets, the reaction temperature, the precursor concentration and the crystal structure of the NC. At a high temperature, the thermodynamic favoured shape will be formed. This is the NC shape with the lowest surface free energy. The facets with a high surface free energy grow the fastest to obtain NCs with the lowest total surface free energy [15]. At low temperature the ligands bind strongly to the facets with a high surface free energy. This makes growth of these facets slower. The low energy facets will grow faster, resulting in the kinetic favoured shape. The relative precursor concentration will also influence which facet can grow the fastest. The crystal structure of the particle determines the surface free energy of the facets [13], and has therefore also has a big influence on the particle shape that will be obtained.

### 2.4 Heteronanocrystals

Although NCs are stabilized by the ligands on the surface, they still degrade or oxidize over time. This is due to the dynamic equilibrium of attached and detached ligands. Detached ligands will expose the NC surface to e.g. oxygen molecules, which form irreversible bonds and induce the formation of NC aggregates due to incompatibility with the solvent. It is difficult to passivate all the cations and anions at the surface with ligands due to steric hindrance, resulting in dangling bonds at the surface [16]. These dangling bonds induce energy levels in the bandgap of the particle. Electrons and holes can be trapped in these states, quenching the luminescence of the particle [13]. Electrons trapped in deep trap states will primarily decay via non-radiative decay paths [11].

The before mentioned trap states in the bandgap can be eliminated by growing a shell of a different material around the NC. This material should have a larger bandgap than and a small lattice mismatch with the material of the core. There are three types of these core/shell nanoparticles: Type-I, Type-I<sup>1/2</sup> and Type II heteronanostructures (Fig 2). The difference between these types is the offset between the HOMO and LUMO of the two materials.

For Type I materials, the bandgap of the core lies within the bandgap of the shell material. Therefore the hole and electron are confined to the core and cannot get trapped by the surface states induced by dangling bonds at the outside of the shell. For Type-II materials, the HOMO of the core has a higher energy than that of the shell. The LUMO of the core has also a higher energy than the LUMO of the shell. As a result, the electron is confined to the shell and the hole to the core. This separation of the electron and hole results in nearly zero overlap between the wavefunctions. This results in NCs with new properties, for example longer exciton lifetimes [17]. For Type I<sup>1/2</sup> one charge carrier is delocalized over the entire crystal and the other charge carrier is confined to either the shell or the core.

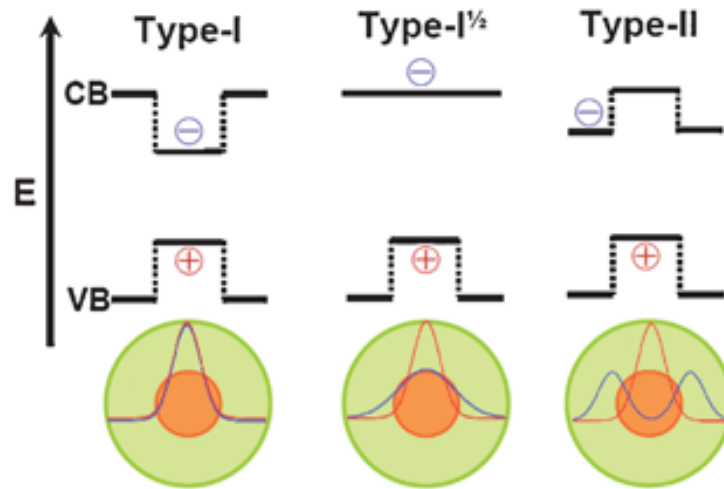


Figure 2: Schematic represent of the different types of heteronanostructures. The offsets between the conduction band (CB) and valence band (VB) of the core and shell for the different types are shown. The lower panel is a schematic representation of the ground-state wavefunctions of the electron (blue) and hole (red) in these NCs. Duplicated from ref.[11].

For passivation of the surface a Type-I shell is synthesised around the particle, because this reduces the trapping of the holes or electron thereby increasing the QY. A problem arising from certain shell materials is that the offset in energy between the two materials is not big enough. For example, the bottom of the conduction band (CB) of CdS is several meV above the CB of CdSe. In a CdSe/CdS core/shell NC the electrons are not confined to the core because of this small offset in energy. The wavefunction of the electron will delocalize into the shell. The electron can then still get trapped by surface

states if the shell is not thick enough.

Synthesizing a thicker shell is not a solution due to the increase of strain within the particle. A better candidate for a shell around a CdSe core would be ZnS, because it has a larger energy mismatch with the LUMO of the CdSe core. However, the lattice mismatch between ZnS and CdSe is too big, resulting in too much strain to successfully synthesize these shells. A solution was proposed by Xie et al [18]. They combined the advantages of both materials (CdS and ZnS) by using both of them. The shells were synthesized layer by layer, increasing the lattice mismatch and the bandgap step by step by gradually changing the ratio between cadmium and zinc. These particles can be made using the SILAR (Successive Ion Layer Adsorption and Reaction) method developed by Peng et al [19]. The QY of these multishell particles was found to be much higher than the QY of core-only particles and the synthesis of a multishell resulted in a higher particle stability as well.

## 2.5 Ion exchange

Ion exchange is a technique which is used to obtain otherwise difficult or even impossible to synthesize chemical compositions and shapes of nanoparticles (NP) [20]. With this technique, the cations or anions in a material are replaced with cations and anions of different elements. The shape of the previous particle is kept after the exchange reaction. Ion exchange is already used for many years for bulk crystals, but got increasingly interesting when exchange on NP turned out to be very efficient at ambient temperatures. The diffusion rate of ions in NCs is very high compared to bulk crystals, due to the larger surface area to volume ratio [21]. These properties make a complete exchange of the ions in a NC possible. Although successful anion exchange has been reported, it is harder to achieve, because anions are bigger than cations, making diffusion harder. During cation exchange, the anion framework stays intact and unaltered, thereby keeping the original shape of the starting material [22].

The exact mechanism for ion exchange is not known yet, but many synthesis conditions and reaction parameters which have an impact on it are known. To start, one of the most straightforward parameters is the solubility of the ions [23]. The solubility of the ion that needs to be extracted from the lattice should be higher than the solubility of ion that is incorporated. If this is not the case, raising the reaction temperature could still make exchange possible. The addition of specific ligands also has an influence, because these ligands can stabilize the extracted ions in solution. Which ligand should be used depends on the hardness of cations that need to be exchanged. Hard cations (hard acids) have a small atomic radius, high oxidation state and a low polarizability [23]. Hard acids bind with strong bases, and vice versa weak acids bind with weak bases. The appropriate ligands should be chosen, depending on the hardness of the incoming and outgoing cations, for the exchange reaction to be favourable. Other factors that influence ion exchange are the lattice energy difference of the starting material and product, the size of the NC, reaction temperature and the surface free energy of the NC facets.

### 3 Previous studies on CdSe nanoplatelets

The synthesis method for CdSe NPLs with a zinc blende structure was developed in 2008 [9]. Since then a lot of research has been performed on these platelets by the group of Dubertret and the group of Peng. Four different thicknesses of CdSe NPLs can be synthesised at this moment; platelets emitting at 395, 460, 510 and 550 nm [24]. The exact thickness of these platelets is debatable. The group of Dubertret assigns a thickness of 2, 3, 4 and 5 monolayers cadmium and selenium plus one addition cadmium layer to these platelets[25]. Our group measured that the platelets emitting at 460 nm are 4 cadmium ions thick and that a platelet contains an equal amount of selenium and cadmium [26]. This implies that there cannot be an extra cadmium layer and that the thickness of the platelets is 3, 4, 5, and 6 monolayers for platelets emitting at 395, 460, 510 and 550 nm respectively.

The complete mechanism for the formation of these platelets is not exactly known. It is known that the formation of NPLs start with the formation of small seeds and that the addition of an acetate salt is necessary for the 2D growth of the initially formed seeds [9]. The group of Dubertret did investigate whether the platelets were formed by self-assembly of seeds or if the seeds extend laterally by continuous reaction with the precursors (Fig. 3) [27]. For example, ultra-thin PbS films are also formed by reactive self-assembly (oriented attachment) of small elementary PbS crystal seeds [28]. These films have a patch-like structure. This patch-like structure is shown in figure 3 route 3; as can be seen, the original constituent nanocrystals can still be recognized in the final structure. This kind of structure is not observed for CdSe NPLs. Therefore it is unlikely that the CdSe NPLS are formed by this mechanism.

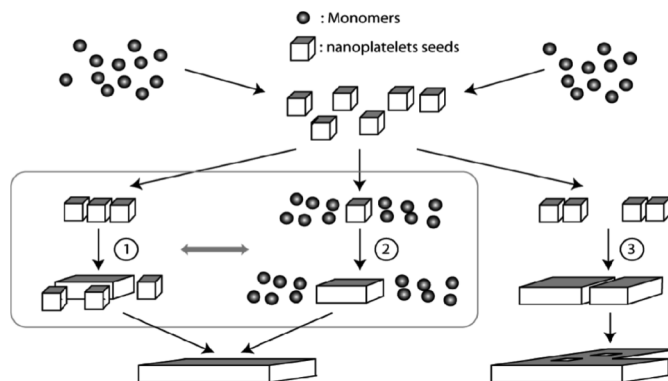


Figure 3: Possible mechanisms for the formation of CdSe NPLs. First small seeds of 2 nm are formed. These seeds could self assemble only at the seed level (route 1) or they can self assemble in patches (route 3). Patch 2 shows the formation of NPLs via a continuous reaction with the precursors. Duplicated from ref.[27].

Another type of assembly that is observed for the formation of NPLs is self-assembly of seeds, followed by recrystallisation. However, the absorption and emission spectra of samples taken during the reaction of CdSe NPLs shifts smoothly to higher wavelengths,

this indicates a continuous growth of the NPLs. A third option is that small clusters of CdSe could continuously attach to the already formed NPLs (Fig. 3, route 1) or the precursors directly react at the edges of the NPLs (Fig. 3, route 2). Which mechanism was most likely was investigated by slowly adding precursors to a mixture of NPLs. The NPLs grew in the lateral dimensions, but there were no small seeds visible on the TEM and also no features of small seeds in the absorption spectra. This strongly suggest that the platelets are formed by continuous reaction of the precursors [27].

The influence of the reaction temperature, ligands, precursor concentration and injection speed on the formation of NPLs was also discussed in the literature [29]. A higher reaction temperature results in NPLs with greater lateral dimensions, but if the temperature is too high (above 260 °C) other shapes of NCs start to form. Which ligands are used during the reaction is very important, as the ligands have an important role in ensuring the 2D growth of the NPLs. If ligands bind strongly to a facet, then the growth at this facet is slow or not possible. For the synthesis of platelets the reactivity along the polar axis is reduced [4]. During the synthesis of CdSe NPLs there are only ligands that bind with cations present. Therefore, it is assumed by the group of Dubertret that the top and bottom of the NPL are terminated with Cd ions. The group of Peng showed that if fatty amines are added during the reaction, they are not present in the sample after purification. This means that these ligands do not bind to the surface of the NPL. This supports the presence of an additional Cd-layer and that the negatively charged oleic acid ligands are needed to neutralize the charge of the NPLs [4].

Next to passivation of the polar facets to induce 2D growth, the addition of Se powder probably also induces 2D growth [4]. Selenium induces 2D growth because the reactivity of Se is low. Therefore the active monomer concentration is low. For growth in the direction of the polar axis, a high concentration of monomers is needed [30] [31].

When the precursors are injected fast the lateral dimensions of the NPLs are small. This is probably because a high concentration of seeds is formed. If the precursors are added slowly, very large NPLs are formed. These NPLs are referred to as nanosheets. The lateral dimensions of these nanosheets can be up to 700 nm [29]. Nanosheets emitting at 510 nm and 550 nm cannot directly be synthesized by the slow addition of precursors. Nanosheets emitting at these wavelength can only be made by using presynthesized 510NPLs or 550NPLs as seeds.

The thinnest nanosheets and NPLs have an addition feature, they tend to roll up to form helices and flower-like structures. The direction in which they fold ([110] direction) is always the same even if the shape of the platelet or nanosheet is not the same. An explanation for the formations of these scrolls could be the difference in alignment of the cadmium atoms at the bottom and top of the NPLs; the link between the cadmium atoms and the selenium atoms are rotated by 90 degrees (Supplementary Figure 1 ref. [29]). The ligands bound to these ions could introduce an asymmetric strain on the NP, inducing the formation of these scrolls [29].

After the development of the methods to synthesize CdSe NPLs with different thicknesses, it became interesting to see whether the same modification could be done on these platelets as for quantum dots or quantum rods. Therefore recently the synthesis

of heteronanoplatelets has been developed. Over the last two year the synthesis of CdS and CdZnS shells around these platelets was reported [32]. But also more exotic shells, like core/crown particles [33] and CdSe platelets with CdS wings are nowadays possible to synthesize [34]. A paper from 2014 by the group of Dubertret showed that CdSe/CdS platelets could be exchanged to ZnSe/ZnS and PbSe/PbS platelets reversibly [35]. Next to research on the modification of NPLs, also research was done on the optical properties of these platelets. As stated before, the absorption and emission spectra of the platelets have very sharp peaks. The QY of these platelets is high compared to other nanostructures and the lifetime at low temperature of these particles is very short. In figure 4 the decay curves of NPLs (red) and QDs (orange) are compared. This figure shows that the fluorescence lifetime of NPLs is shorter than the fluorescence lifetime of QDs. The decay curve of the NPLs is multiexponential at room temperature and single exponential at 6K [29]. Measurements were preformed on single CdSe NPLs, which showed that single NPLs have similar spectroscopic characteristics and lifetimes as an ensemble of NPLs [10]. Also some research has been done on decay pathways in these particles [36], but more research has to be done to get a better insight on these mechanisms.

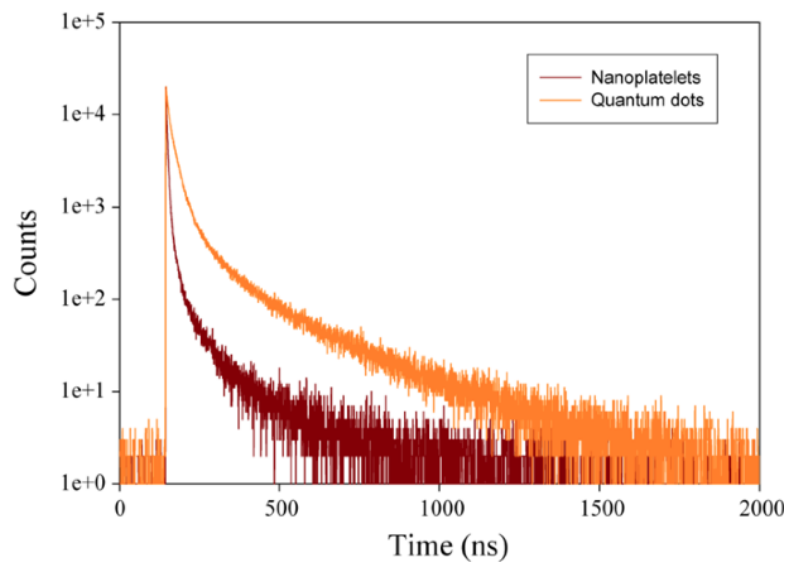


Figure 4: Comparison fluorescence lifetime of 550NPLs (red) and QDs (orange) at room temperature. Duplicated from ref.[24].

## 4 Experimental methods

### 4.1 Chemicals

Methanol (MeOH), ethanol (EtOH), butanol (BuOH), hexane, cyclohexane, toluene, tetrachloroethylene (all anhydrous, 99.8% pure) were obtained from Sigma-Aldrich. Cadmium-, cesium-, cobalt-, lead-, lithium-, magnesium and zinc acetate were also purchased from Sigma-Aldrich (all 99.999% pure on trace metal basis). Potassium-, and sodium acetate were purchased from Merck (99.999% pure on trace metal basis). Acetic acid (99.99%), bis(trimethylsilyl)sulfide (TMS<sub>2</sub>S, 98%), cadmium nitrate tetrahydrate (99.99%, trace metal basis), chlorobenzene (99.5 %), dimethyl sulfoxide (DMSO,  $\geq 99.99\%$ ), mercury(II)chloride (99.5%), octadecanol (ODA, 99%), 1-octadecene (ODE, 90%), oleic acid (OA, 90%), sodium myristate Cd(Myrist)<sub>2</sub>, sulfur (99.98, trace metal basis) and trioctylphosphine (TOP, 90%) were all obtained from Sigma-Aldrich. All chemicals were used without further purification. The acetate salts will be referred to in the text with X(Ac)<sub>2</sub> where X denotes Cd, Zn, Li, Na ect.

### 4.2 Synthesis of nanoplatelets

#### 4.2.1 Synthesis of 460NPLs

The thinnest platelets emitting at 460 nm were synthesised using a method described by Ithurria et al [27]. First, a mixture consisting out of 240 mg Cd(Ac)<sub>2</sub> (0.9 mmol), 15 mL ODE and 285  $\mu$ L OA (0.9 mmol) was degassed for 1 hour at 90 °C under vacuum at the schlenkline. The mixture was then heated to 170°C under N<sub>2</sub> flow. At 170°C 150  $\mu$ L 1 M TOPSe solution was injected. This solution was made by dissolving 0.79 g selenium (10 mmol) in 10 mL TOP. After the injection of the TOPSe the mixture turned yellow. The mixture was kept at 160°C for 50 minutes, no further change in colour was observed. After 50 minutes the mixture was quickly cooled down to room temperature using an air flow to cool the outside of the flask. The mixture was transferred to a nitrogen purged glovebox where 10 mL MeOH and 30 mL BuOH were added to the mixture. After centrifugation at 3000 rpm for 15 minutes, the supernatant was discarded and the precipitate was redispersed in 10 ml hexane. This washing step was repeated. If many dots were present in the obtained dispersion, as observed by TEM analysis, size selection precipitation was performed. This was done by adding MeOH drop-wise until the turbidity could not be shaken away manually. With this method the platelets precipitate during centrifugation, but the dots stay suspended in the supernatant.

#### 4.2.2 Preparation Cadmium myristate for synthesis 510NPLs and 550NPLs

For the synthesis of the platelets emitting at 510 nm and 550 nm a different Cd-precursor was used [27]. This precursor was made by dissolving 1.23 g Cadmium nitrate (5 mmol) in 40 mL MeOH and dissolving 3.13 g sodium myristate (12.5 mmol) in 250 mL MeOH. These two solutions were mixed and the precipitated cadmium myristate was obtained by filtrating the mixture. The product was dried overnight under vacuum.



#### 4.2.3 Synthesis of 510NPLs

The synthesis of 510NPLs was based on a method described by Ithurria [27]. To obtain 510NPLs, 170 mg Cd(Myristate)<sub>2</sub> (0.3 mmol), 12 mg Se (0.15 mmol) and 15 ml ODE were degassed at room temperature for one hour in a roundbottom flask connected to a schlenkline. After degassing, the mixture was transferred into a nitrogen purged glovebox and was heated. During heating the mixture became transparent and at 180°C the mixture started to turn yellow. When the mixture started to turn orange (around 190 °C), 55 mg Cd(Ac)<sub>2</sub> (0.20 mmol) was added. Due to the addition of the acetate salt the colour of the mixture started to turn red. The mixture was heated to 240 °C and was kept at this temperature for 5 minutes. After 5 minutes, the mixture was cooled down to room temperature by adding 14 mL Hexane. At 95 °C 1 mL OA was added. The mixture was washed using 10 mL MeOH and 30 mL BuOH and was centrifugated at 3000 rpm for 15 min. The sediment was dispersed in 4 mL Hexane.

#### 4.2.4 Preparation Se-precursor for synthesis 550NPLS

A solution of 79 mg selenium (10 mmol) in 30 mL ODE was sonicated and slowly added to 70 mL ODE, which was heated to 180 °C. After all the selenium was introduced, the mixture was heated at 220 °C for 30 min. A transparent solution with a molarity of 0.1 M was obtained [27].

#### 4.2.5 Synthesis of 550NPLs

The thickest platelets emitting at 550 nm were synthesized in a similar way as the 510NPLs [24]. After the degassing of the Cd(Myristate)<sub>2</sub>, Se and ODE, the mixture was heated to 240°C. During heating the colour of the mixture changed from grey to yellow to red. At 240 °C 1.5 mL 0.1 M Se in ODE was injected, 10 seconds after the injection 80 mg Cd(Ac)<sub>2</sub> (0.30 mmol) was added. The mixture turned dark red. After 10 minutes the reaction mixture was cooled down to room temperature by adding 14 mL Hexane. The mixture was washed using 10 mL MeOH and 30 mL BuOH and was centrifugated at 3000 rpm for 15 min. The sediment was dispersed in 4 mL Hexane.

### 4.3 Synthesis of heteronano-platelets

#### 4.3.1 Synthesis CdSe/CdS core/shell nano-platelets

The synthesis of a CdS shell around the NPLs was performed using a layer by layer method at room temperature described by Dubertret et al [32]. 1.2 mL of an undiluted CdSe NPL dispersion and 1.2 mL hexane were added to a vial. 50 µL bis-trimethylsilyl sulfide (TMS<sub>2</sub>S) was added while stirring. The mixture was stirred for one hour and washed with 1.5 mL EtOH and centrifuged at 3000 rpm. The precipitate was dispersed in 5 mL Hexane and 20 mg Cd(Ac)<sub>2</sub> was added. The mixture was sonicated for 20 min. 150 µL OA was added in order to prevent the aggregation of the NPLs. Before storing the sample, it was washed with 3 mL EtOH and redispersed in 4 mL hexane.

#### 4.3.2 Synthesis of CdS/Cd<sub>0.5</sub>Zn<sub>0.5</sub>S/ZnS multishell nanoplatelets using layer by layer method

The synthesis of a multishell around the NPLs was done using two methods. First the layer by layer method [32] was used. CdSe/CdS core/shell NPLs were used as starting material for the synthesis of multishells. The same steps were done as for the synthesis of the CdS shell, but instead of adding 20 mg Cd(Ac)<sub>2</sub> a mix of Cd(Ac)<sub>2</sub> and Zn(Ac)<sub>2</sub> was added for the second and third shell. For the last shell only Zn(Ac)<sub>2</sub> was added.

#### 4.3.3 Synthesis of CdS/Cd<sub>0.5</sub>Zn<sub>0.5</sub>S/ZnS multishell nanoplatelets using SILAR method

A second method to synthesize a multishell around the NPLs, makes uses of the SILAR method. The major advantage over the previous method is that it is a one-pot synthesis, which needs no purification steps.

For this synthesis method Cd, Zn and S-Precursor were made. These precursors were made by adding Cd(Ac)<sub>2</sub>, Zn(Ac)<sub>2</sub> or S to ODE, degassing the mixtures and heating them until a transparent solution was obtained. The concentration of all precursors was 0.1 M. A Cd/Zn-precursor can be made by mixing the Cd- and Zn-precursor 1 on 1.

During the first step, 1mL of CdSe/CdS NPLs, 1 g ODA and 3 mL ODE were combined. This mixture was heated to 150°C for half an hour to evaporate the hexane. After half an hour the mixture was heated to 230°C and 100 μL of S-Precursor was added dropwise. After 10 minutes 100 μL of Cd/Zn-precursor was added. These two steps were repeated after 10 minutes. For the last shell 100 μL S-precursor and 100 μL Zn-precursor were added, again waiting 10 minutes after every addition. This method is also preformed using oleyl amine in stead of ODA. Oleyl amine is a less strong coordinating ligand than ODA.

#### 4.4 Hg-Exchange

For the cadmium-to-mercury ion-exchange a method, developed by the group of Hens, was used [37]. For the exchange reaction 5 mL 15 μM CdSe QDs in toluene and 0.5 mL OLA were added to a vial and stirred. 100 μL 0.5 M HgCl<sub>2</sub> was added to the mixture. The mixture turned black in a few seconds. After 5 minutes, the reaction was quenched by adding 5 mL MeOH. The product was washed several times with MeOH and redispersed in toluene.

This method can be used for QDs with a diameter of 4.2 nm. For QDs with a different size, the amount of mercury precursor had to be calculated. This can be done by calculating the concentration of cadmium ions present with equation (6). The diameter and concentration of the QDs can be obtained by the position and intensity of the first excitonic transition in the optical absorption spectrum [38]. An equivalent amount of mercury ions compared to cadmium ions was added. The concentration of NPLs was not know. For the ion exchange reactions on NPLs 500 μL of NPL dispersion was used and the amount of Hg-precursor was varied between 10 μL and 100μL 0.5 M HgCl<sub>2</sub>.

$$[Cd^{2+}] = [QD]\rho\frac{\pi d^3}{6}\frac{1}{M}N_A \quad (6)$$

#### 4.5 Optical measurements

Absorption spectra were measured with a Perkin-Elmer Lambda 950 UV/VIS/NIR spectrophotometer. The emission spectra were recorded using an Edinburgh Instrument FLS920 with a 450 W Xenon Lamp as the excitation source and a Hamamatsu R928 photomultiplier (PMT) detector. The quantum yield was measured using this set-up and an integrating sphere. A 1% neutral density filter was used to measure the intensity of the excitation beam. The lifetime measurements were performed using a laser operating at 441 nm as excitation source and a hamamatsu R928 photomultiplier detector.

The TEM (Transmission electron microscopy) images were obtained with a FEI Technai-10 or FEI Technai-12 operating with an accelerating voltage of 100 or 120 kV. The TEM samples were made by casting a drop of sample on a copper grid coated with a polymer (Formvar) and carbon. The EDX measurement were performed using a FEI Tecnai20FEG instrument operating at 200kV equipped with a Gatan 694 CCD camera and a Fischione HAADF detector.

## 5 Results and Discussion

### 5.1 CdSe nanoplatelets

#### 5.1.1 Nanoplatelets emitting at 460 nm

460NPLs were successfully synthesized using the method described in the experimental method (Chapter 4). The TEM-images of these NPLs are shown in figure 5a and 5b. These thin NPLs tend to roll up and they also aggregate in small groups, forming flower-like structures, as can be seen on the TEM-image. In figure 5b one can see that one such flower-like particle consist out of many NPLs. The estimated size of the NPLs obtained from the TEM-image is 80 nm by 10 nm. The thickness of the synthesized NPLs can be deduced from the emission or absorption spectra. The absorption (black) and emission (red) spectra are shown in figure 6. The peaks at 430 nm and 460 nm in the absorption spectrum are the electron-light hole and electron-heavy hole transitions respectively. The peaks at higher energies are not assigned yet to a particular electronic transition. The emission spectrum gives a clear indication whether there is only one population of NPLs present in the solution, because the emission maxima for the different populations are about 50 nm apart. This emission spectrum has only one peak at 460 nm, meaning that only the thinnest NPLs have been synthesized. A small shoulder is visible at 455 nm, this is probably emission of QDs which could still be present in the sample. These thin NPLs also have a broad trap emission peak from 550 nm to 750 nm (not shown).

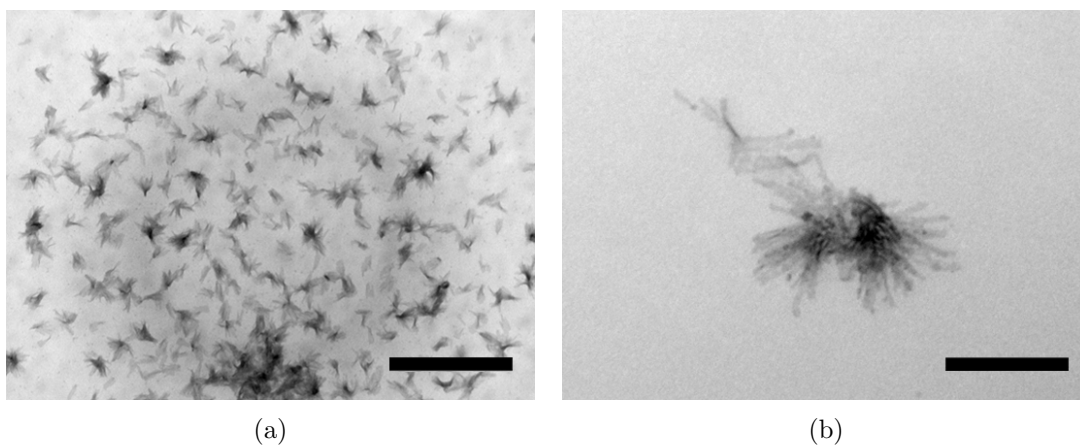


Figure 5: TEM-images of 460NPLs. (a) NPLs tend to aggregate in small groups, forming a flower-like structure. Scale bar 500 nm.(b) Zoomed in image of one flower-like structure. One flower-like structure exist out of many NPLs which are rolled up and folded. Scale bar 100 nm.

#### 5.1.2 Nanoplatelets emitting at 510 nm

510NPLs were synthesized using the method described in the chapter 4. During the synthesis samples were taken to follow the growth of the particles. The TEM-images of these samples are shown in figure 7. The first sample was taken at 185°C, when

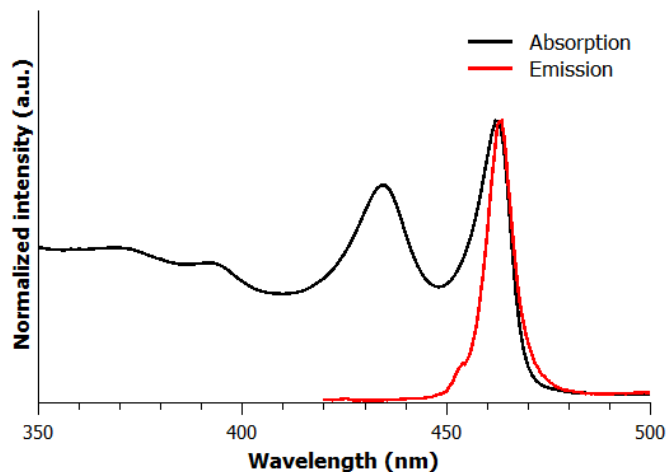


Figure 6: Absorption (black) and emission (red) spectra of 460NPLs. The heavy hole and light hole transitions are visible in the absorption spectrum at 460 nm and 430 nm respectively. The emission spectrum shows the emission of 460NPLs at 460 nm and probably the emission of QDs at 455 nm.

the mixture of Cd(myristate)<sub>2</sub>, Se and ODE started to turn yellow. The TEM-image of this sample is shown in 7a. The picture shows that small seeds of 2 nm had formed at this temperature. The second sample was taken just after the addition of cadmium acetate (Fig 7b). There were still only seeds visible, but when the temperature was increased to 240 °C NPLs started to form (Fig 7c). These NPLs had grown during the 5 minutes of reaction time at 240 °C (Fig 7d) and finally resulted in the product shown in fig 7e.

The growth of the NPLs can also be followed optically by measuring the absorption spectra of the samples. These spectra are shown in figure 8. The absorption spectrum at 185 °C (8, black) has a broad peak at 445 nm which can be assigned to the absorption of the small seeds present in the sample. Directly after the addition of the acetate salt, the peak had shifted to 500 nm (Fig. 8, red). This indicates that the seeds had grown, but the peak was still broad meaning that NPLs had not been formed yet. When the temperature was raised to 240°C a narrow peak started to appear at 510 nm in the absorption spectrum indicating the formation of 510NPLs (8, light blue). The absorption spectra (Fig 8, blue and green) taken during the 5 minutes at 240°C have the same shape as the spectrum of the previous sample. This is because the lateral dimensions of the NPLs were larger than the confinement regime. More growth would therefore not induce a shift of the absorption peak to lower energies.

The absorption and emission spectrum of the final product are shown in figure 9. In the absorption spectrum, the heavy and light hole transitions to the conduction band are visible at 510 nm and 480 nm respectively. The emission spectrum has a peak at 510 nm which is the emission of the 510NPLs. There is also a peak visible with a very low intensity at 460 nm. This peak indicates that there is a low concentration of 460NPLs present in the sample.

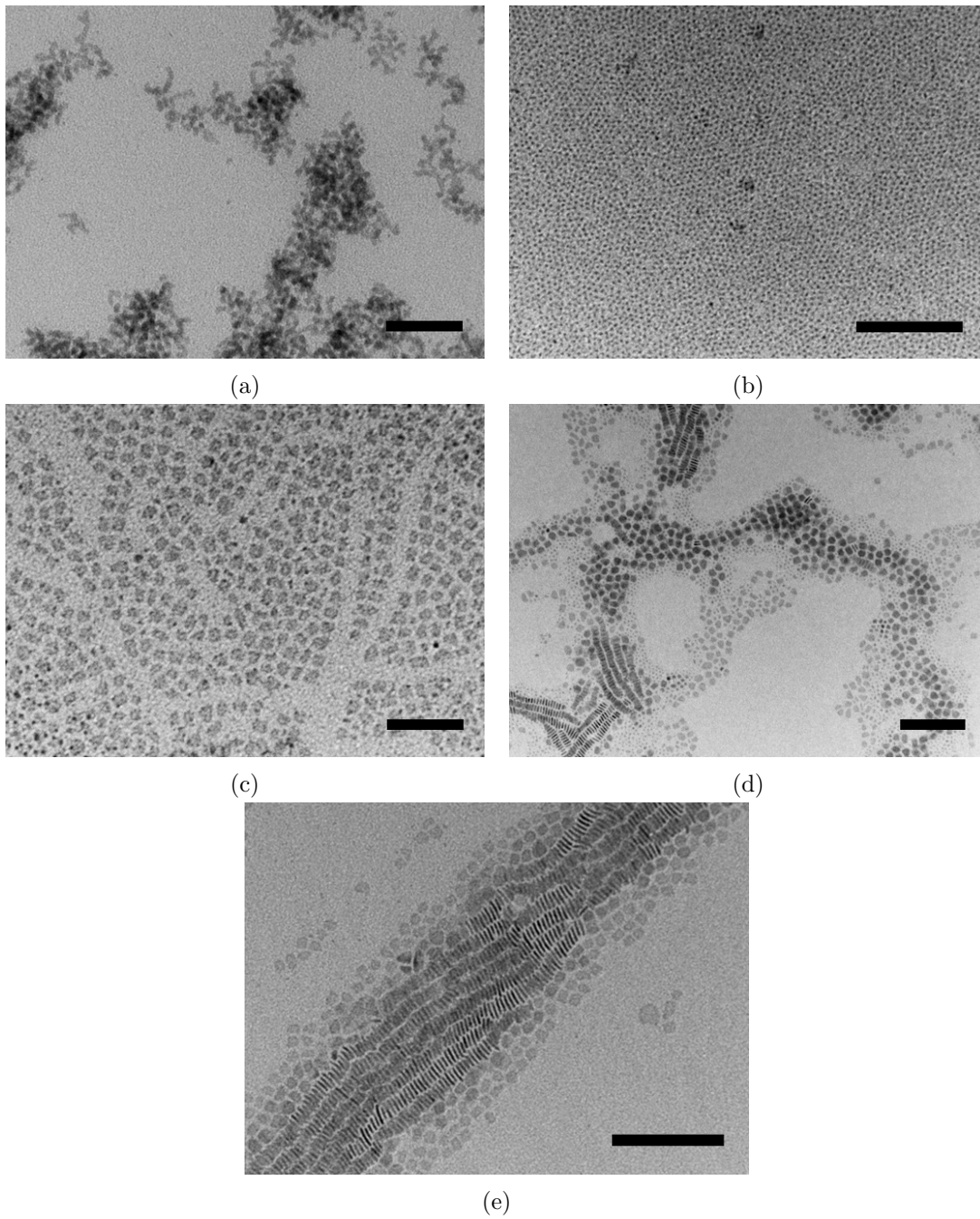


Figure 7: TEM pictures of samples taken during the synthesis of 510NPLs. (a) At 190°C, scale bar 50 nm. (b) Directly after addition  $\text{Cd}(\text{Ac})_2$ , scale bar 100 nm. (c) At 240°C, scale bar 50 nm. (d) After 2 minutes at 240°C, scale bar 100 nm. (e) Final product, scale bar 100 nm.

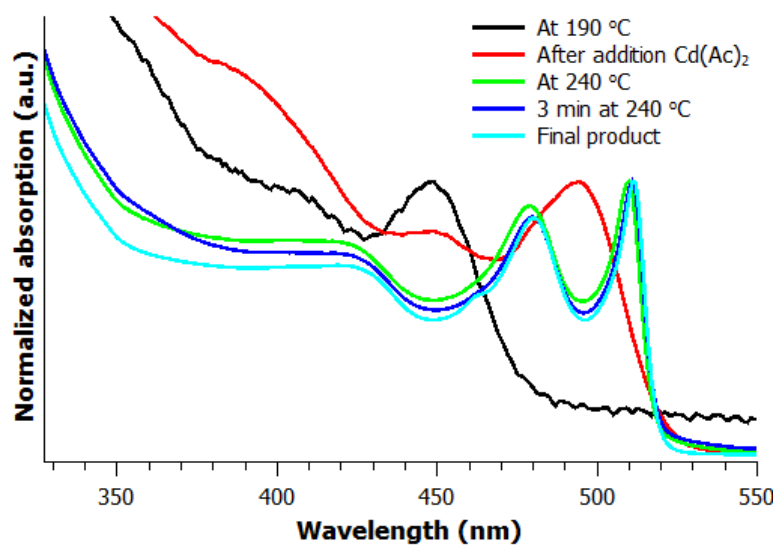


Figure 8: Absorption spectra of samples taken during the synthesis of 510NPLs. At 190°C (black), after the addition of the acetate salt (red), at 240°C (light blue), after 2 minutes at 240°C (green) and the final product (blue).

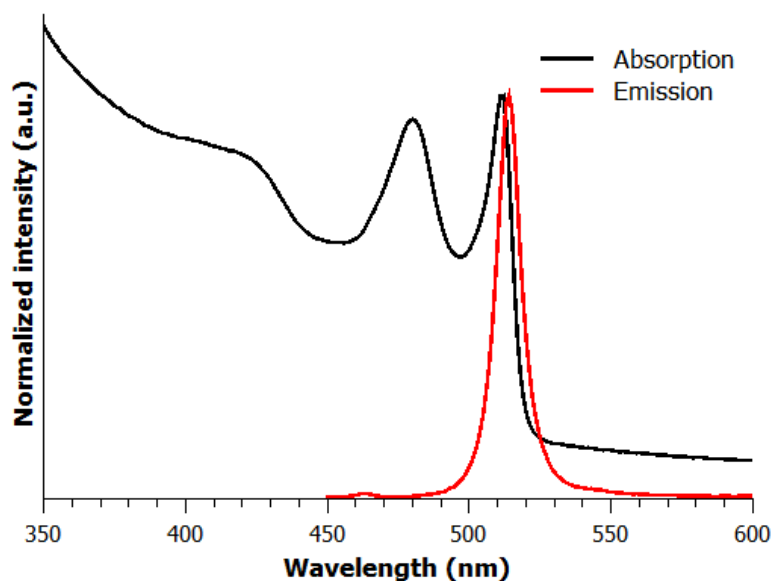


Figure 9: Absorption (black) and emission (red) spectra of 510 NPLs. The heavy and light hole transition are visible in the absorption spectrum at 480 and 510 nm respectively. The emission of the 510NPLs is visible at 510 nm as well as the emission of 460NPLs at 460 nm.

### 5.1.3 Nanoplatelets emitting at 550 nm

The synthesis of the 550NPLs was performed as described in the experimental section (Chapter 4). Samples were taken during this synthesis. The TEM-images are shown in figure 10. The first sample was taken at 190°C, when the mixture of Cd(myristate)<sub>2</sub>, Se and ODE was yellow. There are again only 2 nm seeds visible on the TEM-image (Fig 10a). When the temperature was raised to 240°C, some NPLs had formed (fig 10b). At 240°C Se dispersed in ODE was injected into the reaction mixture followed by the addition of Cd(Ac)<sub>2</sub>. During these steps no significant changes were observed on the TEM-images. The TEM-images of these samples are similar compared to figure 10b. After 3 minutes at 240°C the formation of NPLs was clearly visible (fig 10c). These NPLs grow during the 10 minutes at 240°C resulting in the product shown in figure 10d.

The absorption spectra of all the samples were measured. The spectra are shown in figure 11. The black graph is the absorption spectrum of the sample taken at 190°C. A broad peak at 470 nm is visible, which indicates the formation of seeds. When the temperature is raised to 240°C these seeds have grown significantly, as can be seen from the red-shift of 60 nm of the peak in the absorption spectrum (Fig.11, red). The samples taken directly after the injection of the Se and addition of Cd(Ac)<sub>2</sub> still have an absorption spectrum with a broad peak (Fig.11, green and blue), which means that the concentration of the NPLs seen on the TEM-images is very low. Because of the low concentration the narrow emission features of the NPLs can not be seen in these spectra. The position of the peak in these spectra only shifted 4 nm per sample, indicating that the dots did not grow much. After 3 minutes at 240°C the absorption spectrum had changed a lot. A sharp peak at 510 nm is visible, so NPLs which are one monolayer thinner than the 550NPLs were synthesised. There is a broader peak visible at 545 nm. This could be emission of seeds still present in the sample. The samples taken at 3 minutes, 6 minutes and the final product all had the same absorption spectrum. If the formation of 550NPLs was successful a sharp peak at 550 nm should be visible, but it is not observed.

It was not possible to take samples during the synthesis and obtaining NPLs emitting at 550 nm. Apparently the reaction is disturbed too much when samples are taken. The synthesis of the thickest platelets appears less reproducible and robust than the synthesis of the 460NPLs and 510NPLs. In most experiments a mixture of two populations of NPLs are formed during the synthesis of the 550NPLs. If the ratio is favourable toward the 550NPLs, size selective precipitation can be performed to obtain the 550NPLs. The absorption and emission spectrum of 550NPLs after size selective precipitation are shown in figure 12. There is still a small amount of 510NPLs present in this sample.

### 5.1.4 Conclusion and outlook

The synthesis of 460NPLs, 510NPLs and 550NPLs can be reproduced using the method described by Dubertret et al. However, the ability to get only one population, i.e. one thickness, of platelets seems to be less robust and reproducible, especially during the synthesis of the 550NPLs.



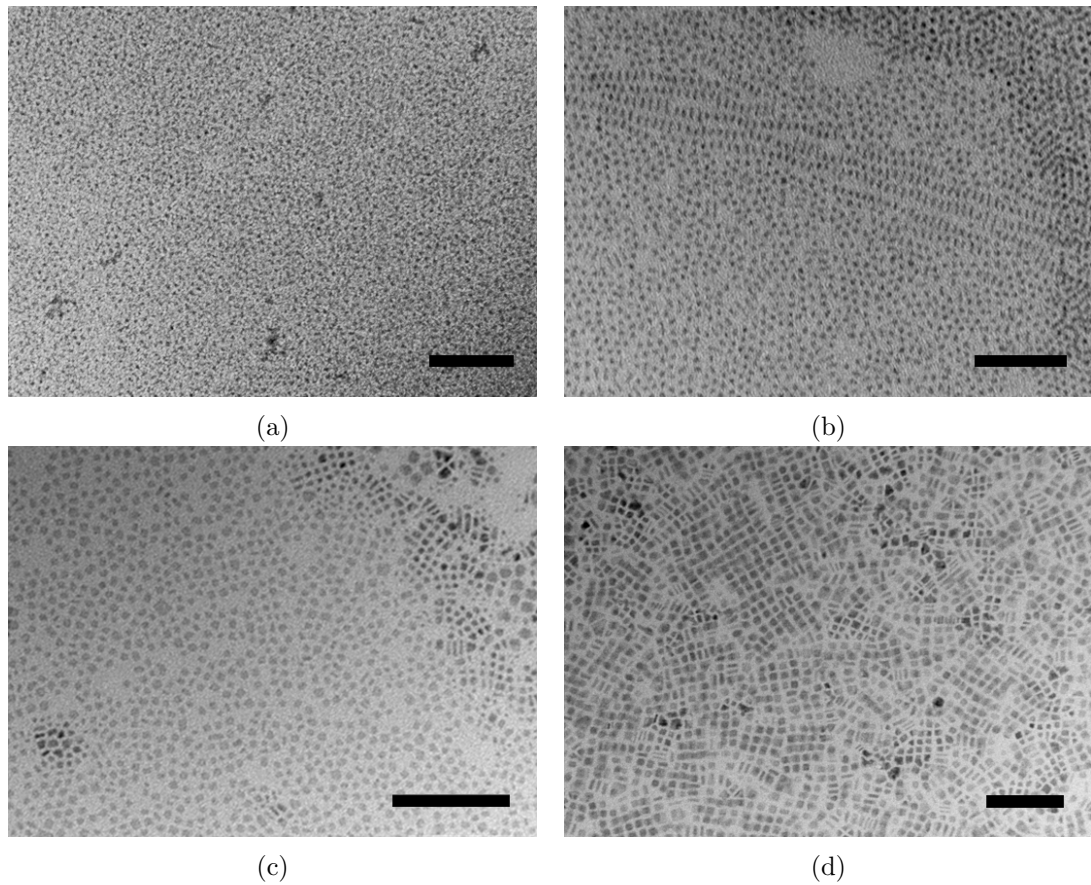


Figure 10: TEM-images of samples taken during the synthesis of 550NPLs. (a) At 190°C, scale bar 50 nm. (b) After raising the temperature to 240°C, scale bar 50 nm. (c) After 3 minutes at 240°C, scale bar 100 nm. (d) Final product, scale bar 100 nm.

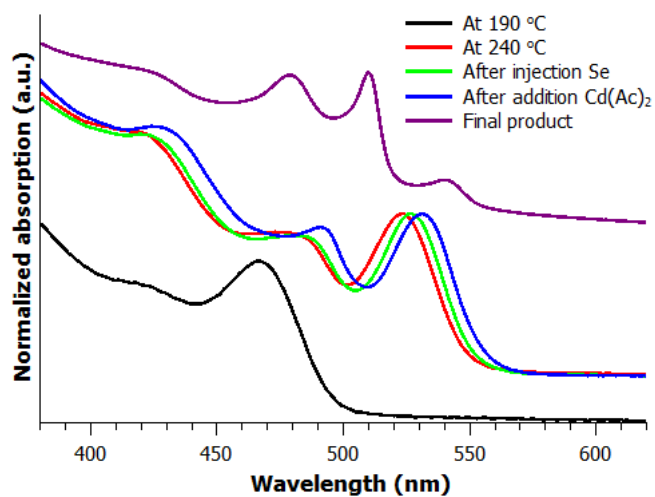


Figure 11: Absorption spectra of samples taken during synthesis of NPLs emitting at 550 nm. At 190 °C (black), at 240 °C (red), after the injection of Se (green) and after the addition of Cd(Ac)<sub>2</sub> (blue).

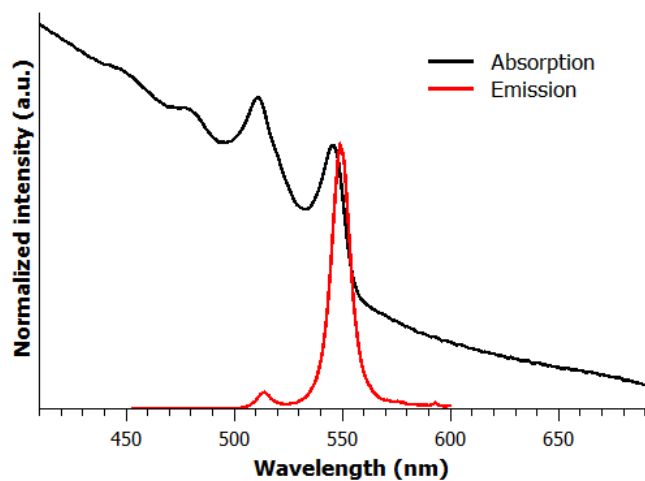


Figure 12: Absorption spectrum (black) and emission spectrum (red) of 550NPLs after size selective precipitation.

## 5.2 Heteronanoplatelets

### 5.2.1 CdSe/CdS core/shell nanoplatelets

A CdS shell was synthesized around CdSe NPLs as described in the experimental methods (Chapter 4). In figure 13a and 13b TEM-images are shown of these core/shell NPLs. Figure 13a is a TEM-image of 460NPLs with a CdS shell. These NPLs lay flat on the TEM-grid. Before the synthesis of the shell these NPLs tend to fold (fig 5a), but with the CdS shell around them they unfold. An explanation for this unfolding is that the core/shell NPLs are two monolayers thicker than the bare platelets, which makes them less flexible.

Figure 13c shows the absorption (black) and the emission (red) spectrum of the 460NPLs with a CdS shell. The emission and absorption maxima of the core/shell NPLs have a large red shift of about 90 nm compared to the emission and absorption maxima of the bare NPLs. The red-shift is due to the increase in thickness of the NPL; the core/shell particles are two monolayers CdS thicker.

CdS shell were also synthesized around the 510NPLs and 550NPLs. The absorption and emission spectra of these particles also have a large red-shift compared to the bare NPLs. 550NPLs with a CdS shell are shown in figure 13b.

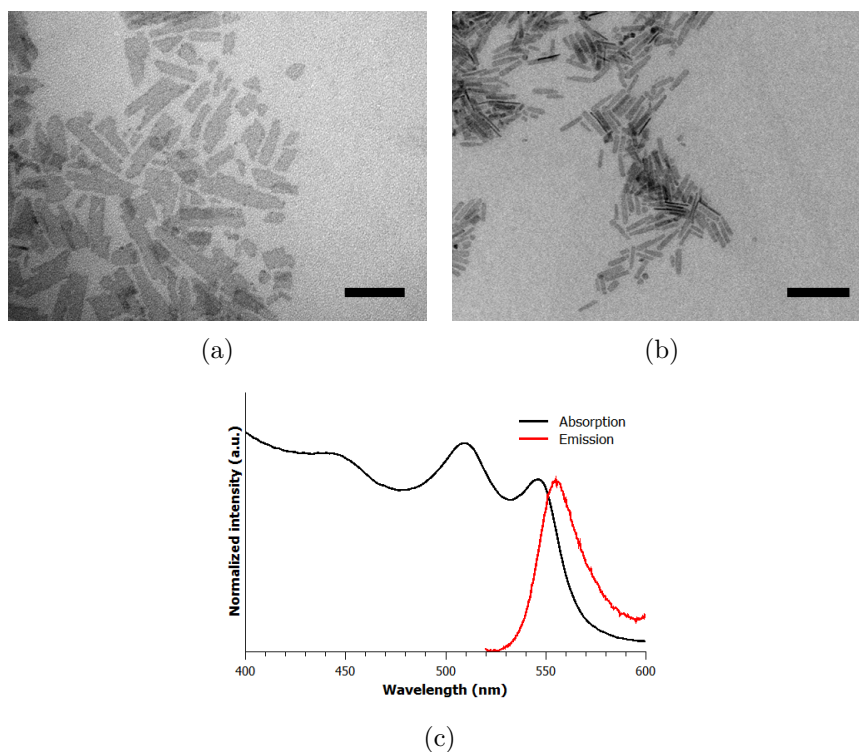


Figure 13: TEM-images of NPLs with shell (a) 460NPLs with a CdS shell (scale bar 50 nm) (b) 550NPLs with a CdS shell (scale bar 100 nm). (c) Absorption (black) and emission (red) spectra of 460NPLs with CdS shell.

### 5.2.2 Nanoplatelets with multishell

The luminescence QY and stability of the NPLs can be increased by synthesizing a multishell around the NPLs. Due to the CdS/Cd<sub>0.5</sub>Zn<sub>0.5</sub>S/ZnS multishell the electron and hole are confined to the core, which reduces the trapping by defects at the surface. The first method used to synthesize these multishells was the layer by layer method described in the experimental methods. The NPLs obtained with this method are shown in figure 14. There are NPLs visible on the TEM-image, but the absorption spectrum of these NPLs has no clear absorption peaks (fig15a). The thickness of the NPLs is probably not uniform, resulting in very broad peaks in the absorption spectrum. In the emission spectrum multiple peaks are visible, but only one is expected. Furthermore, the intensity of the peaks is very low. The multiple peaks in the emission spectrum could be due to background noise.

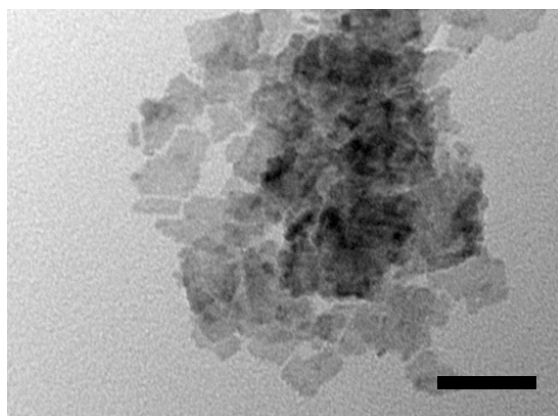


Figure 14: 460NPLs with multishell synthesized using layer by layer method. Scale bar 50 nm

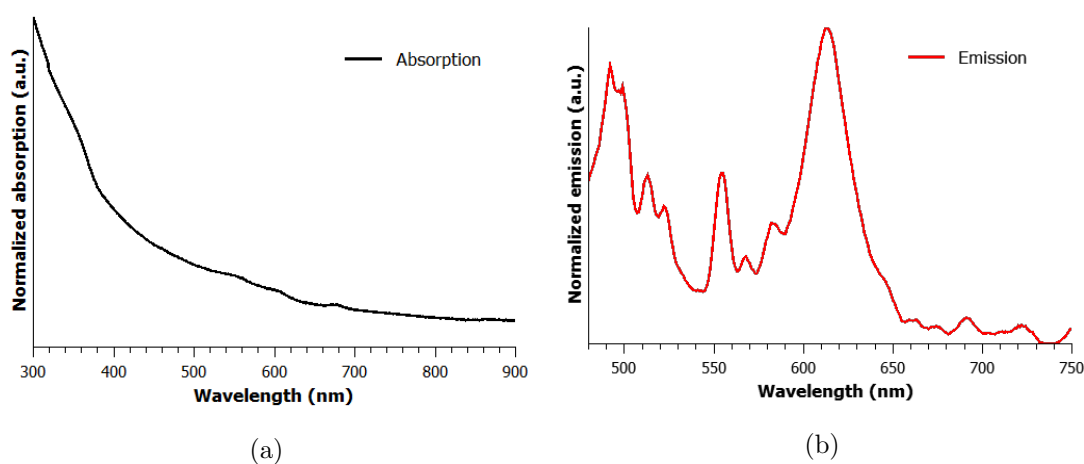


Figure 15: Absorption (a) and emission (b) spectrum of 460NPLs with a multishell synthesised with the layer by layer method.

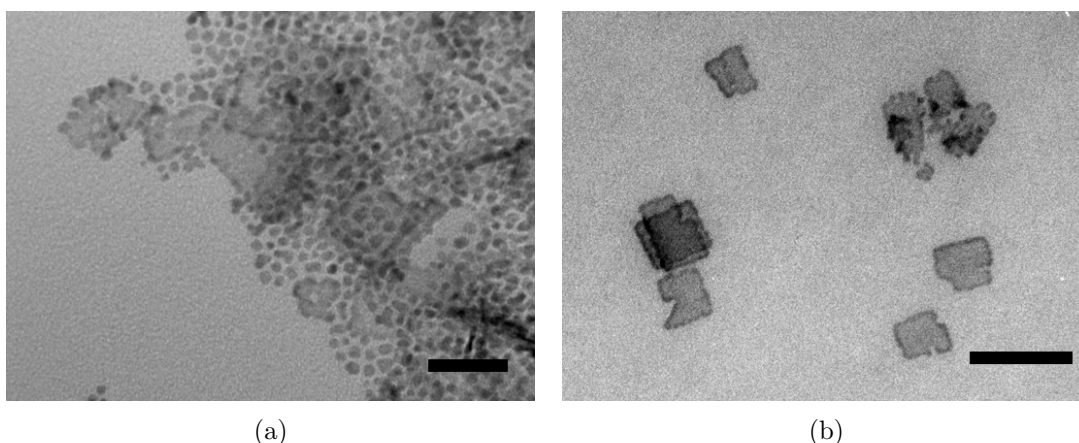


Figure 16: TEM-images of 460NPLs with a multishell synthesized using the SILAR method with adding: (a) octadecanol (scale bar 50 nm) and (b) oleyl amine (scale bar 100 nm).

The layer by layer method was not successful for obtaining NPLs with a stronger emission. A different shell growing method, the SILAR method, was therefore utilized. The TEM-image of the particles obtained with this method are shown in figure 16a. On this image some NPLs can be seen, but also many small particles. These smaller particles are probably synthesized due to secondary nucleation. To reduce the secondary nucleation oleyl amine was added instead of octadecanol. Oleyl amine is a less strong coordinating ligand, which ensures that the secondary nucleation of particles is suppressed. As can be seen in figure 16b no secondary nucleation is observed when oleyl amine is used as coordinating ligand.

The absorption spectrum of these NPLs, shown in figure 17 (black), has again no clear absorption peaks. The emission of these multishells is low compared to the emission of bare NPLs, but is higher than the emission of the multishells made with the layer by layer method. There is one emission peak visible in the emission spectrum (Fig 17, red). The peak is less sharp than the emission of bare NPLs, which could be explained by some thickness variation between the NPLs.

As can be observed from the TEM-images (Fig. 16a and 16b), both adding octadecanol and oleyl amine results in NPLs with a darker edge compared to the centre of the NPLs. To investigate to origin of the darker edge, a High-Angle Annular Dark-Field Scanning TEM (HAADF-STEM) was used. The results are shown in figure 18a and 18b. These images also show that the edge is different than the center of the particle. The edge is brighter than the center. The intensity in HAADF-STEM scales with the atomic number squared and the thickness of the material. The brightness cannot be due to more incorporation of zinc at the edge, because zinc has a lower atomic number than cadmium and would therefore appear less bright on the TEM-image.

To investigate if this intensity difference is due to the distribution of the elements or due to a thickness difference, electron energy loss spectroscopy (EELS) was performed on the multishell NPLs. The elemental maps obtained with these measurements are

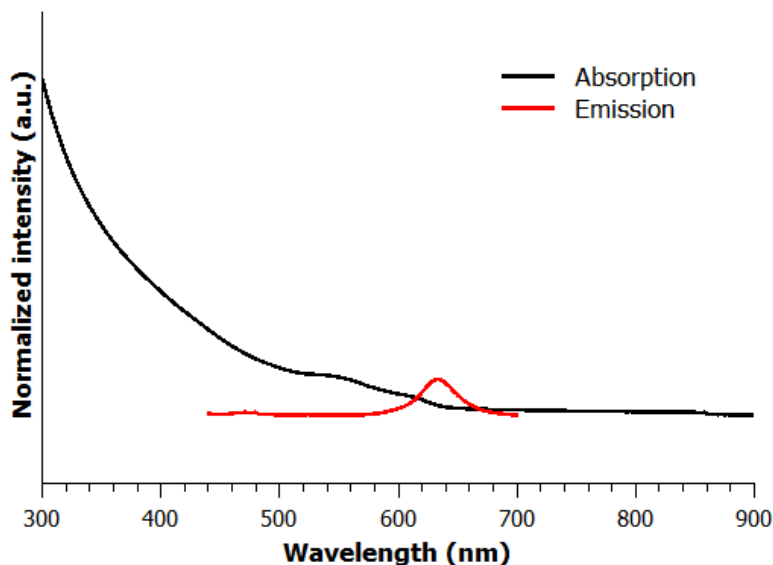


Figure 17: Absorption (black) and emission (red) spectra of 460NPLs with a multishell synthesized using the SILAR method with oleyl amine as coordinating ligand.

show in figure 19. In 19a and 19b images are shown of the NPLs before and after the measurements. The green rectangle indicates the scanned region for the measurements. 19c-19f are the elemental maps of Cd, Zn, S and Se. The measurements show that Zn and Se are homogeneously distributed in the NPL. Cd and S are more concentrated at the edges of the NPL.

The EELS signal could also be used to examine the topography of the NPLs. The results are shown in figure 20. Figure 20a is a STEM-image of multishell NPLs. The scanning area is indicated by the green rectangular. 20b-20d show the topography of the NPL obtained with low loss EELS. The thickness varies between 0.52 nm and 3.34 nm in this measurement. A second measurement on a different NPL had a variation of 0.73 nm to 4.32 nm as result. Considering that one monolayer of CdSe has a thickness of 0.3 nm, this is a significant difference. A thickness of 0.52 nm and 0.73 nm is also thinner than the thickness of the starting material (460NPLs), which has a thickness of 0.9 nm. The reduced thickness could be due to beam damage.

The EELS mapping and the electron tomography results show that the brighter intensity at the edge is mainly due to a difference in thickness. The amount of Zn and Se is constant and does not depend on the thickness of the NPL. The amount of Cd and S are dependent on the thickness of the NPL, an excess of these materials is located at the edge of the NPL. An explanation for this observation is not yet known. A similar observation was reported in literature for a slightly different system where a CdS shell was continuously grown around a CdSe NPL [32]. These particles also had a darker and irregular edge on the TEM-image. Because the formation of a thicker edge is also

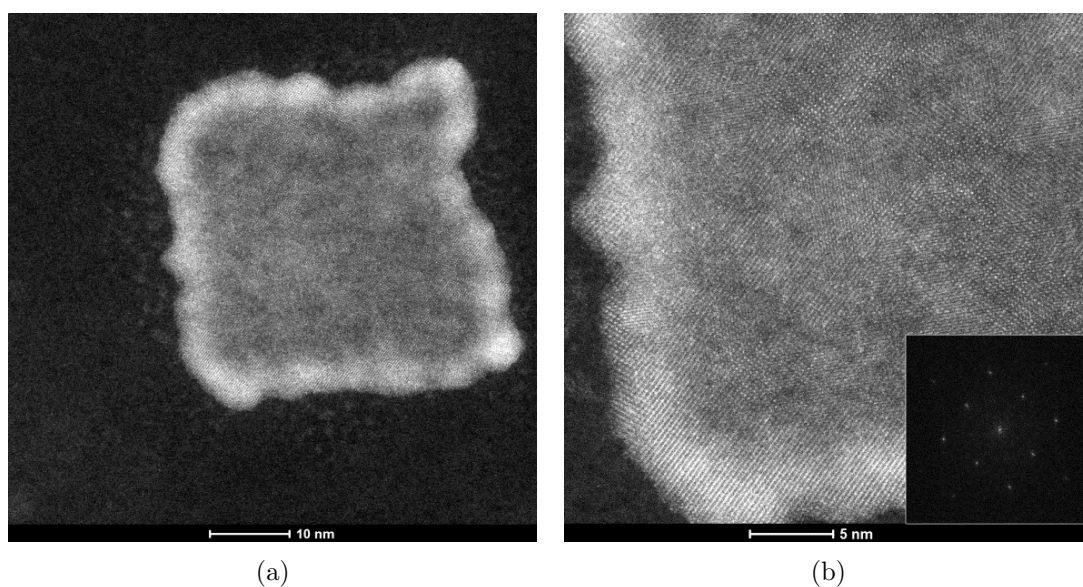


Figure 18: HAADF-STEM images of 460NPLs with a multishells synthesized using SILAR method with oleyl amine. The inset gives the Fast-Fourier-Transform (FFT) of figure (b), indicating that the top facet of the NPL is perpendicular to the [001] direction and that the diagonals of the squared NPL correspond to the  $\langle 001 \rangle$  direction.

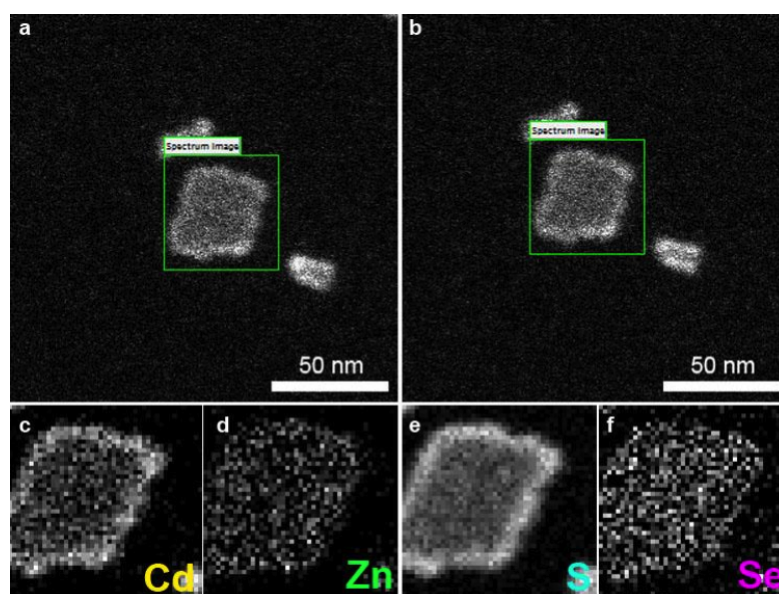


Figure 19: EELS mapping at 80kV of multishell NPLs synthesized with SILAR method using oleyl amine as coordination ligand. (a) and (b) are the images of the NPLs before and after the measurements. The green rectangle indicates the scanned region. (c)-(f) are the elemental maps of Cd, Zn, S and Se respectively.

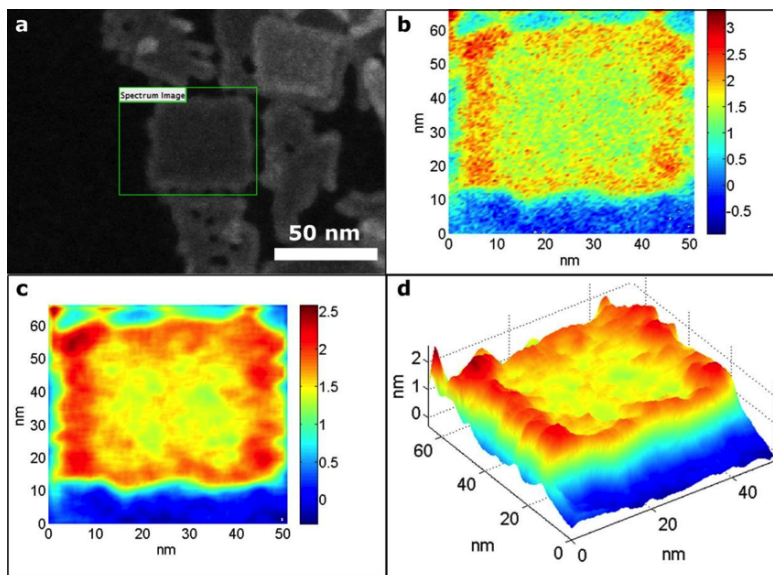


Figure 20: (a) STEM-image of multishell NPL measured on. Green rectangle indicates the selected NPL. (b)-(d) topography using low loss EELS. The estimated thickness of the NPL varies from 0.52 to 3.34.

observed for a CdS shell, the lattice mismatch apparently is not causing this effect. A possible explanation for the observation given in the paper is that the shell grows with a wurtzite or a polytypic structure in the presence of primary amines. This is also observed for CdSe/CdS QDs [39]. However, the thicker edge is also observed in our experiments when octadecanol is added as coordination ligand. Therefore the presence of primary amines cannot explain the observations.

The 460NPLs used as starting material for the synthesis of the multishells were more aggregated than the 460NPLs shown in figure 5. Furthermore, the Fast-Fourier-Transform of the STEM image in figure 18b shows that the diagonals of the squared platelets correspond to the  $\langle 100 \rangle$  direction. The growth direction of 510NPLs and 550NPLs is  $45^\circ$  rotated compared to these NPLs [27]. The growth direction of the flower-like NPLs in figure 5 was not determined, but research on nanosheets emitting at 460 nm showed that the growth direction of these nanosheets depends on the concentration of the Se-precursor (TOPSe) [29]. This precursor was also used for the synthesis of the 460NPLs. It is therefore possible that the 460NPLs used here have a different growth direction compared to the flower-like 460NPLs, which influences the growth of the multishell. Performing the multishell synthesis on a flower-like 460NPLs, 510NPLs and 550 NPLs, also resulted in the formation of an edge with a different contrast (Fig. 21). Therefore it can be concluded that the growth direction and the thickness of the NPL have no influence on the formation of the thicker shell. When 510NPLs and 550NPLs were used, secondary nucleation was observed even though oleyl amine was used as coordinating ligand. It could be that the concentration of precursor was too high, making secondary nucleation possible even with the addition of oleyl amine.



For further research the amount of precursor added during the synthesis of the multishell NPLs should be lowered to investigate if this results in a multishell NPL without a thicker edge. It could be that the amount of precursor added is too high and therefore continuous growth takes place instead of layer by layer growth. As stated before, continuous growth of a CdS shell also resulted in a thicker edge around the particle.

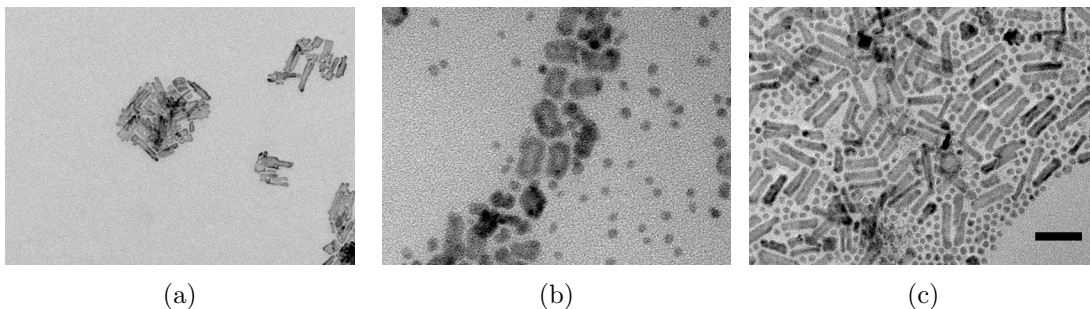


Figure 21: TEM-images of multishell NPLs using the SILAR method with oleyl amine as coordination ligand. Multishells were synthesized on (a) flower-like 460NPLs, (b) 510NPLs and (c) 550NPLs (scale bar 50 nm). Scale of (a) and (b) is not known.

### 5.2.3 Conclusion and outlook

The synthesis of CdSe/CdS core/shell NPLs using the layer by layer method was not successful. Both the layer by layer method and the SILAR method did not result in NPLs with a stronger emission. When using the SILAR method, oleyl amine needs to be used to prevent secondary nucleation, because it is a less strong coordination ligand than octadecanol. The NPLs with multishell had a darker edge on the TEM-images for both using octadecanol or oleyl amine. EELS measurements indicated that a thicker edge had formed around the NPL and that an excess of Cd and S was present at the edge. Zn and Se was homogeneously distributed in the NPLs. When using thicker NPLs and NPLs with a different growth direction, the formation of a thicker shell was still observed. Also comparing the observations with experiments reported in literature did not result in an explanation. For further research the concentration of the precursor added during the growth of the multishells could be varied to investigate if this has an influence on the formation of the thicker edge.

### 5.3 Cadmium-to-mercury ion exchange

To obtain HgSe NPLs, cadmium-to-mercury ion exchange was performed on CdSe NPLs. HgSe nanoparticles are topological insulators; materials that have conductive surface states, but do not conduct in the bulk of the material. This property makes these materials very interesting for all kinds of applications. A method to exchange CdSe QD to HgSe QD was developed by the group of Hens [37]. This method is described in the experimental methods (Chapter 4). 70% of the Cd ions are exchanged to Hg with this method. In this section the reproducibility of these experiments will be discussed as well as the exchange on NPLs and QDs with a multishell.

#### 5.3.1 Cadmium-to-mercury ion exchange on CdSe QDs

The first problem encountered was that the CdSe QDs used in our experiments were smaller than the QDs used by the group of Hens. Therefore different amounts of mercury precursor were added. When the mercury precursor was added the mixture turned black within a couple of seconds. This black mixture was not stable; the particles precipitated over time. Figure 22a to 22c are the TEM-images of experiments where 100 $\mu$ L, 40  $\mu$ L and 10 $\mu$ L mercury precursor was added. No dots are visible on the TEM-images, only clustered particles. In figure 22a big black spots are visible, that vanish during measurements with the TEM. This was probably mercury that was evaporating, due to local heating by the electron beam. There is also a white haze over the TEM-image, probably due to an excess of HgCl<sub>2</sub>. If 10  $\mu$ L mercury precursor is added, no big black spots are visible and also less white haze is observed. The dispersions are also not entirely black, but have a more red-black color. Less particle clustering is also observed in the sample where only 10  $\mu$ L mercury precursor was added, but no stable dispersion was obtained.

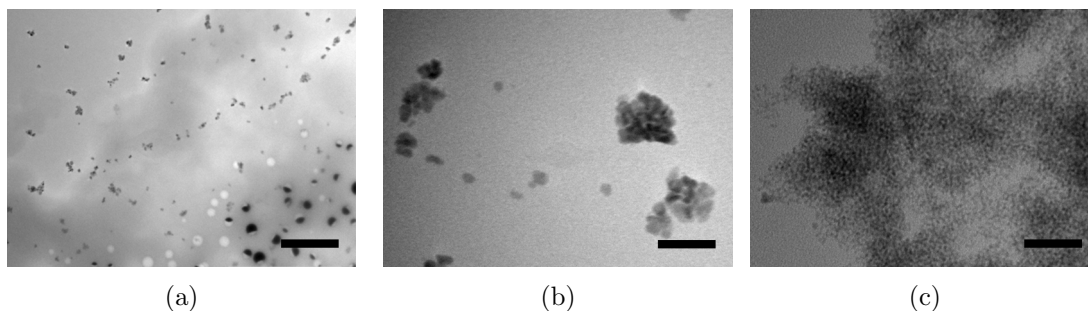


Figure 22: TEM-images of cadmium-to-mercury exchange reaction on CdSe QDs when adding (a) 100 $\mu$ L (scale bar 500 nm), (b) 40  $\mu$ L (scale bar 50 nm) and (c) 10 $\mu$ L mercury precursor (scale bar 50 nm).

The light sensitivity of the mercury precursor was investigated, because the results obtained by the group of Hens could not be reproduced. HgCl<sub>2</sub> is light sensitive, this is not mentioned in the thesis where the cadmium-to-mercury ion exchange is described [37]. Therefore the actual concentration of HgCl<sub>2</sub> could be less than claimed if the precursor was exposed to light. For the light sensitivity experiment, a vial with mercury precursor

was exposed to light for three days (precursor A). The second  $\text{HgCl}_2$  solution (precursor B) was made shortly before the exchange was performed. For these experiments the amount of  $\text{HgCl}_2$  that should be added to obtain solutions with a ratio between mercury and cadmium of 0.5:1, 1:1 and 2:1 were calculated, which is described in the experimental method. In the experiments by the group of Hens one equivalent of Hg ions compared to Cd ions was added.

The addition of precursor A and precursor B did both not result in the formation of stable dispersions; all particles precipitated over time. The absorption spectra are shown in figure 23 for the synthesis where a half equivalent (red and green) and one equivalent (light blue and blue) mercury were added. There is a difference in the shape of the absorption spectra if more mercury precursor is added, but there is no difference in the absorption spectra for added precursor A or B. Exposure to light for 3 days does not influence the concentration of the precursor.

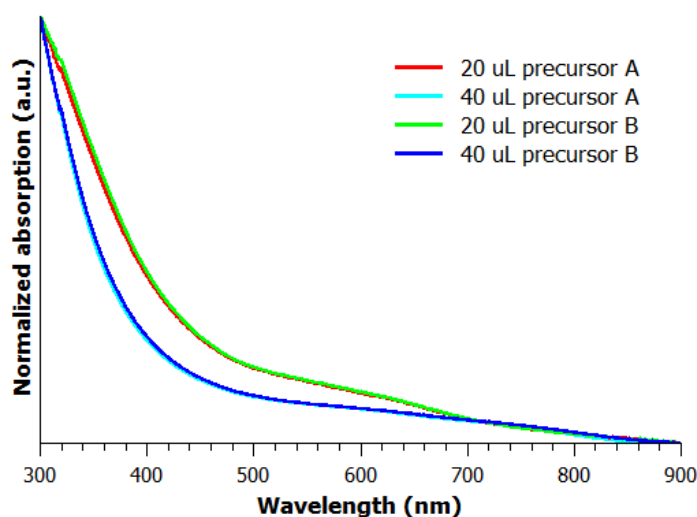


Figure 23: Absorption spectra of CdSe QDs treated with a precursor that was exposed to light (precursor A) and not exposed to light (precursor B). 20 and 40  $\mu\text{L}$  precursor was added, which corresponds to 0.5 and 1 equivalent of mercury compared to cadmium.

Another explanation why the exchange was not successful could be that the ligands on the QD disturb the reaction. The QDs used by the group of Hens are passivated with oleic acid (OA), whereas the QDs used in the previous experiments are passivated with TOPO, TOP and OA. Therefore the ligands were exchanged to OA by adding an excess of OA to a mixture with CdSe QDs. The mixture was stirred for 12 hours and washed. An amount of a half, one, two and four equivalents of mercury precursor compared to cadmium were added. Again particle instability was observed. On the TEM-images big black dots and a white haze are observed if four equivalents Hg was added (Fig. 24a). When a half equivalent Hg was added some clustered dots were visible (Fig. 24b). It can be concluded that ligand exchange did not result in stable QDs after Hg-exchange.

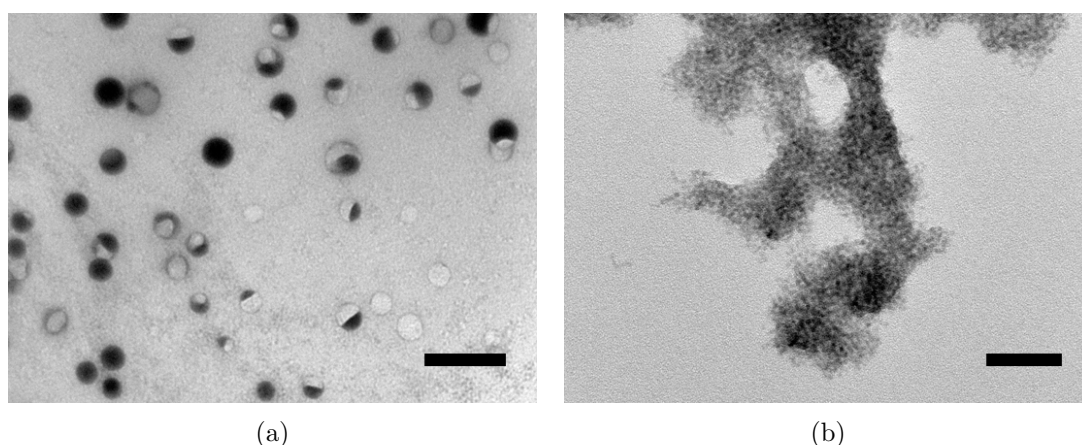


Figure 24: TEM-images of QDs with exchanged ligands treated with  $\text{HgCl}_2$ . (a) addition of four equivalents mercury precursor, scale bar 100 nm. (b) addition of a half equivalent Hg-precursor, scale bar 100 nm.

### 5.3.2 Cadmium-to-mercury ion exchange on CdSe nanoplatelets

The exchange reaction to mercury was also preformed on CdSe NPLs. Because the concentration of the NPLs is not known, different amounts of mercury precursor were added. The exchange reaction was first preformed on 460NPLs. After the addition of the Hg-precursor the mixtures turned black. The Hg-exchange did not result in stable solution with NPLs; the platelets precipitated. On the TEM-images only a few NPLs were visible, but mostly clustered particles (Fig25a and 25b).

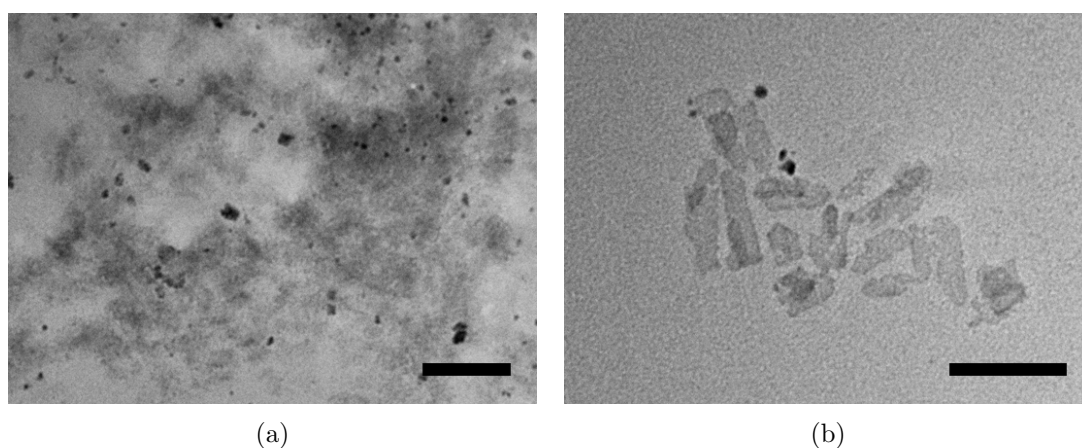


Figure 25: TEM-images of 460NPLs treated with  $\text{HgCl}_2$ . (a) with addition of 6  $\mu\text{L}$  Hg-precursor (scale bar 200 nm). (b) with addition of 40  $\mu\text{L}$  Hg-precursor (scale bar 100 nm)

The synthesis method for the CdSe QDs used by the group of Hens and the synthesis method for 510NPLs are similar. In both cases cadmium myristate is use as a Cd-precursor and OA is added at the end of the reaction. Therefore an exchange reaction

was also performed on 510NPLs. Figure 26a shows the TEM-image of 510NPLs before exchange and figure 26b shows the TEM-image of 510NPLS after Cadmium-to-mercury exchange reaction. There are still NPLs visible, but they appear to be more deformed than before the exchange reaction.

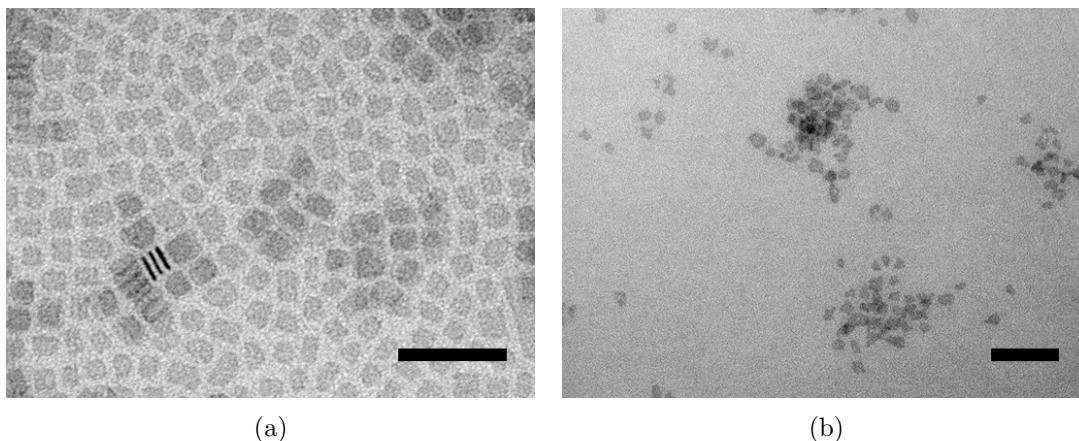


Figure 26: TEM-images of 510NPLs before cadmium-to-mercury cation exchange reaction (a) and after (b). Scale bar 50 nm for both images.

To see if the Cadmium-to-mercury cation exchange reaction was successful, EDX (Energy dispersive X-ray spectroscopy) was performed on these NPLs. The EDX spectrum is shown in figure 27. The EDX spectrum shows that there is Hg present in the sample. This could indicate that the exchange was successful. The atomic percentage of the elements present in the sample was calculated by integrating the peaks for each element (Table 1). 12% of the sample consist out of Hg, but there is also 18% Cd present. Apparently the Cd was not fully exchanged into Hg. There is also a large percentage of Cl present in the sample. Therefore, it is also possible that Hg is not incorporated in the NPLs, but that it is still present in the sample as a precursor. For further experiments the samples could be washed more times. If the percentage of Hg present in the sample decreases when the sample is washed more times, then the Hg is not incorporated in the NPL.

Element	Atomic %
Chloride	31.93
Selenium	38.03
Cadmium	18.25
Mercury	11.77

Table 1: Quantitative determination of the composition of the NPLs after cadmium-to-mercury exchange reaction.

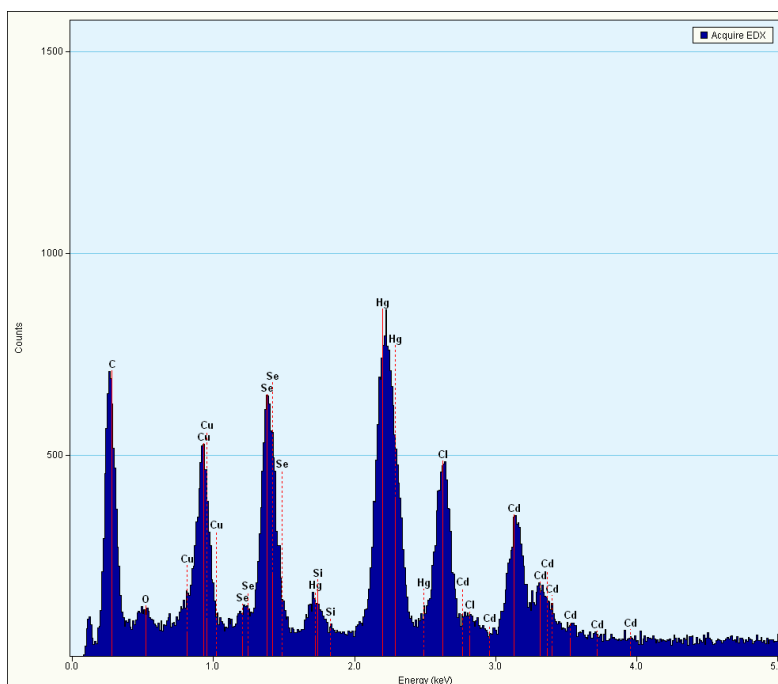


Figure 27: EDX spectrum of 510NPLs on which the Cadmium-to-mercury ion exchange reaction was performed. Hg is present in the sample, there is less Cd present than Se, but there is also a lot of Cl present.

### 5.3.3 Cadmium-to-mercury ion exchange on multishell quantum QDs

Exchange was partially successful on QDs with a multishell. After the exchange reaction many dots were still visible on the TEM-image, as can be seen in figure 28. Different amounts of mercury precursor were added, samples with a low concentration of  $\text{HgCl}_2$  turned yellow and with a high concentration of  $\text{HgCl}_2$  orange. To investigate if exchange had taken place, EDX was performed on the samples (Fig. 29). A large peak at 2.2 keV is visible in the spectrum. This peak can be assigned to Hg, but the S peak is at almost the same position. This means that the peak of Hg could be overestimated during quantitative analysis. There is also a peak around 10 keV which also indicates that Hg is present. There is a small peak visible at 2.6 keV, which can be assigned to Cl. The intensity of the peaks in an EDX spectrum depends on the atomic number of the element. If the amount of Cl would be equal to the amount of Hg present, then the intensity of the chlorine peak would still be lower, because Cl has a lower atomic number. In this case the Cl peak is much lower. This means that not all Hg is present as a salt, but some could be incorporated in the dots. More washing steps to remove the excess Cl, followed by more EDX analysis could prove this. Quantitative analysis of the EDX data could not be performed on this sample.

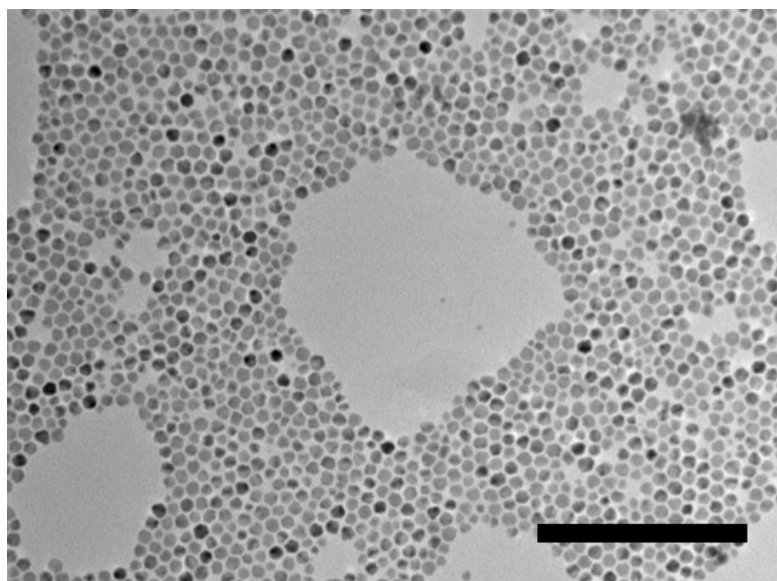


Figure 28: TEM-figure ion exchange on multishell particles. scale bar 200 nm

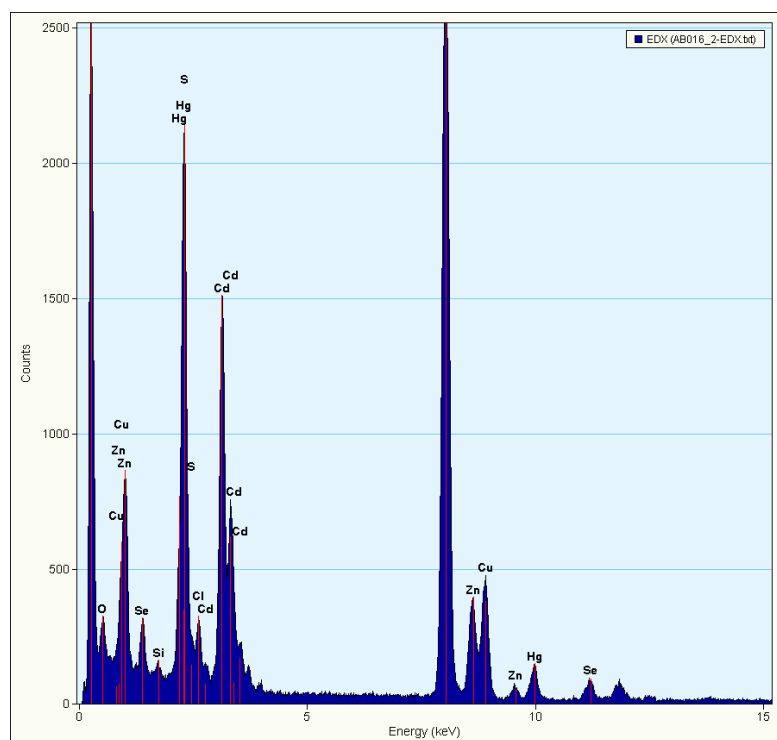


Figure 29: EDX spectrum of multishell particle exposed to  $\text{HgCl}_2$ . There is an intense signal of mercury and the signal of chloride is low. This could indicate that ion-exchange was successful to some extent.

### 5.3.4 Conclusion and outlook

Ion-exchange from cadmium-to-mercury was not successful on 460NPLs and CdSe QDs with a size of 3 nm or smaller. Exchange reactions on multishells and 510NPLs was more successful. Exchange on multishell particles resulted in a stable dispersion and the TEM-images showed that there were still dots present in the sample. The TEM-images of the samples with 510NPLs treated with  $\text{HgCl}_2$  showed that there were still NPLs present, but these samples were no stable dispersions. From the EDX measurement it is not clear if the Hg is incorporated in the NPLs. This is because there is also Cl present in the sample, which could mean that the signal of Hg is due to the  $\text{HgCl}_2$  salt still present in the sample after purification steps. Washing the particles more after ion exchange could give insight on whether the Hg is incorporated in the particle or present as precursor.

An explanation why the ion-exchange on QDs could not be reproduced, could be that the size of the QDs is too small. If the reaction zone is large compared to the dimensions of the particle, then the original shape of the NP cannot be preserved. This could also be the reason why the exchange reaction on NPLs does not work. E.g. in a paper published by the group of Dubetret, the exchange of 1.2 nm thick CdSe platelets to CuSe was also not successful. Exchange on core/shell NPLs with 1 to 3 CdS was possible [35]. It would be interesting to investigate if Hg-exchange is possible on CdSe/CdS core/shell particles.



## 5.4 Adaptation to original synthesis

### 5.4.1 Addition of different acetates salts

The addition of a different acetates salts than cadmium acetate during the synthesis of the 510NPLs also resulted in the formation of 510NPLs. This is also stated in papers published by Dubertret et al. [9] and Peng et al [4]. In these papers it is stated that the formation of the NPLs is acetate facilitated, but there is nothing published on the influence of the cation that is added. The influence of the cation on the formation of NPLs will be the topic of this section.

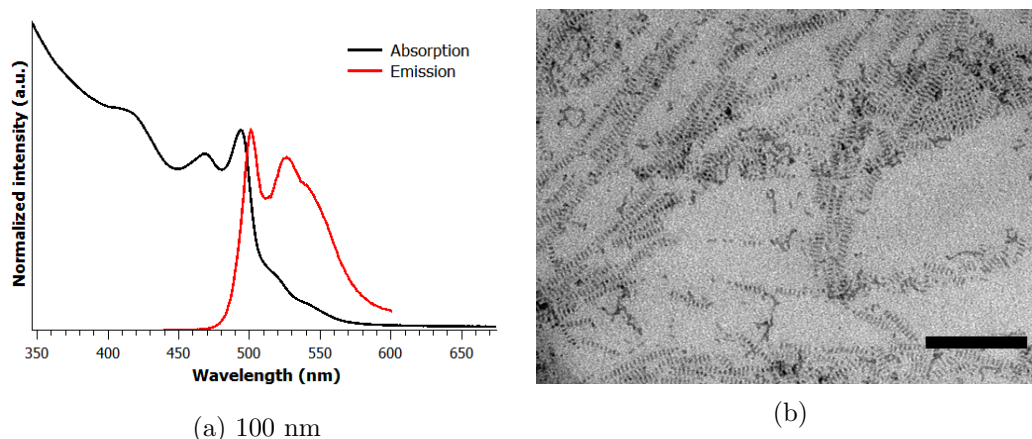


Figure 30: (a) Absorption (black) and emission (red) spectra of NP synthesized when no acetate salt is added during the reaction. (b) TEM-image of sample where no acetate salt was added during the reaction (scale bar 100 nm).

First some experiments were done to verify that the addition of an acetate salt is necessary for the formation of 510NPLs. In the first experiment, no acetate salt was added during the reaction. If no acetate salt was added there were still some NPLs synthesized during the reaction, but mostly dots were synthesized as can be seen on the TEM-image (Fig. 30b). The absorption and emission spectra of the obtained dispersion are shown in (Fig. 30a). A sharp peak is visible at 490 nm in the absorption spectrum and at 500 nm in the emission spectrum. This is not the expected peak position in the absorption and emission spectrum for these NPLs when synthesized according to the standard procedure. Because the peak has a small FWHM, it is unlikely that the absorption and emission at this position originates from QDs or nanorods. However, no CdSe NPLs have been synthesized so far that emit and absorb at these wavelengths. It is possible that the lateral dimensions of the NPL are not large enough to exceed the confinement regime. If this is indeed the case, there is still confinement in the lateral dimensions, resulting in emission and absorption at higher energies. It could also be that these NPLs have a thickness in between the thickness of the 460NPLs and the 510NPLs. This would mean that these NPLs are half a monolayer thicker than the 460NPLs. This thickness is not reported by other groups.

Next to the sharp peak, the emission spectrum of this sample also has a double peak around 540 nm. These peaks are broader and probably originate from the dots visible on the TEM-image. Although the type of particles formed during this synthesis is unclear, it can be stated that the formation of 510NPLs is not successful when no acetate salt is added.

Addition of a different cadmium source (cadmium myristate) did not result in obtaining a dispersion with only NPLs. A few NPLs can be identified on the TEM-image (Fig. 31b), but mostly QDs are observed. The absorption and emission spectra (Fig. 31a) have broad peaks which confirms that mostly QDs were synthesized.

From these two experiments, the addition of no acetate salt and the addition of cadmium myristate, it can be concluded that for the formation of 510NPLs the addition of an acetate salt is essential.

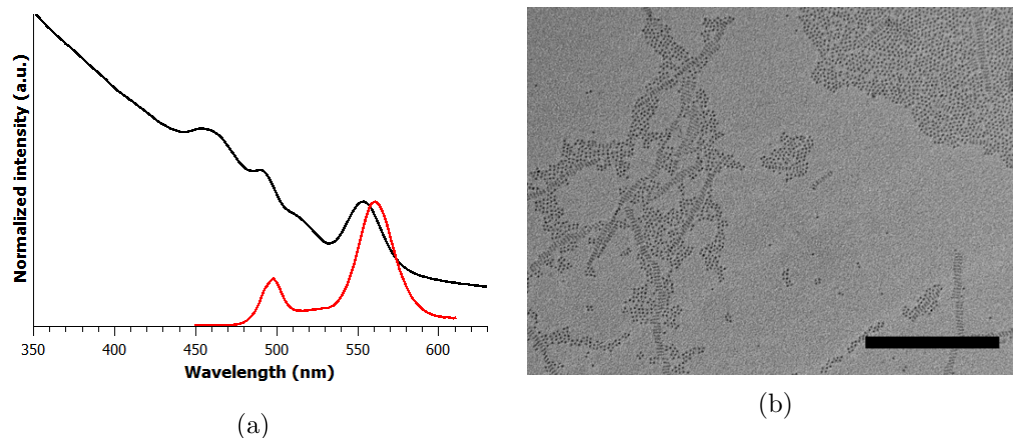


Figure 31: (a) Absorption (black) and emission (red) spectra of NP synthesized when  $\text{Cd}(\text{myr})_2$  is added. (b) TEM-image of a sample where  $\text{Cd}(\text{myr})_2$  was added during the reaction (scale bar 100 nm)

Different acetates salts were added to investigate if NPLs would form. Addition of zinc-, cobalt-, magnesium- and lead acetate all resulted in the formation of NPLs. Addition of copper acetate did not result in the formation of NPLs. The TEM-images, absorption spectra and emission spectra of these samples are included in appendix (A). A selection of acetates salts was made to investigate the influence of the cation on the formation of the NPLs. Acetic acid (hydrogen acetate), lithium acetate, sodium acetate, potassium acetate and cesium acetate, the first group in the periodic table, were added during the reaction.

When acetic acid was added, many different kinds of particles were obtained. The TEM-image (Fig. 32b) shows that the dispersion contained dots, small NPLs or rods and large NPLs. The large NPLs tend to stack in the middle, but the ends of the NPLs are twisted and lay flat on the TEM-grid. The absorption (Fig. 32a, black) and emission (Fig. 32a, red) spectra also show that there was more than one population of NP present in the dispersion.

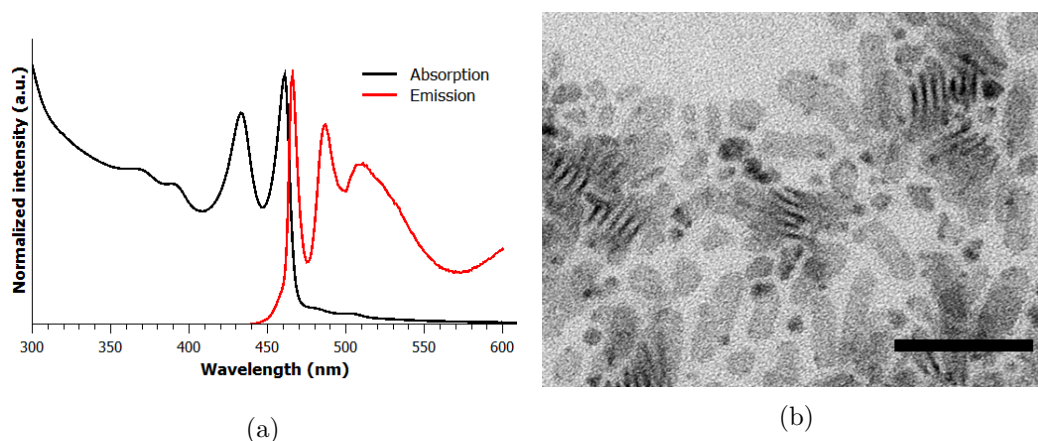


Figure 32: (a) absorption (black) and emission (red) spectra of a sample where 40  $\mu\text{L}$  acetic acid was added during the reaction. (b) TEM-image of a similar sample as in (a) (scale bar 50 nm).

In the absorption spectrum mainly features characteristic for 460NPLs can be seen; The sharp peaks at 460 nm and 430 nm and the bumps at higher energies. There are also some peaks visible with a low intensity at longer wavelength than 460 nm. These peaks are more prominent in the emission spectrum than in the absorption spectrum. This difference in ratio between the peaks in the emission and absorption spectrum will be discussed in chapter 5.5. The emission spectrum also indicates the presence of 460NPLs, because there is a sharp emission peak at 460 nm. There is also a sharp peak around 490 nm, which is a position in between the absorption and emission maximum of the 460NPLs and 510NPLS. This peak was also seen when no acetate salt was added, but it is not at the exact same position. The peak could be the emission of small NPLs where there is still confinement in the lateral dimensions, or it could be the emission of NPLs which are half a monolayer thicker than the 460NPLs. The first explanation is more plausible considering that the peak is not at the same position as when no acetate salt was added. The third peak in the emission spectrum is broad, therefore it is probably emission of QDs present in the sample. The start of a fourth peak is also visible. This is the trap emission of 460NPLs [24].

If less acetic acid is added during the synthesis, a sharp peaks becomes visible 510 nm (Fig 33a). This sharp peak is emission of 510NPLS. However, there is also a broad peak at the same position with a lower intensity, which is again probably emission of dots present in the sample. Furthermore, the absorption and emission spectra have the characteristic peak at 460 nm, indicating that there are also 460NPLs present in the sample. These experiments show that addition of acetic acid results in the formation of NPLs, but also other NP are obtained.

When lithium acetate or sodium acetate was added only 510NPLs were formed. The emission spectra and absorption spectra only show features of the 510NPLs (Fig 34a and 35a). If different amounts of lithium or sodium acetate were added, there was still only one peak visible at 510 nm. This is different compared to cadmium acetate, where

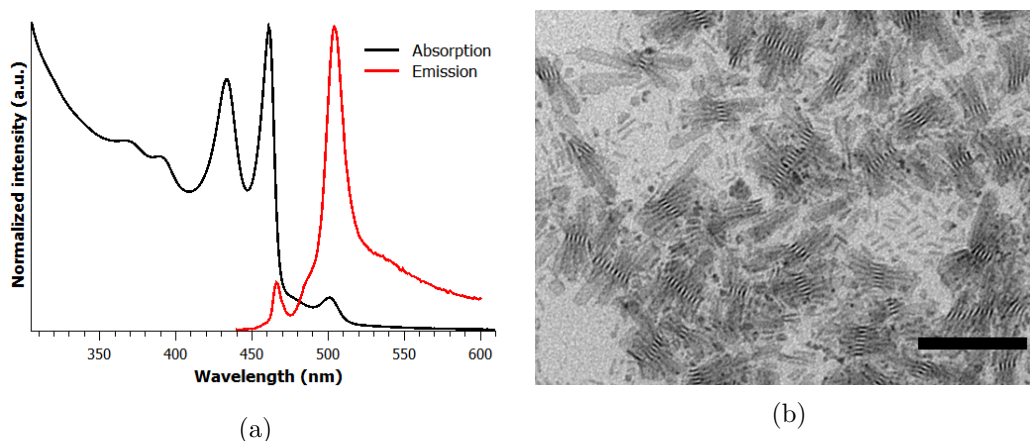


Figure 33: (a) absorption (black) and emission (red) spectra of a sample where 27  $\mu\text{L}$  acetic acid was added during the reaction. (b) TEM-picture of a similar sample as in (a) (scale bar 100 nm).

the trend was that if less cadmium acetate was used also 460NPLs were present in the sample and when more cadmium acetate was used 550 NPLs were present. The addition of sodium acetate gives more square-like particles than when lithium acetate is added (34b and 35b).

When potassium or cesium acetate was added, no or almost no NPLs were formed. When potassium acetate was added, some NPLs were formed as can be seen on the TEM-image (Fig 36b), but also triangular particles and particles with an even less well defined structure were formed. The triangular particles could be bipyramids or tetrahedrals, because there appears to be contrast difference within one particle. The absorption spectrum (Fig 36a, red) of the dispersion has almost no distinct features, indicating that no NPLs were formed during this reaction, but rather three dimensional NPs with a large polydispersity. The particles did show photoluminescence (PL), but the PL signal was very low. The emission spectrum is shown in black in figure 36a. There are small peaks visible at 460 nm and 510 nm, which could indicate that some 460NPLs and 510NPLs were present in the sample. The broad peak at 560 nm confirms that three dimensional particles were present in the sample. The addition of cesium acetate resulted in particles where the PL signal was almost completely quenched (Fig 37a, red). There are no clear features present in the absorption spectrum either (Fig 37a, black). On the TEM-image shown in figure 37b only particles with a not well-defined shape are observed.

To summarize, the addition of acetic acid gave a mixture of NP including NPLs. Adding lithium- and sodium acetate resulted in the formation of NPLs, whereas the addition of potassium and cesium acetate did not. A trend in the above results becomes visible when the ionic radius of the cations is compared to the ionic radius of a cadmium ion. If the ionic radius of the cation has a similar or smaller size than the ionic radius of the cadmium ion, then there appear to be NPLs forming with well defined absorption and emission features, which is confirmed by TEM and optical measurements. The ionic

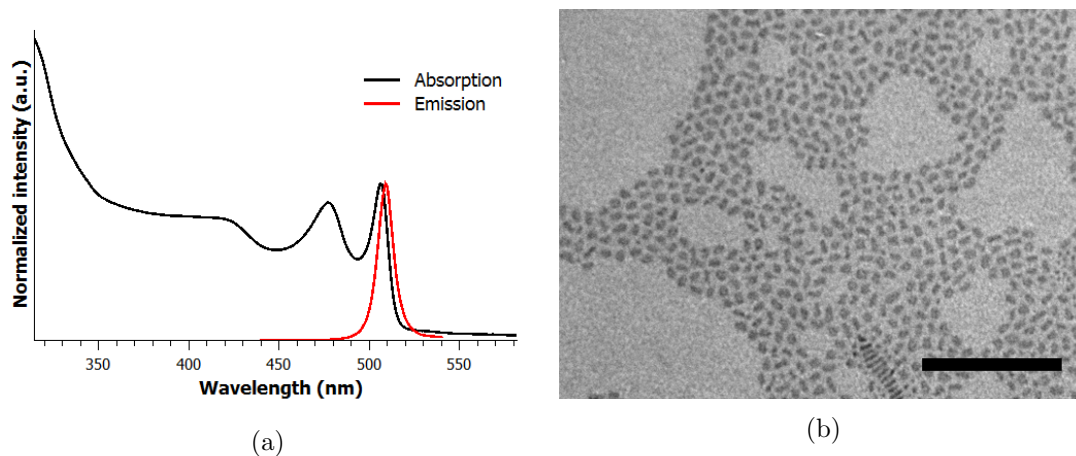


Figure 34: (a) absorption (black) and emission (red) spectra of 510NPLs with addition of 46 mg Li(Ac) (b) TEM-image of 510NPLs with addition of 46 mg Li(Ac) (scale bar 100 nm).

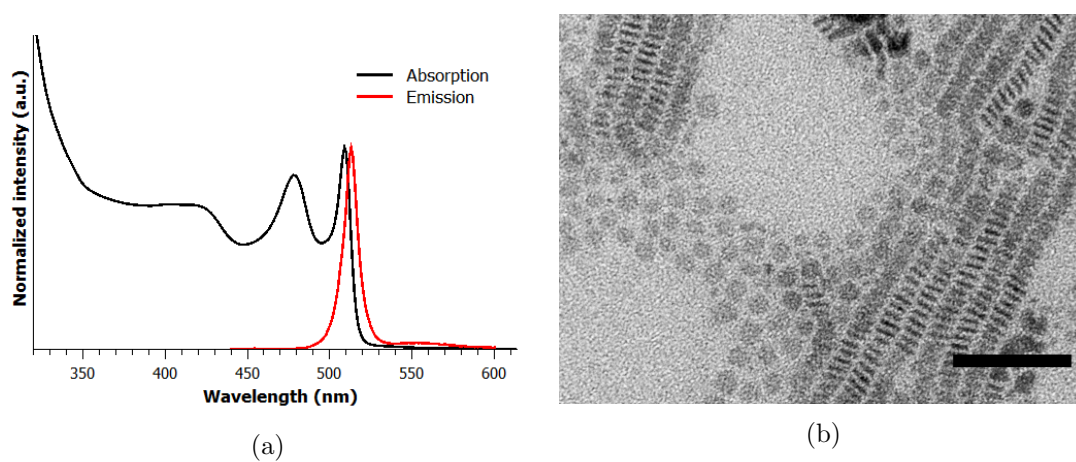


Figure 35: (a) absorption (black) and emission (red) spectra of 510NPLs with addition of 39 mg Na(Ac) (b) TEM-picture of 510NPLs with addition of 39 mg Na(Ac) (scale bar 50 nm).

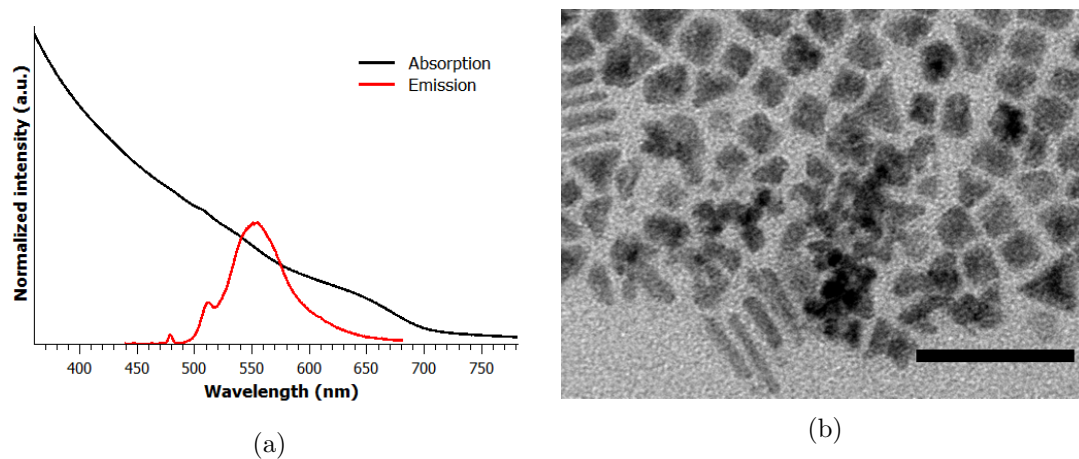


Figure 36: (a) absorption (red) and emission (black) spectra of a sample where 47 mg K(Ac) was added. (b) TEM-image of a similar sample as in (a). scale bar 50 nm.

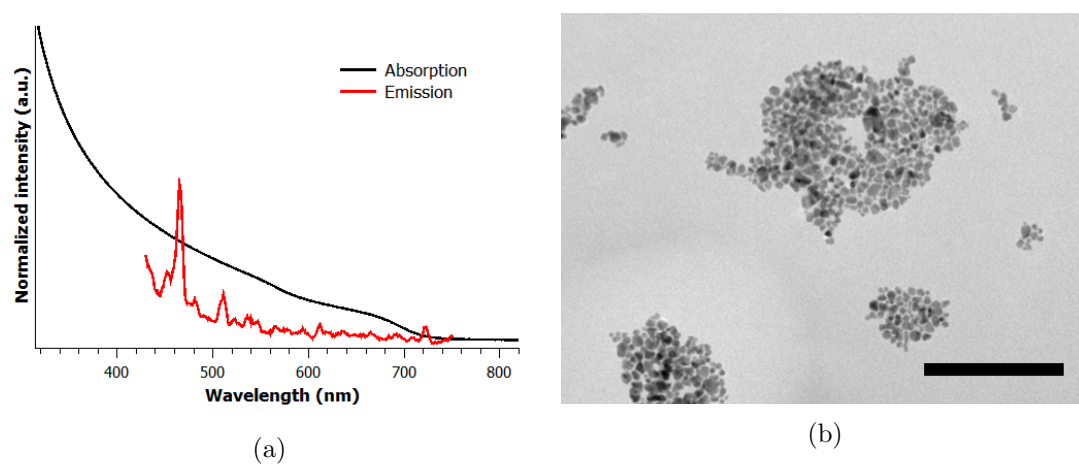


Figure 37: (a) absorption (black) and emission (red) spectra of a sample where 133 mg Cs(Ac) was added. (b) TEM-image of corresponding particles. scale bar 200 nm.

radii of the cations is shown in figure 38. An explanation for the observed trend cannot be given by the information available at this point, but the dissociation energy of the cation-acetate ionic bond could play a role. This could influence the active concentration of the monomers in the solution during the reaction, which has a big influence on the formation of NPLs (see section 2.3 and chapter 3). Further research has to be done to investigate this hypothesis.

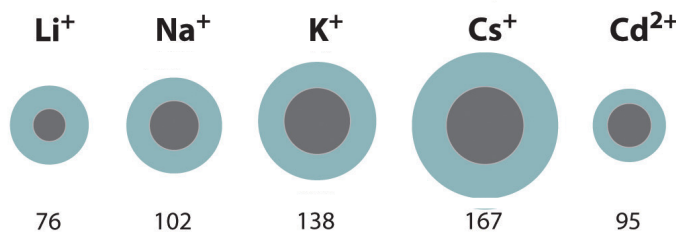


Figure 38: Schematic representation of the ionic radii of lithium, sodium, potassium, cesium and cadmium. Gray circles indicate the size of the ions and the colored circles indicate the size of the neutral atoms. Size of the ionic radius is given in picometers. Data duplicated from ref. [40].

#### 5.4.2 EDX-measurements

The absorption and emission spectra of the NPLs obtained when adding lithium- or sodium acetate are the same as the absorption and emission spectra of the NPLs obtained when cadmium acetate is added. This indicates that lithium and sodium are not incorporated in the NPL. Incorporation of these ions would result in a different band structure and therefore different absorption and emission maxima. To be sure that these ions are not incorporated, elemental analysis using EDX was performed on these particles. This could only be done on the sample where sodium was added, because the detector used for the measurements was equipped with a beryllium window, making elemental analysis on elements with a lighter atom mass than sodium not possible. Figure 39 shows the EDX spectrum of a sample where sodium acetate was added during the synthesis of the NPLs. Instead of using a conventional Cu TEM-grid, a Ni TEM-grid was used, as the Cu emission lines overlap strongly with the Na emission lines. The peak around 1.40 keV indicates that there is Se present in the sample. There is also a peak of Cd at 3.1 keV, which has the same intensity as the selenium peak. The peak of Na should be positioned at 1.04 keV. Figure 40 is a zoom of the EDX spectrum. In this spectrum there is a small bump around 1 keV, but this peak could not be distinguished from the background noise. Another measurement was done on a different spot on the TEM-grid. In this measurement there is no peak visible at 1 keV (Fig 41). Keeping in mind that 49.1 mg sodium acetate (0.67 mmol Na) and 170 mg cadmium myristate (0.30 mmol Cd) were added during the reaction, one would expect to measure the presence of Na in the resulting NPLs if it is incorporated. These EDX measurements show that Na is not incorporated in the NPLs, and are most likely removed in subsequent purification steps.

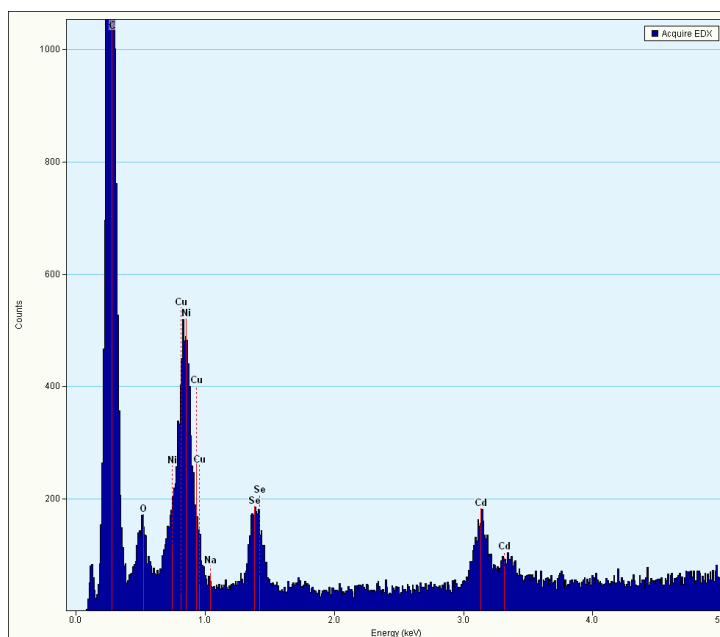


Figure 39: EDX of 510NPLs with addition of  $\text{Na}(\text{Ac})_2$ .

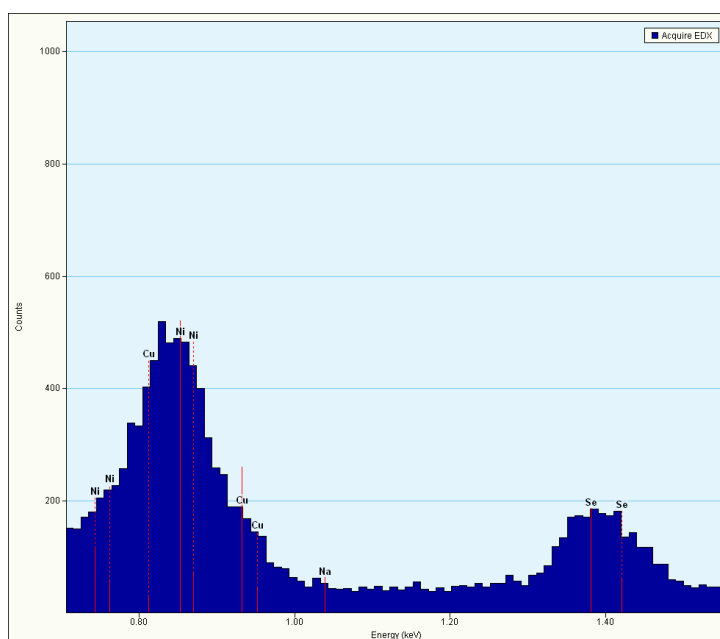


Figure 40: Zoom in the energy region between 0.7 and 1.5 keV of the EDX spectrum shown in figure 39.



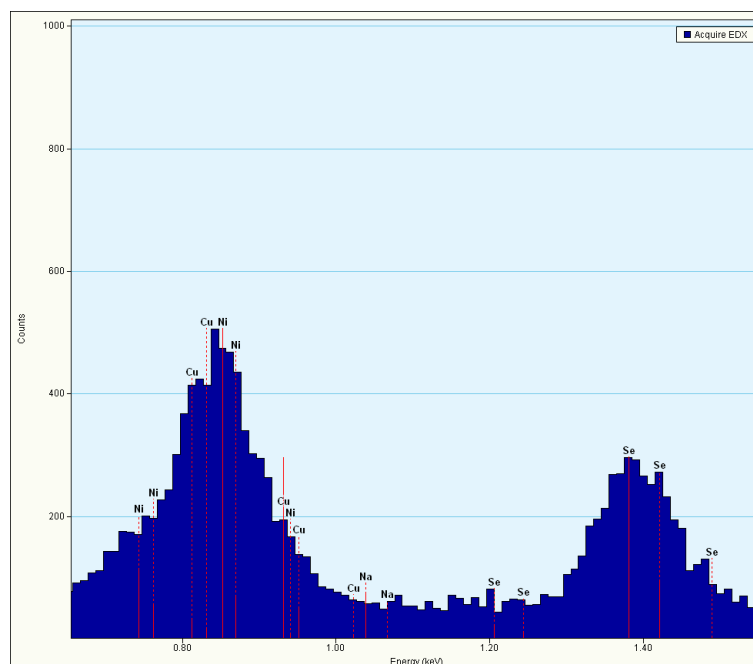


Figure 41: Zoom in the energy region between 0.7 and 1.5 keV of EDX spectrum of second measurement on 510NPLs with addition of  $\text{Na}(\text{Ac})_2$ .

#### 5.4.3 Photoluminescence quantum yield measurements

The addition of lithium- and sodium acetate results in the formation of NPLs. The emission and absorption spectra show that lithium and sodium are not incorporated in the NPLs. This was confirmed by the EDX-measurements. To see whether there is a difference in the optical quality of the NPLs when lithium-, sodium-, or cadmium acetate were added during the reaction, the PL-quantum yield (QY) was measured. The QY measurements were performed using an integrating sphere. The QY was measured of samples where different amounts of acetates salts were added. In the case of cadmium acetate 40 mg, 55 mg and 80 mg was added. An equivalent amount of moles acetate was added in the case of lithium- and cadmium acetate. The amounts are listed in table 2. The QY was measured for two excitation wavelengths. The results are listed in table 2. The first observation is that the QY is higher when the NPLs are excited at 430 nm than at 480 nm. This is an unexpected result, since there is no physical reason for the QY to be different for the NPLs when exciting at these two wavelengths. Differences in QY when exciting at different wavelengths can be observed when the cuvette absorbs as well. However, the quartz cuvettes used in these measurements should absorb stronger at shorter wavelengths, which would result in a lower QY when exciting at 430 nm. This is the opposite of what is observed in these measurements. There could be some other particles in the sample that disturb the measurements, but the TEM-images, absorption spectra and emission spectra do not give reason to assume this. The measurements could be done using a dye to investigate if this difference in QY is also seen.

$X(\text{Ac})_x$	Amount of acetate salt (mg)	QY exciting at 430 nm (%)	QY exciting at 480 nm (%)
$\text{Cd}(\text{Ac})_2$	40	48	16
	55	40	13
	80	33	13
$\text{Na}(\text{Ac})$	29	16	6.0
	39	18	6.0
	57	17	4.0
$\text{Li}(\text{Ac})$	23	26	6.1
	32	19	6.9
	46	11	3.5

Table 2: Comparison of measured QY when adding different acetate salts

Even though it proves to be difficult to measure the absolute QY, a trend is observed nonetheless between the different NPLs. The QY when adding cadmium acetate is higher than when lithium- or sodium acetate is added. A possible explanation for this is that the concentration of cadmium was not high enough during the synthesis where lithium- or sodium acetate was added and therefore defects were introduced in the NPLs, reducing the QY.

A second trend that can be observed is that the QY is higher when less acetate salt is added, except for when sodium acetate is added; The QY of these NPLs is roughly the same. From these measurements it can be concluded that NPLs with the highest optical quality can be obtained by adding 40 mg, or presumably even less, of cadmium acetate during the synthesis. The problem is however that if less cadmium acetate is added, more 460NPLs are formed during the reaction next to 510NPLs. It would be ideal if only one population is present. The NPLs can to some extent be separated with size-selective precipitation, but this reduces the emission (and hence the QY) of the NPLs. Washing removes the unbound ligands present in the solvent. A new equilibrium between ligands in solution and ligands bound to the NPLs surface will be established when the particles are redispersed. This means that after every washing step less ligand will be bound to the surface of the NPLs. This will result in more dangling bonds at the surface, which result in more trapping and hence the QY will be reduced. It would be ideal if size-selective precipitation could be avoided by finding a method to synthesize only one population of NPLs. When only cadmium acetate is added it proves to be difficult to obtain one population. If more acetate salt is added, there is no formation of 460NPLs, but then a mixture of 510NPLs and 550NPLs is obtained. What stands out is that when sodium- or lithium acetate is added only formation of 510NPLs is observed, independent of the amount of acetate salt added. If a mixture of  $\text{Cd}(\text{Ac})_2$  and  $\text{Na}(\text{Ac})$  or  $\text{Cd}(\text{Ac})_2$  and  $\text{Li}(\text{Ac})$  is added during the reaction, it could be possible to obtain only one population of NPLs which do have a high QY.

A mixture of cadmium acetate and sodium acetate was added during the reaction to investigate if one population of NPLs with a high QY can be obtained. The amount of

cadmium acetate was kept the same for all experiments. The amount of sodium acetate was varied. The measured QY of these samples are shown in table 3. All samples have a high QY compared to when only sodium acetate is added. If a mix of 40 mg cadmium acetate and 20 mg sodium acetate is added, then the QY is even higher than when only cadmium acetate is added.

The remaining question is if there is only one population of NPLs obtained when a mixture is added. Therefore the absorption spectra of these samples were measured. Using the emission spectra would make it easier to distinguish between the two populations, but the difference in QY would also influence the ratio between the peaks. The absorption spectra are shown in figure 42. All absorption spectra have a peak at 510 nm and 480 nm, which are the heavy and light hole transitions of the 510NPLs. In the blue, light blue and red spectra there is also a small peak visible at 460 nm, which is the heavy hole transition of the 460NPLs. This peak disappears upon addition of more sodium acetate. With the addition of a mixture of cadmium- and sodium acetate one population of NPLs can be obtained with a high QY.

Cd(Ac) <sub>2</sub> (mg)	Na(Ac) (mg)	QY exciting at 430 nm (%)	QY exciting at 480 nm (%)
40	0 mg	48	16
40	5 mg	47	38
40	10 mg	49	40
40	20 mg	61	44

Table 3: Comparison of measured QY when adding mixture of cadmium- and sodium acetate.

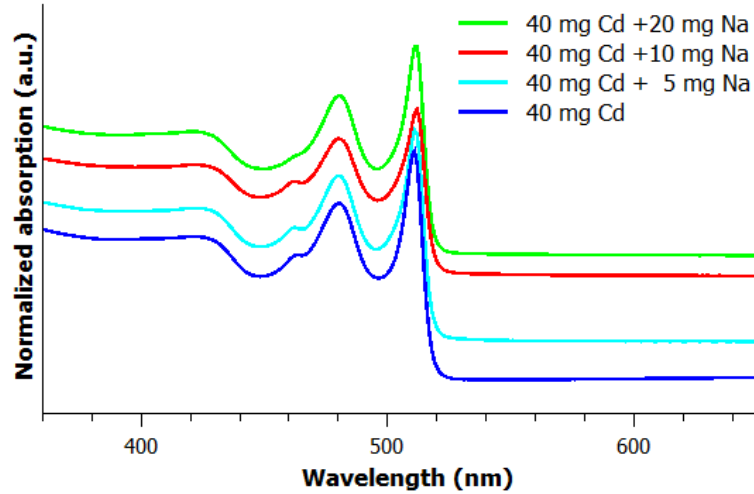


Figure 42: Absorption spectra NPLs when adding mixture of cadmium- and sodium acetate.

#### 5.4.4 Conclusion and outlook

Addition of an acetate salt is necessary to obtain CdSe NPLs, but it is not necessary to add cadmium acetate. Addition of cobalt acetate, zinc acetate, magnesium acetate, lithium acetate and sodium acetate also results in the formation of NPLs. The cation of the added acetate salt has an influence on the formation of the NPLs. If a cation which has a larger ionic radius than cadmium is added, the reaction does not result in the formation of NPLs. A possible explanation could be that the dissociation energy of the acetate salt has an influence on the formation of the NPLs, however more research has to be done to confirm this statement.

NPLs with a higher QY are obtained when cadmium acetate is added. However, when cadmium acetate is added, a mixture of different populations of NPLs are obtained. Addition of a mixture of cadmium acetate and sodium acetate result in the formation of one population of NPLs with a high QY. This adaptation to the synthesis method of the 510NPLs results in NPLs with a high QY and no size-selective precipitation, which results in degradation of the optical properties of the NPLs, is required.

It would be interesting to investigate whether this adaptation would also work for the formation of 550NPLs, as with the current synthesis method for these NPLs a mixture of several NPL thicknesses is obtained as well. Sometimes the ratio of obtained NPLs is one-to-one, which makes the isolation of 550NPLs with size selective precipitation very difficult without reducing the QY.

## 5.5 Energy transfer

### 5.5.1 Energy transfer in dispersion obtained when adding acetic acid

The absorption and emission spectra of the sample where acetic acid was added during the reaction (see figure 43), hinted towards possible energy transfer (ET) between the NPs in the dispersion, as the ratio between the peaks in the absorption spectrum differs from the ratio between the peaks in the emission spectrum. The intensity of the peaks at 485 nm and 510 nm is relatively higher in the emission spectrum than in the absorption spectrum when comparing it with the intensity of the peak at 460 nm. A first explanation for this observation is that the obtained NPs have different QYs. A second explanation is that ET occurs from 460NPLs to the other NPs present in the dispersion. This process can occur non-radiatively or radiatively. ET occurs radiatively if the emitted photon by the 460NPLs is reabsorbed by the particles that absorb at lower energies. Energy can also be transferred through a strongly distance dependent dipole-dipole coupling; a non-radiative process. The observation of non-radiative ET, would be very interesting. In order to confirm the presence of ET, the concentration of the NP dispersion was varied and excitation spectra were measured (Fig. 44 and 45).

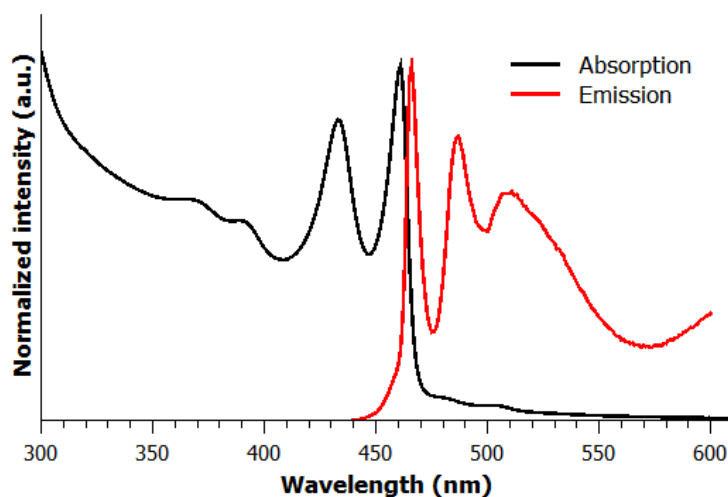


Figure 43: (Absorption (black) and emission (red) spectra of a sample which was synthesized with the addition of 40  $\mu$ L acetic acid.

The amount of ET between the particles increases if the interparticle distance is decreased, both for radiative and non-radiative transfer pathways. The emission spectra for different concentrations of the sample are shown in figure 44a. The concentrations were varied qualitatively by adding 10uL (black), 50uL (red) and 100 uL (green) of a NPL dispersion to 3 mL of hexane. The spectra are normalized on the emission peak of the 460NPLs. The intensity of the peaks at 490 nm and 510 nm increase with respect to the peak of the 460NPLs upon increasing the relative concentration of the NP solution.

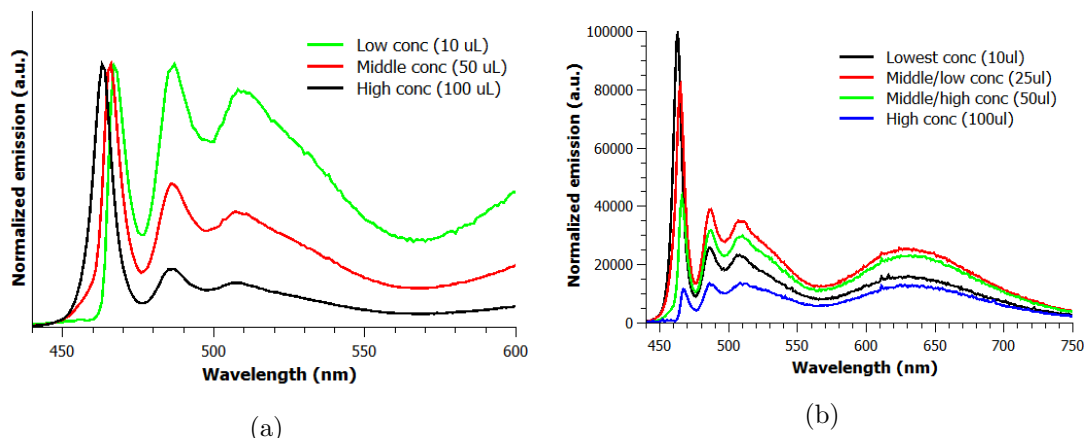


Figure 44: (a) normalized emission spectra of different concentration of a sample where acetic acid was added during the reaction. Relative sample concentrations: 10  $\mu\text{L}$  (black), 50  $\mu\text{L}$  (red) and 100  $\mu\text{L}$  (green) of sample in 3 ml hexane. (b) Not-normalized emission spectra of this sample. Relative sample concentrations: 10  $\mu\text{L}$  (black), 25  $\mu\text{L}$  (red) and 50  $\mu\text{L}$  (green) and 100  $\mu\text{L}$  (blue) of sample in 3 ml hexane.

This is an indication for ET between the 460NPLs and the particles that emit at 490 nm and 510 nm. With these experiments we cannot distinguish between radiative and non-radiative ET between the 460NPLs and the other NPs. What we can conclude from these experiments is that there is radiative ET (reabsorption) taking place between the 460NPLs, seen by the red-shift of the emission peak at 460 nm for higher concentrations. This red-shift occurs because the absorption and emission maximum do not coincide, due to the Stokes-shift between the absorption and emission features. Due to this Stokes-shift, the photons emitted at higher energy are more strongly reabsorbed than the photons emitted at lower energy, resulting in a red-shift of the emission peak. Comparing the absolute intensities of the emission features (Fig 44b shows that other processes next to the possible ET are occurring. For example, the peak at 490 nm does not increase by 2.5 times in intensity when the concentration of the dispersion is increased by 2.5 times (Fig 44b black and red). If ET is occurring, the intensity should increase more than 2.5 times, if the concentration is increased by 2.5 times. It should be noted that there is much overlap between the peaks, making it hard to estimate how much the intensity is increased. When the green and blue spectrum in figure 44b are compared, it is even more certain that more processes are occurring; upon increasing the concentration of the dispersion, the intensity of the emission decreases. This could be due to concentration quenching. Concentration quenching occurs when the amount of ET is very high, so the stored energy can migrate through the sample until it reaches a defect and is quenched. A second explanation for the reduced emission could be that the concentration of the sample is so high that the light of incoming beam during the measurements is absorbed before the focal point of the beam. The emission is measured in the focal point of the beam, but if the incoming light is mostly absorbed before this point, then there is less excitation in the focal point and therefore less emission that will be measured.

Although the emission spectra measured at different concentrations do not give a clear view if there is ET between the NPs, the excitation measurements give further evidence for ET (Fig 45). These spectra were measured for the emission maxima, seen in figure 45a, and were normalized on the peak at 460 nm. We can observe several features in the excitation spectrum recorded for an emission wavelength of 464 nm, namely the light hole (430 nm) and the heavy hole (460 nm) transitions of 460NPLs. The excitation spectra of the other emission wavelengths (486 nm and 508 nm) have the same features, indicating the presence of ET from the 460NPLs to the other NPs. However, there is overlap between the peaks and therefore we probe not only one emission feature, hence not only one type of NP present in the solution. If more than one type of NP is excited, this could result in measuring the same excitation features. Furthermore, the origin of the emission peaks at 490 nm and 510 nm are not known at this time, so definitive conclusions from these experiments cannot be made. For example, the broad peak at 510 nm could be from the seeds which are formed at the beginning of the reaction. These seeds also emit and absorb at 460 nm, but have a trapping peak at 510 nm [27]. These seeds will have a similar excitation spectrum as the 460NPLs.

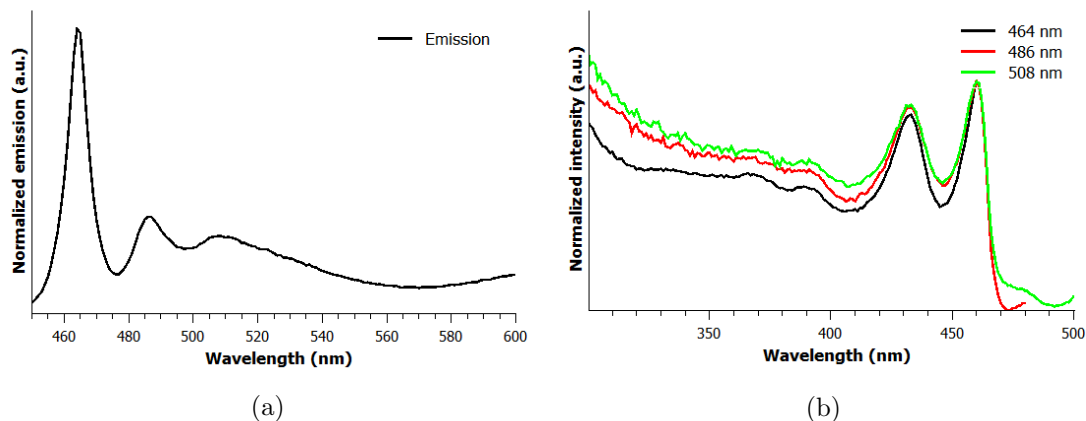


Figure 45: (a) Emission spectrum of the sample where acetic acid was added during the reaction (b) Excitation spectra for the peaks at 464 (black), 486 (red) and 503 (green) nm.

### 5.5.2 Energy transfer between 460NPLs and 510NPLs

Even though the results of investigating ET are inconclusive, it would seem reasonable to assume ET occurs between NPLs in general. As the NPLs have facets with a higher surface area than QDs, there should be ET occurring, as it is also observed in QDs [41]. To further study the possibility of ET, two NPL populations, 460 NPLs and 510 NPLs, were mixed. It is easier to interpret the results for this system, because the origin of the emission features for these NPLs are known. Emission spectra were measured for various concentrations of NPLs, which are shown in figure 46. The spectra are normalized on the emission peak of the 460NPLs. If the concentration of the mixture of 460NPLs and 510NPLs is increased, the intensity of the emission of the 510NPLs and the trap emission

of the 460NPLs (at 630 nm) increases compared to the emission of the 460NPLs. This can again indicate ET between 460NPLs and 510NPLs. As a red-shift of the 460NPL emission peak is observed again, reabsorption seems to be occurring as well.

To investigate if the change in ratio is due to radiative ET (reabsorption) or due to non-radiative ET, time-resolved PL measurements can be performed. If the change in ratio is only due to reabsorption then the lifetime of the 460NPLs would not change, but if there is non-radiative ET then there is an extra decay path for the exciton in the 460NPLs at higher concentrations. This extra decay path lowers the lifetime of the 460NPLs. There should be no difference for the lifetime of the 510NPLs if there is ET. Measuring the lifetime of the 460NPLs and 510NPLs in this sample will not give clear information, as their emission peaks overlap significantly. Because of the broad trap emission peak of the 460NPLs, the lifetime of the 510NPL emission cannot be measured without having significant contributions from the trap emission. Especially at high concentrations of the dispersion. The lifetime will be a convolution of the lifetime of the 510NPLs and the trapped excitons/charge carriers of the 460NPLs.

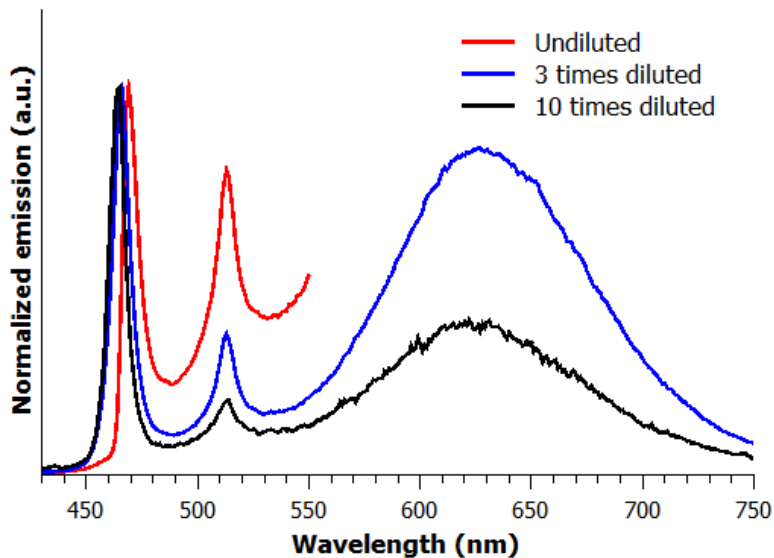


Figure 46: Emission spectra of a mixture of 460NPLs en 510NPLs with different concentrations. The spectra are normalized on the the emission peak at 460 nm.



### 5.5.3 Energy transfer between 510NPLs and 550NPLs

To be able to investigate ET between the NPLs two problems had to be solved. First, there should be less overlap between the emission peaks. Second, the platelet-platelet distance should be decreased without increasing the overall concentration of the solution. At high concentration other processes can occur next to non-radiative ET, like concentration quenching and reabsorption. The concentration could also be so high that all light is absorbed before the focus of the beam. The first issue can be solved by mixing 510NPLs and 550NPLs, as these NPLs have no trap emission. The second issue can be solved by adding a anti-solvent to the mixture. Addition of a anti-solvent induces the formation of stacks of NPLs in solution as their stability in the solvent is decreased [42]. Therefore, if more anti-solvent is added, the distance between the NPLs will be reduced, hence increasing the possibility of ET.

In figure 47 the emission spectra are shown of a mixture of 510NPLs and 550NPLs where a 1:4 (v/v) methanol/butanol mixture was added stepwise. When adding more anti-solvent a relative increase of the intensity of the 550NPLs emission was observed. This could indicate that there is an increase of ET from the 510NPLs to the 550NPLs upon increasing the amount of anti-solvent. To investigate whether this is non-radiative ET, the lifetime of the emission of 510NPLs was measured. The lifetime curves are shown in figure 48. The lifetime of the emission of 510NPLs becomes shorter when more anti-solvent is added. This is a convincing observation that there is non-radiative ET, because non-radiative ET induces an extra decay path, shortening the lifetime of the emission of the 510NPLs. However, the not normalized emission spectra (Fig 50) show quenching for both the emission of the 510NPLs and the 550NPLs when more anti-solvent is added. Furthermore, the lifetime of the 550NPLs also decreases when more anti-solvent is added (Fig 49). These two observations make the existence of ET from the 510NPLs to the 550NPLs debatable.

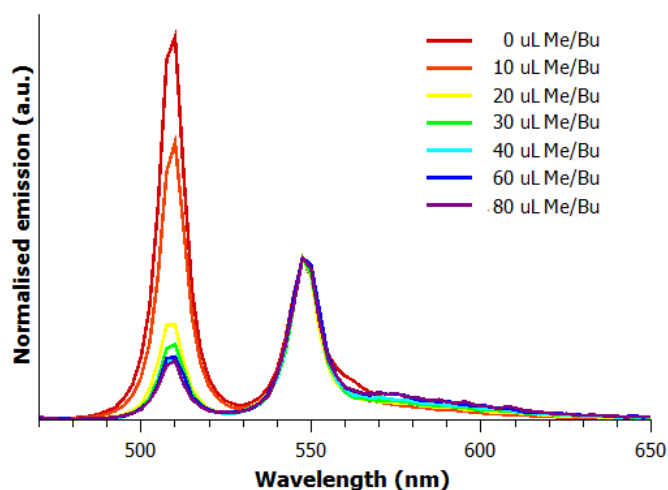


Figure 47: Emission spectra of the mixture of 510NPLs and 550NPLs where different amounts of Me/Bu are added. Spectra are normalized on the emission peak of the 550NPLs.

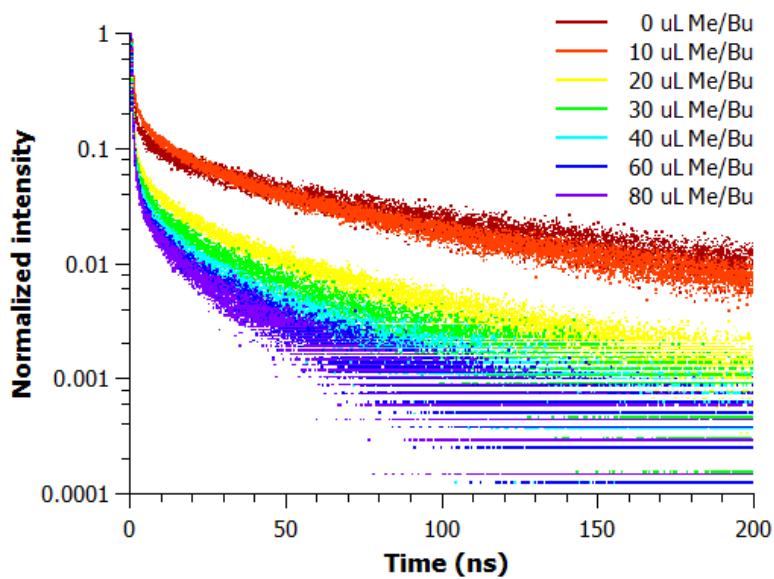


Figure 48: Lifetime of the 510NPLs emission in a mixture of 510NPLs and 550NPLs. More Me/Bu was added stepwise.

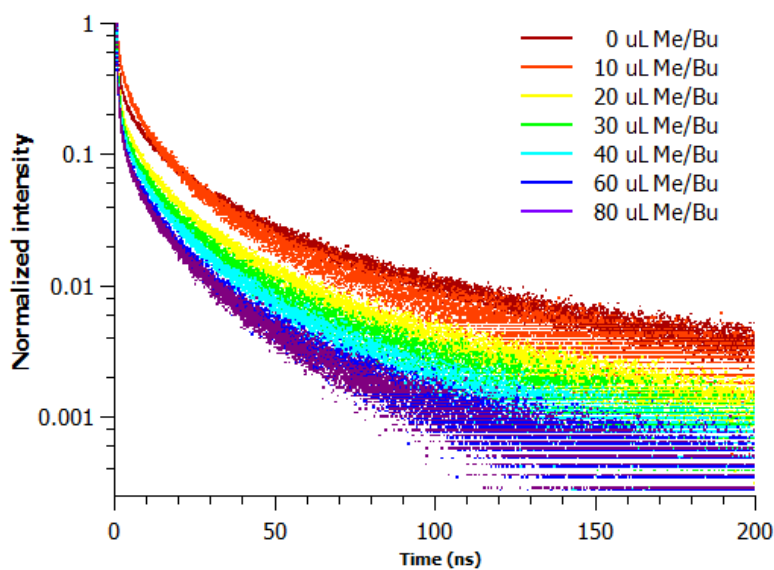


Figure 49: Lifetime of the 550NPLs emission in a mixture of 510NPLs and 550NPLs. More Me/Bu was added stepwise.

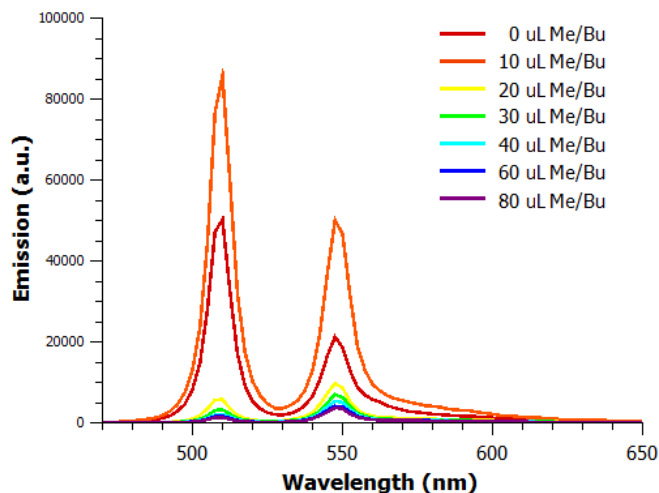


Figure 50: Emission spectra of a mixture of 510NPLs and 550 NPLs with different amounts of added Me/Bu solution.

The existence of ET from the 510NPLs to the 550NPLs is debatable, because there are two possible explanations for the observations in the emission and lifetime measurements. First explanation, there is non-radiative ET from the 510NPLs to the 550NPLs. This explains the shorter lifetime of the 510NPLs and the change in ratio between the emission peaks upon the addition of more anti-solvent. The decrease of the emission of both NPLs and the shorter lifetime of the emission of 550NPLs can be explained by an increase in ET between NPLs of the same thickness when more anti-solvent is added. Due to this increases in ET between the same NPLs, the probability of quenching the emission is increased, as the energy can migrate to non-emitting NPLs.

A second explanation is that the anti-solvent interacts with the NPLs, which results in quenching of the emission. This explains the lower emission intensity and the decrease in lifetime when more anti-solvent is added. The change in ratio between the emission peaks can be explained by that the quenching of the emission, due to the anti-solvent, will be stronger for the 510NPLs than the 550NPLs. As the surface-to-volume ratio of the 510NPLs is bigger, their effective interaction with the solvent will be larger than for the 550NPLs. What the possible mechanism is behind the quenching due to the anti-solvent is not known. Further research has to be done to investigate if one of these two explanations is true.

#### 5.5.4 Conclusion and outlook

It is shown that there could be ET occurring between the NPLs, but the results are inconclusive. Overlap between the emission peaks of different NPLs forms a problem, because it makes it difficult to conclude if there is ET between the NPLs. Due to the high concentration that have to be used to observe ET between these NPLs, other processes like concentration quenching also start to play a role. These problems could be

circumvented by adding an anti-solvent to a mixture of 510NPLs and 550 NPLs. For the measurements on this sample it was also not clear if there was ET between the particles. The anti-solvent could also quench the emission, which could also explain all observations. For future research, a different anti-solvent could be added to see what the effect is on the emission and luminescence lifetime. A second measurement that could be done is adding a Me/Bu mixture to a lower concentration of 510NPLs and 550NPLs. Due to the lower concentration, shorter stacks will be formed. This will lower the ET between the NPLs and also decrease the chance that an exciton gets trapped. Therefore the decay curves will be longer compared to the decay curves in figure 48 and 49. However, if our obtained data is due to quenching of the emission by the anti-solvent, there should be no difference in the lifetime.

## 5.6 Influence refractive index on the decay rate and the quantum yield

### 5.6.1 Background information

510NPLs were dispersed in solutions with different refractive indices to obtain more information about the radiative and non-radiative decay. The non-radiative decay rate is invariant when changing the refractive index of the solvent, but the radiative decay rate is affected. The radiative decay rate is higher in solvents with a higher refractive index. For an emitter in a homogeneous dielectric surrounding an expression for this dependence is given by equation (7), where  $\Gamma$  is the radiative decay rate,  $\Gamma_0$  the radiative decay rate in vacuum and  $n$  the refractive index of the solvent [43]. However, in a real system the dielectric surroundings are not perfectly homogeneous. Therefore the local field factor  $\chi$  is introduced (Eq (8)) [44].

$$\Gamma = \Gamma_0 n \quad (7)$$

$$\Gamma = \Gamma_0 n \chi^2 \quad (8)$$

There are many models to obtain an expression for this local field factor. The model that will be used here is the empty cavity model, because this model accounts for the fact that the emitter and the solvent cannot occupy the same space and that the emitter has a different refractive index than the solvent [43]. The expression for  $\chi$  in this model is given by equation (9). One adaptation has to be made to this expression, because the cavity where the emitter is located does not have a refractive index of vacuum ( $n = 1$ ). The refractive index of the cavity in our system is the refractive index of the CdSe NC ( $n = 2.65$ ). This results in an expression for  $\chi$  and  $\Gamma$  given by equation (10) and (11) respectively [45].

This model has an spherical cavity shape, which cannot describe the decay rate of all shapes of emitter accurately. The NPLs used in this system could probably be better described with an empty ellipsoidal cavity model [43]. The expression for this model is given in equation (12).  $L_\mu$  should be substituted by  $L_X$ ,  $L_Y$  or  $L_Z$  depending on whether the transition moment  $\mu_{ji}$  is parallel to the  $x$ ,  $y$  or  $z$  axis. In the case of CdSe NPLs it should be substituted by  $L_X$  or  $L_Y$  [42]. The values for the  $a_X$ ,  $a_Y$  and  $a_Z$  are the sizes of the NPL, which is 14 by 14 nm by 1.2 nm. Note that for the special case that  $a_X = a_Y = a_Z$  we obtain  $L_X = L_Y = L_Z = \frac{1}{3}$  and the expression for the ellipsoidal model (Eq. (12)) simplifies to the expression for the spherical cavity model (Eq.(11)).

$$\chi = \frac{3n^2}{2n^2 + 1} \quad (9)$$

$$\chi = \frac{3n^2}{2n^2 + n_{NC}^2} \quad (10)$$

$$\Gamma = \Gamma_0 n \left( \frac{3n^2}{2n^2 + n_{NC}^2} \right)^2 \quad (11)$$

$$\Gamma = \Gamma_0 \frac{n^5}{((1 - L_\mu)n^2 + L_\mu n_{NC})^2} \quad (12)$$

$$L_x = \int_0^\infty \frac{a_x a_y a_z ds}{2\sqrt{(s + a_x^2)^3 (s + a_y^2)(s + a_z^2)}} \quad (13)$$

### 5.6.2 Lifetime measurements

In this chapter the dependence of the lifetime and the dependence of fraction of emission trough the fast components on the refractive index of the solvent will be discussed. To investigate this dependence, 50  $\mu$ L of a sample with 510NPLs was dispersed in 3 mL solvent. The solvents that were used and the refractive indices of these solvents are listed in table 4. The lifetime of these samples were measured using a pulsed laser with intervals of 50 ns and 2  $\mu$ s and an excitation wavelength of 441 nm. All measurements were done for 2 minutes. The measurements with a high frequency of the pulsed laser were done to measure the fast component of the decay curve more accurately. The obtained decay curves were normalized and are shown in figure 51 and 52.

Solvent	refractive index
Hexane	1.375
Hexane/cyclohexane mixture (1:1)	1.4005
Cyclohexane	1.426
Trichloroethylene	1.4777
Trichloroethylen/toluene mixture (1:1)	1.48685
Toluene	1.496
Toluene/chlorobenzene (1:1)	1.51005
Toluene	1.52411

Table 4: Refractive index of solvents used for measurements

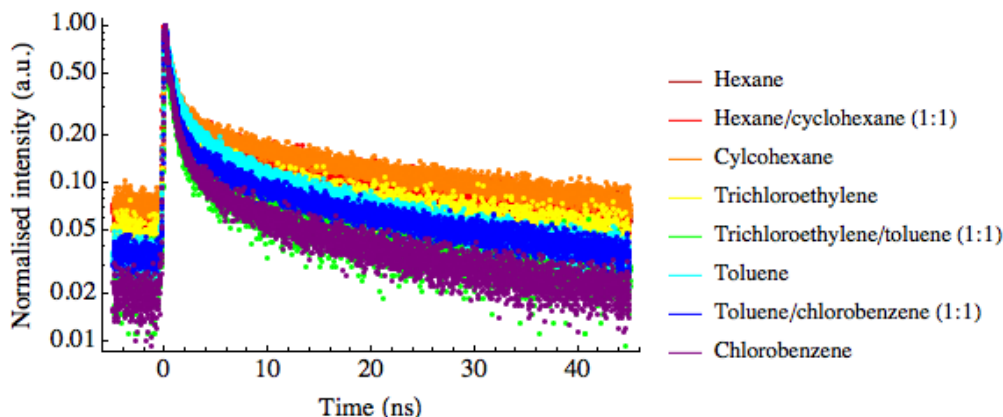


Figure 51: Decay curve of emission 510NPLs in different solvents measured with pulsed laser with intervals of 50 ns. Solvents: Hexane (dark red), cyclohexane/hexane (red), cyclohexane (orange), trichloroethylene (yellow), trichloroethylene/toluene (green), toluene (cyan), toluene/chlorobenzene (blue) and chlorobenzene (purple).

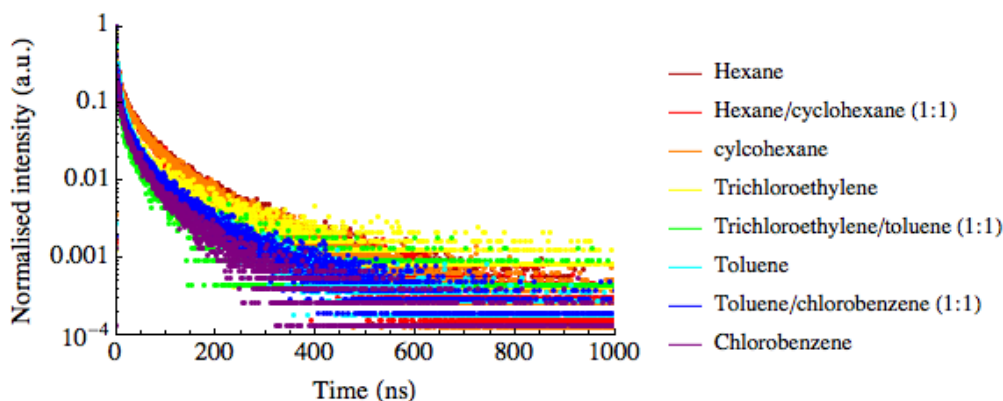


Figure 52: Decay curve of emission 510NPLs in different solvents measured with pulsed laser with intervals of 2  $\mu$ s. Solvents: Hexane (dark red), cyclohexane/hexane (red), cyclohexane (orange), trichloroethylene (yellow), trichloroethylene/toluene (green), toluene (cyan), toluene/chlorobenzene (blue) and chlorobenzene (purple).

### 5.6.3 Dependence lifetime

The decay curves in figure 51 and 52 are multi-exponential. The decay curves are different for the different solvents, but there is no relation between between the shape of the decay curves and the refractive index of the solvent.

The decay curves were fitted to see whether there is a trend in the individual components of the lifetime. The decay curves obtained when pulsing every 50 ns can be fitted with a triple-exponential decay curve (Eq. (14)).

$$I(t) = A_1 e^{t/\tau_1} + A_2 e^{t/\tau_2} + A_3 e^{t/\tau_3} \quad (14)$$

The obtained values for the lifetime of these components are shown in figure 53a and 53b in blue ( $\tau_1$ ), orange ( $\tau_2$ ) and red ( $\tau_3$ ). For these individual components there is no trend in the lifetime versus the refractive index. Since the rate ( $1/\tau$ ) of a radiative processes depends on the solvents refractive index ((12)), we must conclude that none of the three lifetime components is predominantly radiative. This is an unexpected result, because the fast components in the photoluminescence decay of NPLS have previously been ascribed to radiative recombination of the exciton [36].

The average lifetimes of the slow components were also determined. These average lifetimes were calculated using the data from 20 ns to 1  $\mu$ s shown in figure 52. The results are shown in figure 53b in green. Again, the lifetime does not decreases when the refractive index is increased, but this is what we would expect. The slow components are probably due to trapping. This process is mostly non-radiative.

The average lifetime at  $n = 1.466$  and  $n = 1.48685$  are longer than the other values. These two point are from the samples where trichloroethylene was the solvent. The intensity of these samples were lower during the measurements. It is possible that due to the presence of trichloroethylene there is more trapping, resulting in a slower decay rate. The reason for the increase in trapping when trichloroethylene is present cannot be given at this point. Photocatalytic decomposition of trichloroethylene has been reported, but this decomposition occurred in the presence of oxygen and water [46].

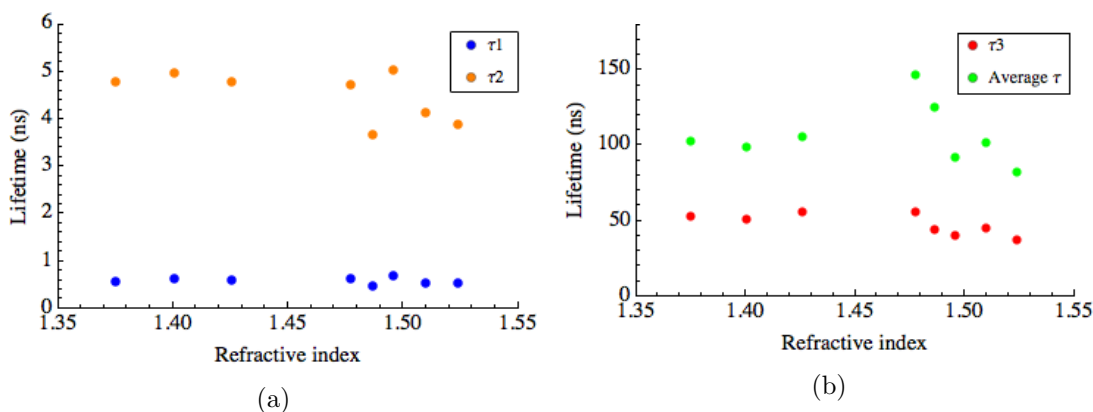


Figure 53: (a) Fitted lifetime of  $\tau_1$  (blue) and  $\tau_2$  (orange). (b) Fitted lifetime of  $\tau_3$  (red) and the average lifetime of the long components (green).

#### 5.6.4 Dependence fraction of emission through fast components

The dependence of the fraction of emission through the fast components on the refractive index can be determined by integrating the area under the decay curves. With integration a number for the directly emitted photons ( $I_{\text{fast}}$ ) can be obtained. This number can be divided by the total area under the decay curve ( $I_{\text{tot}}$ ) to obtain the fraction of photons directly emitted.  $I_{\text{fast}}$  is obtained by integrating the first two components (fast components) of equation (14). The values for  $\tau_1$ ,  $\tau_2$ ,  $A_1$  and  $A_2$  were obtained



by fitting the decay curves in figure 51 with equation (14). The values for  $A_1$  and  $A_2$  had to be corrected, because the intensity of the decay curves in figure 51 is not zero after 50 ns. The intensity of first and second component are zero after 50 ns. The third component, on the other hand, does not completely decay in one repetition period of the laser. Consequently, the photoluminescence decay after a certain laser pulse contains contributions from slowly decaying NPLs which were excited by the pulse before. The apparent amplitude,  $A_3$ , of the third component is therefore higher than it would be at a lower repetition rate. To correct for this experimental artefact, an expression was found for the  $A_3$  in terms of the real value of  $A_3$  ( $A_3^*$ ). The value of  $A_3$  is  $A_3^*$  plus the sum of the intensity of all previous measured decay curves. The resulting expression is given in Eq (15). This expression can be substituted in equation (14) to obtain equation (16). Figure 54 shows the effect of this adaptation. The green curve is the fit of equation (16) and the red curve is what the decay curve would look like when it was measured at a lower repetition rate of the pulsed laser. The values of  $A_1$ ,  $A_2$  and  $A_3^*$  were normalized to obtain the correct values for the amplitude of the first two components. This resulted in an expression for  $I_{\text{fast}}$  given in equation (17).

$$A_3 = A_3^* + A_3^* \sum_{n=1}^{+\infty} e^{nT/\tau_3} = A_3^* \sum_{n=0}^{+\infty} e^{nT/\tau_3} = A_3^* \frac{e^{T/\tau_3}}{e^{T/\tau_3} - 1}, (T = 50ns) \quad (15)$$

$$I(t) = A_1 e^{t/\tau_1} + A_2 e^{t/\tau_2} + A_3^* \frac{e^{50/\tau_3}}{e^{50/\tau_3} - 1} e^{t/\tau_3} \quad (16)$$

$$I_A = \frac{A_1}{A_1 + A_2 + A_3^*} \tau_1 + \frac{A_2}{A_1 + A_2 + A_3^*} \tau_2 \quad (17)$$

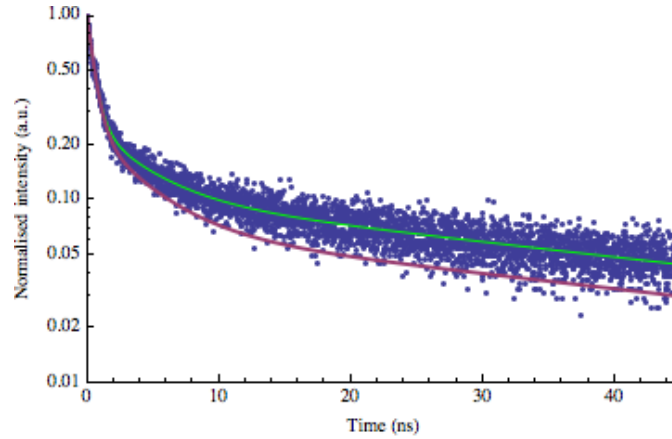


Figure 54: Correction of the measured decay curve. The original data point is shown in blue, fit of equation (16) is shown in green and the adapted decay curve is shown in red.

The values obtained after integration of the different components as a function of the refractive index are shown in figure 55. The values obtained for the first and second component (orange and blue) do not depend on the refractive index. The values obtained for the third component (red) decreases when the refractive index of the solvent is increased.  $I_{\text{fast}}$  is given by the sum of the two fast components shown in blue and orange.

The total area under the decay curve was determined by summing the values of all points in the measured decay curve shown in figure 52 and multiplying this by the step size. The results are shown in figure 55 in green. The value for the total area under the normalized decay curve also decreases when the refractive index of the solvent is increased.

The fraction of emission through the fast component for all samples were calculated by dividing  $I_{\text{fast}}$  by  $I_{\text{tot}}$ . The results are shown in figure 56. The fraction of emission through the fast components increases when the refractive index of the solvent increases and is also only 10 to 20% of the total emission.

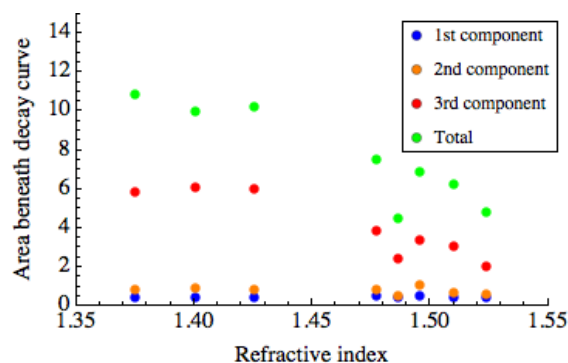


Figure 55: Number of photons emitted by the first component (blue), second component (orange) and third component (green). The total emitted number of photons is shown in green

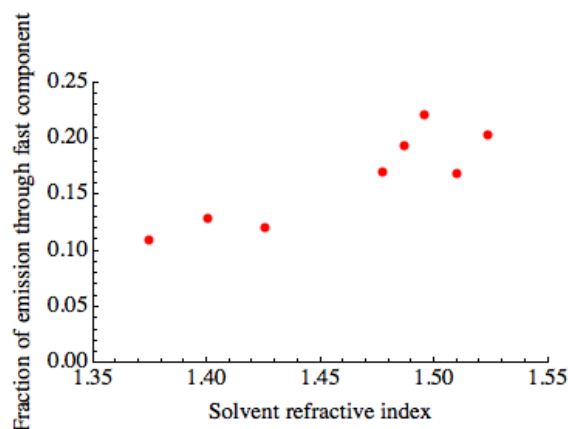


Figure 56: Fraction of emission through fast component as function of the refractive index of the solvents.

## 5.6.5 Fitting of the models

The underlying assumption is that an excited NPLs can decay at a fast rate by emission or can trap a charge carrier and then decay at a slow rate. The schematic representation of this proposed model is shown in figure 57. In this figure, the fast decay path is shown in red and the slow decay path is shown in black. The fast decay is due to a direct decay from the conduction band (CB) to the valence band (VB). This is a radiative process and therefore depends on the refractive index of the solvent. The slow decay is due to a temporarily trapping of the charge carrier followed by decay from the CB to the VB. The assumption is made that the trapping is a non-radiative process and is therefore independent of the refractive index of the solvent. The trapped charge carrier can also decay non-radiatively from the trapping state to the valence band (Fig. 57, curly arrow).

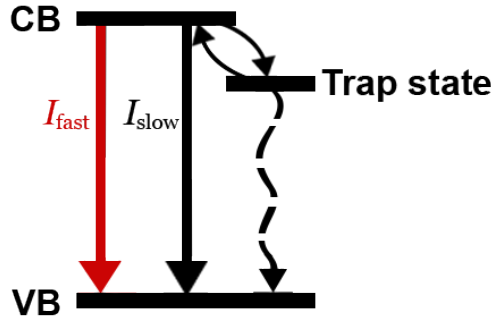


Figure 57: Model of decay paths in a NPL. The fast (radiative) decay path from the CB to the VB is shown red. The slow (non-radiative) decay path is shown in black. The curly arrow indices the possible non-radiative decay of the charge carrier from the trapping state to the VB.

In the previous section it was shown that there is a dependence between the fraction of emission by the fast components and the refractive index of the solvent. To investigate if this dependence is consistent with the theory discussed in section 5.6, the data points in figure 56 were fitted with the ellipsoidal empty cavity model. The fraction of emission through the fast components or the ratio between  $I_{fast}$  and  $I_{tot}$  is equal to the ratio between the radiative decay ( $\Gamma_{rad}$ ) rate and the total decay rate ( $\Gamma_{tot}$ ). The expression for  $\Gamma_{rad}$  is given by the ellipsoidal empty cavity model (Eq. (12)).  $\Gamma_{tot}$  is the sum of  $\Gamma_{rad}$  and  $\Gamma_{nonrad}$ .  $\Gamma_{nonrad}$  is a constant, because the non-radiative decay rate does not depend on the refractive index of the solvent. The constant is multiplied with a factor  $\eta$ , which accounts for the non-radiative decay from the trapping state to the VB. This result in an expression (Eq. (18)) which can be fitted to the obtained data points in figure 56.

$$QY = \frac{I_{fast}}{I_{tot}} = \frac{\Gamma_{rad}}{\Gamma_{tot}} = \frac{\Gamma_{rad}}{\Gamma_{rad} + \eta constant} = \frac{\Gamma_0 n \left( \frac{n^2}{(1-L_\mu)n^2 + L_\mu n_{NC}^2} \right)^2}{\Gamma_0 n \left( \frac{n^2}{(1-L_\mu)n^2 + L_\mu n_{NC}^2} \right)^2 + \eta c} \quad (18)$$

The datapoint were fitted for  $L_\mu = 0.07$ ,  $L_\mu = \frac{1}{3}$  and  $L_\mu = 1$ .  $L_\mu = 0.07$  is the value you obtain if the size of the NPL is 14 by 14 by 1.2 nm and the transition moment is perpendicular to the short axis of the platelet.  $L_\mu = \frac{1}{3}$  is a special case were the Ellipsoidal Cavity Model is reduced to the Spherical Cavity Model.  $L_\mu = 1$ , is the case for when the lateral dimensions of the NPLs are infinite compared to the thickness of the NPL and the transition moment is parallel to the short axis. The fits for  $L_\mu = 0.07$  (purple),  $\frac{1}{3}$  (red) and 1 (green) are shown in figure 58. The value for  $\eta$  is set to 1, meaning that these fits do not take the radiative decay from the trapping state to the VB into account.

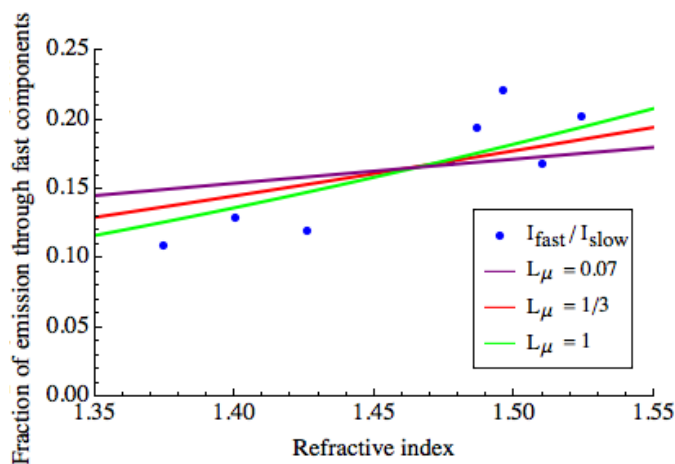


Figure 58: QY as function of the refractive index (blue) fitted with equation 18 for  $L_\mu = 0.07$  (purple),  $L_\mu = \frac{1}{3}$  (red) and  $L_\mu = 1$  (green).

The fit shown in purple should be the best fit, because the value for  $L_\mu$  used for the fit is the value that  $L_\mu$  should have for the NPLs measured on. This fit is however the worst fit of the three. The data points cannot be fitted well by any of the values for  $L_\mu$ . The slope of fit should be higher, but this is only possible if  $L_\mu$  becomes larger than 1. A value larger than 1 cannot be obtained for  $L_\mu$ .

A possible reason why the data points cannot be fitted by any of the models is that the solvents have an influence on the non-radiative decay rate. The solvent could for example induce more trapping due to a reaction with a charge carrier. As stated before the emission of the samples with trichloroethylene had a lower intensity. This solvent quenches the luminescence. There is an influence of the solvents on the non-radiative decay rate, but it is hard to say if all solvents used have an influence. The increase of the fraction of emission through the fast components when the refractive index of the solvent is increased will only fit the models discussed when the solvents do not provide any non-radiative decay channels [45].

A second explanation for why the data points cannot be fitted by the models is that the assumption that the first two components are due to radiative decay is not correct. Because the decay curves are multi-exponential, it is hard to say what processes are occurring. Some research on these processes have been published, but only the first 5 ns

of the decay was taken into account [36]. The conclusions of Ref. [36] were that there are NPLs with and without a quenching site. The second component of the lifetime is assumed to be non-radiative. The statement that there are two kinds of NPLs present contradicts a previous paper where it was stated that the lifetime of a single NPL is very similar to the lifetime of an ensemble [10].

#### 5.6.6 Conclusion and outlook

The decay curves are different for the different solvents, but there is no relation between the shape of the decay curves and the refractive index of the solvent. A decrease of the lifetime of the radiative decay (two fast components) as a function of the refractive index was not observed. There was also no trend visible in the lifetime of the slow components. This was expected, because the non-radiative decay rate does not depend on the refractive index according to the theory. The lifetime of the NPLs in trichloroethylene had, in comparison with the other solvents, a longer lifetime. This could be because this solvent induces other decay pathways.

The fraction of emission through the fast components did depend on the refractive index of the solvent, but the trend could not be fitted by any of the models. The NPLs do not show the same behaviour as other emitters in solvents. There is no clear explanation for why the obtained results cannot be fitted with any of the models. More research on the possible decay pathways would give more insight on these strange observations. It could be that the NPLs interact with the solvents, resulting in other non-radiative decay paths.

For further research, it would also be interesting to do these measurements on NPLs that are not washed so many times. To obtain one population of NPLs, size selective precipitation was performed on the platelets used for these experiments. This could reduce the QY of the platelets, because more surface defects are introduced. It would be interesting to see if the NPLs obtained with the adapted synthesis method reported in section 5.4 would give the same results as the NPLs obtained with many washing steps.

## 6 Conclusion and outlook

NPLs emitting at 460, 510 and 550 nm can be successfully synthesized using the method described by the Dubertret et al. CdSe/CdS core/shell particles can also be synthesized, but the formation of CdSe/Cd<sub>0.5</sub>Zn<sub>0.5</sub>S/ZnS multishell NPLs proved to be more difficult. Multishell NPLs containing Cd, S<sub>6</sub>, Zn and S are obtained when the SILAR method with oleyl amine as coordinating ligand is used, but the QY of these NPLs is very low compared to bare NPLs. The TEM/HAADF-STEM images show that the contrast of the edge of the multishell NPLs is different than the center. EELS measurements show that the edge is thicker than the center of the particle and that an excess of cadmium and sulphur is present at the edge of the particle. The formation of a thicker edge is also observed for thicker NPLs with a different growth direction. What causes the formation of the thicker shell is not known yet. Formation of a thicker edge was also observed for the continuous growth of CdS around CdSe NPLs. The concentration of precursor used in our experiments could have been too high and therefore continuous growth was taking place instead of layer by layer growth. For further experiments the concentration of the precursors could be lowered, to investigate if this has an influence on the thickness of the edge.

When a Hg-exchange reaction is performed on CdSe NPLs no stable dispersions are obtained. The method used for the exchange reaction was developed by the group of Hens for QDs, but exchange on QDs could also not be reproduced. A possible explanation could be that the QDs used for the experiment were too small and the NPLs too thin. When the reaction zone is larger than the size of the NC, then the particle will disintegrate during the reaction. The exchange reaction is partially successful on QDs with a multishell according to TEM and EDX-measurements. These experiments also resulted in stable dispersions. For future experiments it would be interesting to investigate whether exchange is possible on CdSe/CdS core/shell NPLs, because these particles are thicker.

As stated before, NPLs emitting at 460 nm, 510 nm and 550 nm can successfully be synthesized, it is however difficult to obtain only one population of NPLs. When adding sodium acetate or lithium acetate during the synthesis of 510NPLs only one population of NPLs is obtained, but these platelets have a lower QY than when cadmium acetate is added. Adding a mixture of cadmium acetate and sodium acetate resulted in a single population of NPLs with a high QY of 60%. Recommendation for further experiments are investigating if the same adaptation to the synthesis method of 550NPLs will also result in one population of NPLs with a high QY.

Whether ET is occurring between NPLs was also investigated. The results obtained when varying the concentration of the samples to investigate this phenomenon were inconclusive. The change in ratio between the emission intensity of different populations of NPLs can be explained by ET, but also by concentration quenching. As there is overlap between the emission peaks, it is also hard to measure the lifetime of only one population. These lifetime measurements could confirm if ET is taking place. When adding an anti-solvent to reduce the distance between the NPLs instead of increasing

the concentration, the results were still inconclusive. The lifetime of both 550NPLs and 510NPLs changes and also the ratio between the emission peaks change, but the total intensity of the emission for both populations is lower when more anti-solvent is added. The changes in the lifetime when more anti-solvent is added could be explained by ET, but can also be explained by quenching of the emission due to the interaction with the added anti-solvent. Adding different anti-solvents or adding a anti-solvent to lower concentration of NPLs and comparing the decay curves to the experiments already done can give more information if ET is taking place.

The influence of the refractive index of the solvent on the lifetime and the fraction of emission through the fast components was also investigated. All components of the lifetime are independent of the refractive index. This is not expected, as the radiative decay rate depends on the refractive index of the solvent. Because no dependence is measured, it can be concluded that non of the lifetime components are mainly radiative. The fraction of emission through the fast components did depend on the refractive index, but the observed trend could not be fitted by the proposed models. More research has to be done on the decay path of the charge carriers in NPLs, in order to come up with a better model for the decay pathways.





## 7 Acknowledgements

First of all, I would like to thank my daily supervisor Jaco for all his help during my thesis, for the thorough checking of my thesis and for not forgetting me when you were in France! Furthermore, I would like to thank Relinde for being my substitute supervisor and for answering all my questions about synthesis. I would also like to thank my second supervisor Daniël Vanmaekelbergh for the helpful discussions of my results.

Many thanks to all PhD's, masterstudents and the entire CMI group. I had a great time during the one and a half year I was there! Special thanks to Freddy and Elleke for helping me with measurements and Carlo for borrowing your cuvettes many times. Thanks to Marieke for helping me with Mathematica during the last weeks, it was of great help. Thanks to Maro, Adriaan and Paolo for the discussion about our results and problems. I really enjoyed that. I also really enjoyed the fun I had with my fellow masterstudents (e.g. taping Stephan to a chair. Yes, I have pictures!).

Finally, I would like to thank my brother for always being interested in what I do and for not getting annoyed when I only called because I had a problem with my laptop. Thanks to all for the great one and a half year I had!



## References

- [1] Marcel Bruchez Jr. and Mario Moronne. Semiconductor nanocrystals as fluorescent biological labels. *Science*, 281(5385):2013 – 2016, 1998.
- [2] Wandy U. Huynh, Janke J. Dittmer, and A. Paul Alivisatos. Hybrid Nanorod-Polymer Solar Cells. *Science*, 295(5564):2425, 2002.
- [3] V. L. Colvin, M. C. Schlamp, and A. P. Alivisatos. Light-emitting diodes made from cadmium selenide nanocrystals and a semiconducting polymer. *Nature*, 370(6488):354–357, 1994.
- [4] Zheng Li and Xiaogang Peng. Size/Shape-Controlled Synthesis of Colloidal CdSe Quantum Disks: Ligand and Temperature Effects. *Journal of the American Chemical Society*, 133(17):6578–6586, 2011.
- [5] C. B. Murray, D. J. Norris, and M. G. Bawendi. Synthesis and characterization of nearly monodisperse CdE (E = sulfur, selenium, tellurium) semiconductor nanocrystallites. *Journal of the American Chemical Society*, 115(19):8706–8715, 1993.
- [6] Xiaogang Peng and Liberato Manna. Shape control of CdSe nanocrystals. *Nature*, 404(6773):59, 2000.
- [7] Liberato Manna, Delia J. Milliron, Andreas Meisel, Erik C. Scher, and A. Paul Alivisatos. Controlled growth of tetrapod-branched inorganic nanocrystals. *Nat Mater*, 2(6):382–385, 2003.
- [8] W. William Yu, Lianhua Qu, Wenzhuo Guo, and Xiaogang Peng. Experimental determination of the extinction coefficient of cdte, cdse, and cds nanocrystals. *Chemistry of Materials*, 15(14):2854–2860, 2003.
- [9] Sandrine Ithurria and Benoit Dubertret. Quasi 2D Colloidal CdSe Platelets with Thicknesses Controlled at the Atomic Level. *Journal of the American Chemical Society*, 130(49):16504–16505, 2008.
- [10] Mickaël D. Tessier, Clémentine Javaux, Ivan Maksimovic, Vincent Lorientte, and Benoit Dubertret. Spectroscopy of Single CdSe Nanoplatelets. *ACS Nano*, 6(8):6751–6758, 2012.
- [11] Celso de Mello Donega. Synthesis and properties of colloidal heteronanocrystals. *Chem. Soc. Rev.*, 40:1512–1546, 2011.
- [12] S. V. Gaponenko. *Introduction to Nanophotonics*. Cambridge University Press, New York, 1st edition, 2010.
- [13] Jin Chang and Eric R. Waclawik. Colloidal semiconductor nanocrystals: controlled synthesis and surface chemistry in organic media. *RSC Adv.*, 4:23505–23527, 2014.

- 
- [14] Yongan Andrew Yang, Huimeng Wu, Kathryn R. Williams, and Y. Charles Cao. Synthesis of CdSe and CdTe Nanocrystals without Precursor Injection. *Angewandte Chemie International Edition*, 44(41):6712–6715, 2005.
- [15] Yin Yadong and A. Paul Alivisatos. Colloidal nanocrystal synthesis and the organic/inorganic interface. *Nature*, 437(7059):664 – 670, 2005.
- [16] J. E. Bowen Katari, V. L. Colvin, and A. P. Alivisatos. X-ray Photoelectron Spectroscopy of CdSe Nanocrystals with Applications to Studies of the Nanocrystal Surface. *The Journal of Physical Chemistry*, 98(15):4109–4117, 1994.
- [17] Rajib Ghosh Chaudhuri and Santanu Paria. Core/shell nanoparticles: Classes, Properties, Synthesis Mechanisms, Characterization, and Applications. *Chemical Reviews*, 112(4):2373–2433, 2012.
- [18] Renguo Xie, Ute Kolb, Jixue Li, Thomas Basch, and Alf Mews. Synthesis and Characterization of Highly Luminescent CdSe-core CdS/Zn<sub>0.5</sub>Cd<sub>0.5</sub>S/ZnS multishell Nanocrystals. *Journal of the American Chemical Society*, 127(20):7480–7488, 2005.
- [19] J. Jack Li, Y. Andrew Wang, Wenzhuo Guo, Joel C. Keay, Tetsuya D. Mishima, Matthew B. Johnson, and Xiaogang Peng. Large-Scale Synthesis of Nearly Monodisperse CdSe/CdS Core/Shell Nanocrystals Using Air-Stable Reagents via Successive Ion Layer Adsorption and Reaction. *Journal of the American Chemical Society*, 125(41):12567–12575, 2003.
- [20] Jessy B. Rivest and Prashant K. Jain. Cation exchange on the nanoscale: an emerging technique for new material synthesis, device fabrication, and chemical sensing. *Chem. Soc. Rev.*, 42:89–96, 2013.
- [21] Dong Hee Son, Steven M. Hughes, Yadong Yin, and A. Paul Alivisatos. Cation Exchange Reactions in Ionic Nanocrystals. *Science*, 306(5698):1009–1012, 2004.
- [22] Karol Miszta, Dirk Dorfs, Alessandro Genovese, Mee Rahn Kim, and Liberato Manna. Cation Exchange Reactions in Colloidal Branched Nanocrystals. *ACS Nano*, 5(9):7176–7183, 2011.
- [23] Shuchi Gupta, Stephen V. Kershaw, and Andrey L. Rogach. 25th Anniversary Article: Ion Exchange in Colloidal Nanocrystals. *Advanced Materials*, 25(48):6923–6944, 2013.
- [24] S. Ithurria, M. D. Tessier, B. Mahler, R. P. S. M. Lobo, B. Dubertret, and A. L. Efros. Colloidal nanoplatelets with two-dimensional electronic structure. *Nat Mater*, 10(12):936–941, 12 2011.
- [25] Ramzi Benchamekh, Nikolay Gippius, Jacky Even, O. Nestoklon, Mikhail, Jean-Marc Jancu, Sandrine Ithurria Lhuillier, Benoît Dubertret, Alexander Efros, and Paul Voisin. Tight-binding calculations of image charge effects in colloidal nanoscale platelets of CdSe. *Physical Review B (Condensed Matter)*, 89(3):035307, 2014.

- [26] Eline M. Hutter, Eva Bladt, Bart Goris, Francesca Pietra, Johanna C. van der Bok, Mark P. Boneschanscher, Celso de Mello Donegá, Sara Bals, and Daniël Vanmaekelbergh. Conformal and Atomic Characterization of Ultrathin CdSe Platelets with a Helical Shape. *Nano Letters*, 14(11):6257–6262, 2014.
- [27] S. Ithurria, G. Bousquet, and B. Dubertret. Continuous Transition from 3D to 1D Confinement Observed during the Formation of CdSe Nanoplatelets. *Journal of the American Chemical Society*, 133(9):3070–3077, 2011.
- [28] Constanze Schliehe, Beatriz H. Juarez, Marie Pelletier, Sebastian Jander, Denis Greshnykh, Mona Nagel, Andreas Meyer, Stephan Foerster, Andreas Kornowski, Christian Klinke, and Horst Weller. Ultrathin PbS Sheets by Two-Dimensional Oriented Attachment. *Science*, 329(5991):550–553, 2010.
- [29] Cécile Bouet, Benoit Mahler, Brice Nadal, Benjamin Abecassis, Mickael D. Tessier, Sandrine Ithurria, Xiangzhen Xu, and Benoit Dubertret. Two-Dimensional Growth of CdSe Nanocrystals, from Nanoplatelets to Nanosheets. *Chemistry of Materials*, 25(4):639–645, 2013.
- [30] Liberato Manna, Erik C. Scher, and A. Paul Alivisatos. Synthesis of Soluble and Processable Rod-, Arrow-, Teardrop-, and Tetrapod-Shaped CdSe Nanocrystals. *Journal of the American Chemical Society*, 122(51):12700–12706, 2000.
- [31] Z. Adam Peng and Xiaogang Peng. Mechanisms of the Shape Evolution of CdSe Nanocrystals. *Journal of the American Chemical Society*, 123(7):1389–1395, 2001.
- [32] Benoit Mahler, Brice Nadal, Cecile Bouet, Gilles Patriarche, and Benoit Dubertret. Core/Shell Colloidal Semiconductor Nanoplatelets. *Journal of the American Chemical Society*, 134(45):18591–18598, 2012.
- [33] Mickaël D. Tessier, Piernicola Spinicelli, Dorian Dupont, Gilles Patriarche, Sandrine Ithurria, and Benoit Dubertret. Efficient Exciton Concentrators Built from Colloidal Core/Crown CdSe/CdS Semiconductor Nanoplatelets. *Nano Letters*, 14(1):207–213, 2014.
- [34] Anatol Prudnikau, Andrey Chuvilin, and Mikhail Artemyev. CdSe-CdS Nanoheteroplatelets with Efficient Photoexcitation of Central CdSe Region through Epitaxially Grown CdS Wings. *Journal of the American Chemical Society*, 135(39):14476–14479, 2013.
- [35] Cécile Bouet, Donatien Laufer, Benoit Mahler, Brice Nadal, Hadrien Heuclin, Silvia Pedetti, Gilles Patriarche, and Benoit Dubertret. Synthesis of Zinc and Lead Chalcogenide Core and Core/Shell Nanoplatelets Using Sequential Cation Exchange Reactions. *Chemistry of Materials*, 26(9):3002–3008, 2014.

- 
- [36] Lucas T. Kunneman, Juleon M. Schins, Silvia Pedetti, Hadrien Heuclin, Ferdinand C. Grozema, Arjan J. Houtepen, Benoit Dubertret, and Laurens D. A. Siebbeles. Nature and Decay Pathways of Photoexcited States in CdSe and CdSe/CdS Nanoplatelets. *Nano Letters*, 14(12):7039–7045, 2014.
- [37] Ward De Jonghe. Mercury chalcogenide quantum dots by cation exchange, 2013.
- [38] W. William Yu, Lianhua Qu, Wenzhuo Guo, and Xiaogang Peng. Experimental Determination of the Extinction Coefficient of CdTe, CdSe, and CdS Nanocrystals. *Chemistry of Materials*, 15(14):2854–2860, 2003.
- [39] Benoît Mahler, Nicolas Lequeux, and Benoît Dubertret. Ligand-Controlled Polytypism of Thick-Shell CdSe/CdS Nanocrystals. *Journal of the American Chemical Society*, 132(3):953–959, 2010.
- [40] R. D. Shannon. Revised effective ionic radii and systematic studies of interatomic distances in halides and chalcogenides. *Acta Crystallographica Section A*, 32(5):751–767, 1976.
- [41] Y. Q. Li, A. Rizzo, R. Cingolani, and G. Gigli. Bright white-light-emitting device from ternary nanocrystal composites. *Advanced Materials*, 18(19):2545–2548, 2006.
- [42] Benjamin Abécassis, Mickael D. Tessier, Patrick Davidson, and Benoit Dubertret. Self-Assembly of CdSe Nanoplatelets into Giant Micrometer-Scale Needles Emitting Polarized Light. *Nano Letters*, 14(2):710–715, 2014.
- [43] Dmitri Topygin. Effects of the Solvent Refractive Index and Its Dispersion on the Radiative Decay Rate and Extinction Coefficient of a Fluorescent Solute. *Journal of Fluorescence*, 13(3):201–219, 2003.
- [44] B Henderson and G. F. Imbusch. Optical Spectroscopy of Inorganic Solids. *Journal of Modern Optics*, 37(10):1688–1688, 1990.
- [45] Tim Senden, Freddy T. Rabouw, and Andries Meijerink. Photonic Effects on the Radiative Decay Rate and Luminescence Quantum Yield of Doped Nanocrystals. *ACS Nano*, 9(2):1801–1808, 2015.
- [46] Kyeong Youl Jung, Seung Bin Park, Masaya Matsuoka, and Masakazu Anpo. In-situ investigations of the photoluminescence properties of  $\text{SiO}_2/\text{TiO}_2$  binary and boron- $\text{SiO}_2/\text{TiO}_2$  ternary oxides prepared by the sol-gel method and their photocatalytic reactivity for the oxidative decomposition of trichloroethylene. *International Journal of Photoenergy*, 5(1):31–36, 2003.

A Appendix A

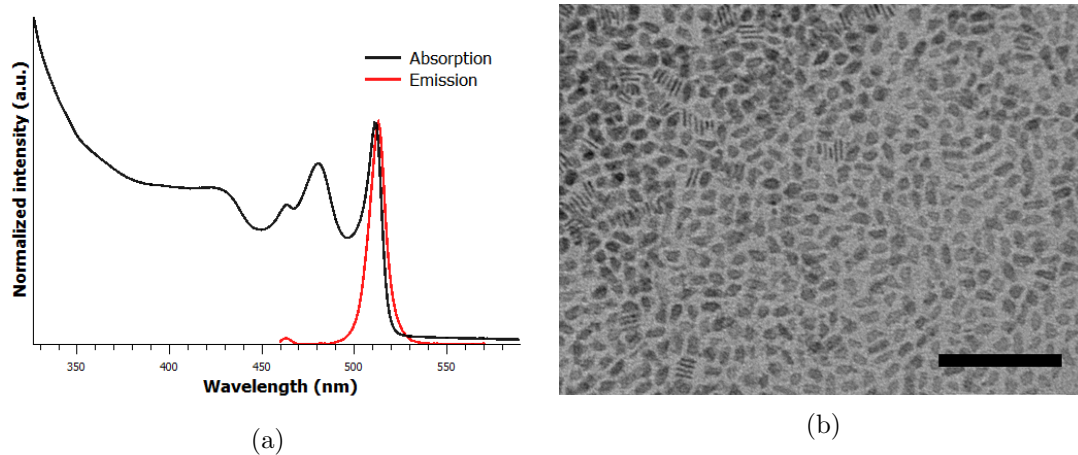


Figure 59: (a) Absorption spectrum of 510NPLs synthesized with the addition of  $Zn(Ac)_2$  (b) TEM picture of these particles. scale bar 100 nm.

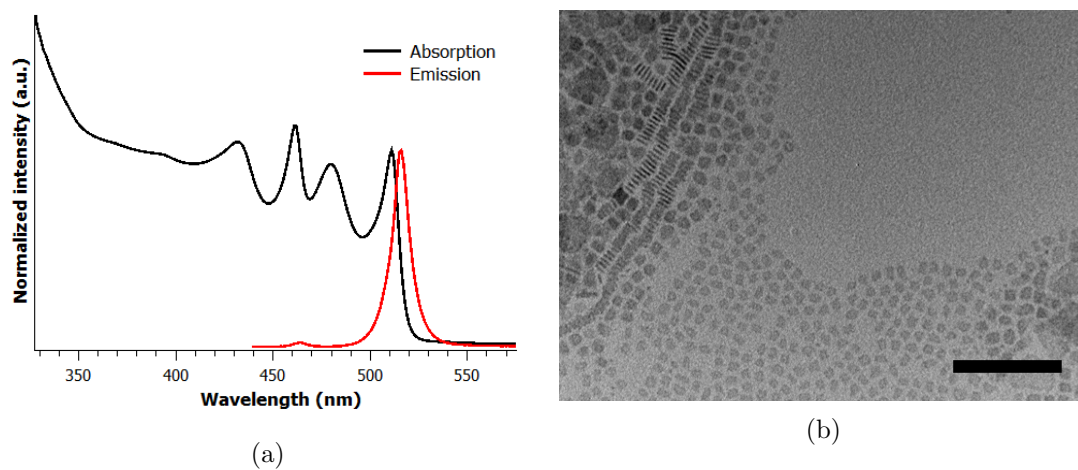
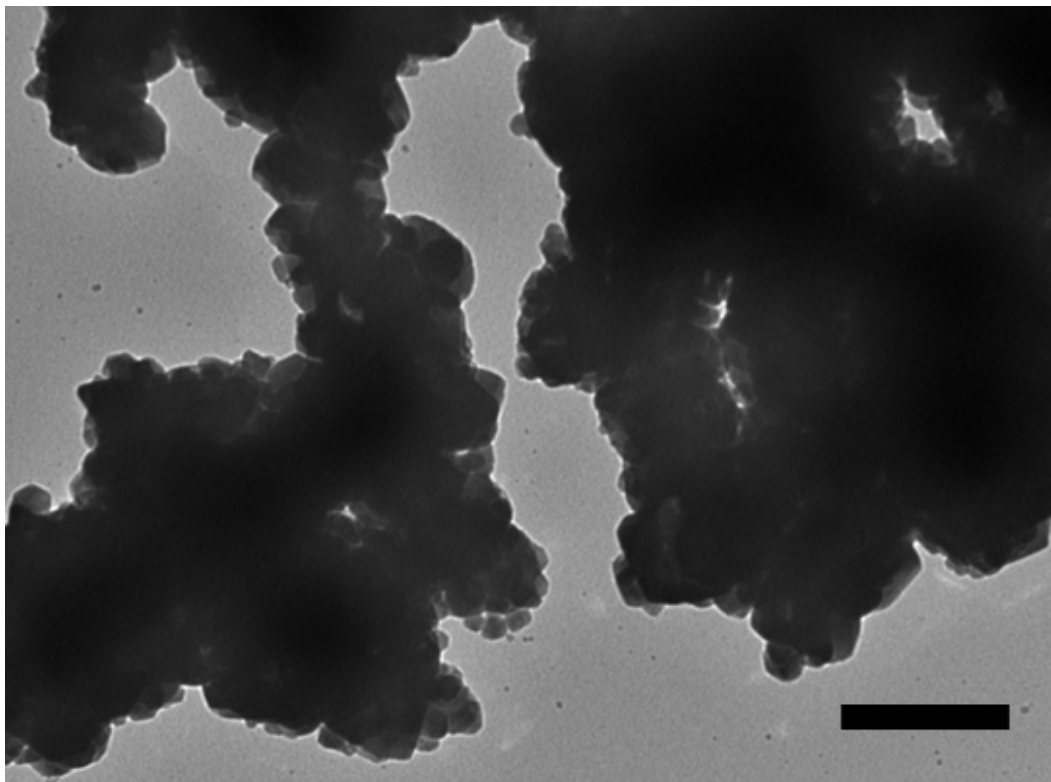
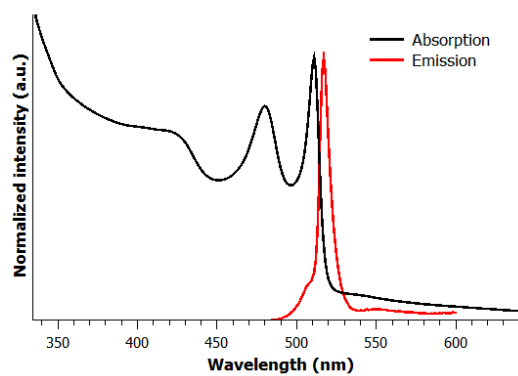


Figure 60: (a) Absorption spectrum of 510NPLs synthesized with the addition of  $Co(Ac)_2$  (b) TEM picture of these particles. Scale bar 100 nm.

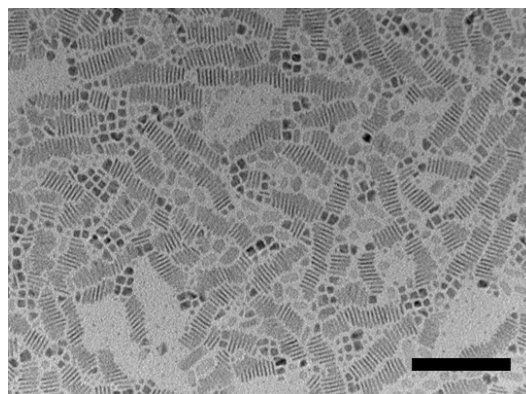


(a)

(b) TEM picture of 510NPLs synthesized with the addition of  $\text{Cu}(\text{Ac})_2$ . Scale bar 200 nm



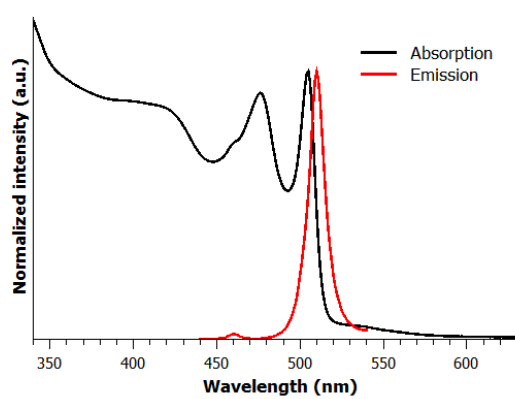
(a)



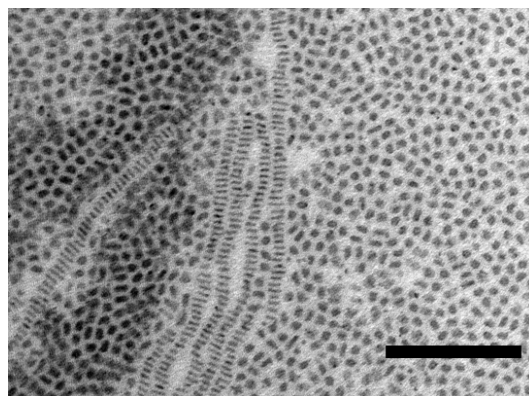
(b)

Figure 62: (a) Absorption spectrum of 510NPLs synthesized with the addition of  $\text{Pb}(\text{Ac})_2$  (b) TEM picture of these particles. Scale bar 100 nm.





(a)



(b)

Figure 63: (a) Absorption spectrum of 510NPLs synthesized with the addition of  $\text{Mg}(\text{Ac})_2$  (b) TEM picture of these particles. Scale bar 100 nm.